2012

A MEMS viscosity sensor for conductive fluids

Luis Gan Chau

A MEMS VISCOSITY SENSOR FOR CONDUCTIVE FLUIDS

by

Luis Alberto Gan Chau

A Thesis submitted in partial fulfillment of the requirements for the degree of

MASTER OF SCIENCE

IN

ELECTRICAL ENGINEERING

Approved by:

Prof. _____
Thesis Advisor – Dr. Lynn F. Fuller

Prof. _____
Thesis Advisor – Dr. Ivan Puchades

Prof. _____
Thesis Advisor – Dr. Sergey E. Lyshevski

Prof. _____
Department Head – Dr. Sohail A. Dianat

Department of Electrical and Microelectronic Engineering
Kate Gleason College of Engineering
ROCHESTER INSTITUTE OF TECHNOLOGY
Rochester, New York
2012

DEDICATION

To my parents, sister, brothers and family, who in the distance have been supportive of all my decisions:

"What this power is, I cannot say. All I know is that it exists...and it becomes available only when you are in that state of mind in which you know exactly what you want...and are fully determined not to quit until you get it."

-Alexander Graham Bell

ACKNOWLEDGEMENTS

To my fellow colleagues, faculty, and mentors thanking you is the least I could do, but I will always remember you for how much you have helped me change as a person and become a better engineer.

To Dr. Lynn Fuller and Dr. Ivan Puchades who were present at all times helping me accomplish this project. Without your guidance, I would have not learned the graduate aspect of the research environment. Pushing me all the time to make sure I understand what I was doing every step of this project. At the same time thinking in what needed to be done, and the consequences of following the decisions made, and WHY that decision was taken with background knowledge. That is the biggest one I will always remember, the special "WHY".

To Dr. Sergey Lyshevski who helped me comprehend the different ways actual theorems are solved, and why we use those theorems in different applications. Without that background I would have not understood how and why it was occurring.

To Team GALT, Dan, Nick, you two have helped me see how to take the different paths in life. Regardless of the path just make sure to take the easiest and shortest path rather than the hardest and longest one. Understanding how to work as a team and provide insight regardless of how much experience one has, it is always good to have different point of views.

"It is always the simple things that change our lives."

-Donald Miller

ABSTRACT

MEMS Viscosity sensors are widely used in different applications nowadays. MEMS sensors are created by making them small in size almost penny-like sized. With low power consumption, cheap costs of production, and mass production of the devices. These sensors are able to measure viscosity through three different characteristics, the frequency, amplitude and the quality factor. Each of these describes the fluids viscosity, by using a vibrational type viscometer. The sensor has been proven to work in conductive fluids after a post process fabrication of a protective layer of Parylene C. The sensors performance has been altered due to a thicker membrane, but still operates as expected. The MEMS viscosity sensor has been tested in various glycerol water mixtures to simulate conductive fluids with varying viscosity. The tests had positive outcomes, and the sensors performance was not altered, they worked as predicted. Different tests were accomplished to make sure the sensors performance remained close to normal operations after adding the protective layer of Parylene C. Four distinct oils were chosen to accomplish this variation test. Oil was chosen rather than a conductive liquid in order to prevent the sensor from damaging itself, and having to repackage another sensor and running all the previous tests. With these tests the sensor proved that adding a thin layer of Parylene C does not alter the sensors performance, but it does tend to change some of the theoretical calculations because there are various factors involving the addition of a protective layer post fabrication. In this case a layer of 0.5μm of Parylene C is thick enough to protect against conductive fluid. Overall the addition of the protective layer shielded the sensor from conductive fluids and prevented the electrical currents to expand through the conductive fluid.

Outline

List of Tables

List of Figures

1.0 Introduction

Fluids are the essence of life, without understanding their characteristics and flow properties we would not be able to comprehend their behavior. As an engineer it is pertinent to understand how fluids affect our everyday lives, because it can enhance our learning by facilitating peoples lives with new tools or gadgets. With this new knowledge it is possible to create systems, which rely on the control of fluids by making them more efficient. A *system* in this paper talks about a *whole*, which is composed of smaller sections or channels that allows the fluid to flow freely. If the fluidity of the system is not behaving correctly then there are constraints found within the conduit, thus leading to inefficient flowness. From these problems it's understood that the fluid in question requires to be analyzed. Therefore a sensor is used to analyze and understand what is restraining the fluid in the channels and why this is happening. A way to assess this problem is by identifying and measuring the internal resistance of a fluid within the channels of a system.

The flow of fluids in a system can be used to determine its quality and viscosity, compared to other types of liquids. With these two important factors one can establish a result and compare it with other referential values that meet certain requirements for the liquid. This can become a standard to determine the lifestyle of a fluid. Just like humans have a choice of where to live depending on the quality of life standards a city has to give.

From the viewpoint of scientists the flow of liquids can determine how a stream or system is behaving. This behavior can be interpreted through the use of viscosity sensors. In complex systems where fluids are implemented, it is nearly impossible to understand whether the fluid is flowing adequately, without these types of viscosity sensors. The performance of this system is measured through the use of sensors. An example of complex systems using fluids can be seen in our bloodstream, where the blood composition is not like oil, which does conduct electricity. Blood is made out of different kinds of liquids, gases, plasma, etc. and sometimes, different kinds of chemicals are added to help purify the body or fight diseases. All of these small particles contain different kinds of electrical properties that make the overall fluid conductive.

For testing purposes the sensor is placed in different mediums where conductive liquids are present, this requires the sensor to be packaged in a distinct manner. This is one of many reasons as to why different integrated circuit chips have a certain number of packaging codes. Overall the packaging method implemented can help the device defend itself from conductive fluids. Else problems would arise and the device would not operate to normal conditions, causing inefficiency in the system.

This example can be related to the fluidity of a liquid in a system by measuring its internal resistance to flow. This observation helps determine the quality of resistance in a liquid, or obtain its viscosity measurement.

1.1.0 Quick Overview of Device (Problem Statement)

This project discusses about an enhancement to the innovative *thermally actuated micro electro mechanical system (MEMS) viscosity sensor* [1], which was researched under Ivan Puchades Ph.D. thesis. The device presented below in Figure 1, can be used to analyze oil by obtaining its flow properties, measured through thermal vibrations using a diaphragm made out of silicon.

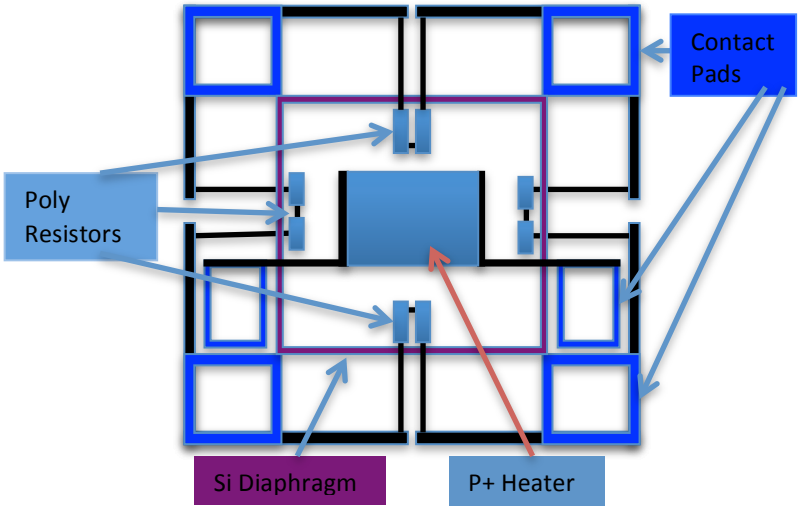

Figure 1.1 – Thermally Actuated Viscosity Sensor MEMS sensor Top View [1]

The device has been tested in different oil temperatures and compositions, for which viscosity measurements were taken. Taking the sensor to the next level leads to be able to measure viscosity in conductive liquids, because oil is a non-conductive medium it does not affect the sensors performance. But if a conductive fluid is present then everything changes, and the sensor stops working after a given period of time. Some of the problems encountered while testing the devices in conductive fluids are visible under a microscope by broken interconnects. The top layer of protection cracks due to pinholes that lead to the failure of the device. Thus the protective layer is very important when placing the sensor in conductive fluids.

Post processing fabrication of the protective layer has been chosen to be able to take advantage of all the existing viscosity sensors. At the same time this was chosen because if the fabrication steps were altered then the device would work at different specifications.

This is why many different MEMS-chips contain different packaging methods depending on the application that the sensor is going to be used upon. With this said, a new protective coating method will be

implemented and presented to the existing viscosity sensors. Afterwards they will be subject to test in order to find the corresponding viscosity measurements. All of these technological advancements have led MEMS to become a very sophisticated and useful technique to enhance various hi-technological devices, which are used throughout the entire world.

1.2.0 Micro-Electro Mechanical Systems (MEMS) & Biomedical-MEMS (Bio-MEMS)

MEMS devices are known throughout the world because they are part of large components, various MEMS devices together produce a system. It is a link between the mechanical and electrical systems that operate together in a smaller scale. They have a variety of applications that are used today, in "the automotive industry, in process control and automation,

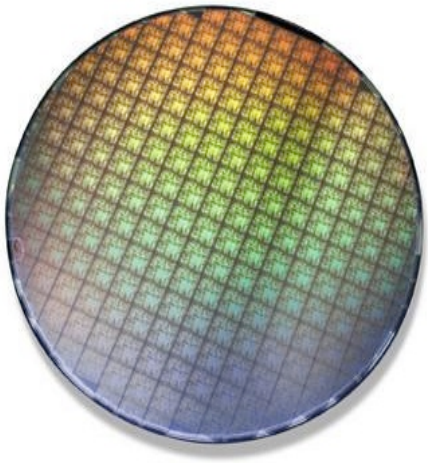

Figure 1.2 - NeoSense wafer with numerous MEMS devices [2]

scientific and medical instrumentation, telecommunication, commodity products, environmental monitoring, etc." [3] With these broad applications this technology is advantageous for it has various uses in industry and affects people's everyday life. The fascinations of using MEMS technology are its similar processes like the ones found in integrated circuit (IC) techniques [4]. Or the capability of mass production by using micro or nano scale devices on 4, 6, and 9-inch wafers (see Figure 1.2).

MEMS technology focuses on a wide variety of applications. But many researchers tend to emphasize on a specific one, in order to enhance such techniques and enhance the technologies even further. These involve bulk micromachining, surface micromachining, wafer bonding and MEMS packaging. [3] The latter is very specific to an application because it depends where and for what reason the sensor will be used as. The device is produced using low costs due to their small size and current integrated circuits (IC) techniques. Another important fact is that they

are composed of mechanical and electrical parts. Both parts together make a whole system, which is capable to move and give an electrical output, or vice-versa.

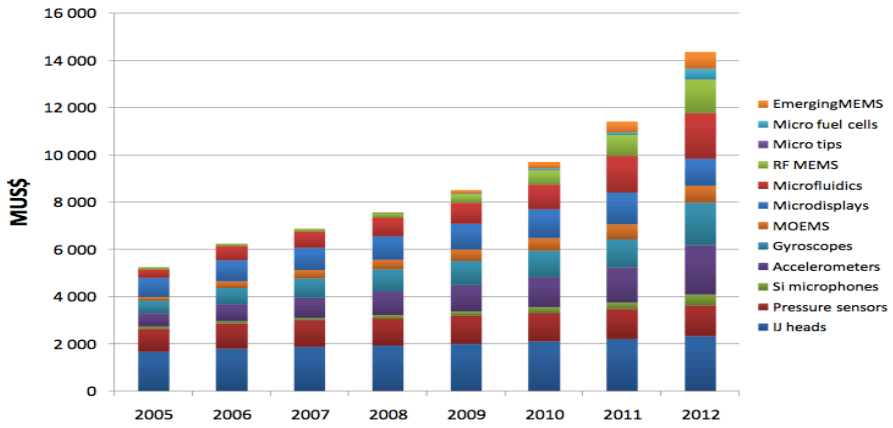

Figure 1.3 - Emerging MEMS market worldwide [5]

MEMS devices are very powerful and can be used to sense, feel, detect, or identify a specific problem, substituting our senses in case we are set to test something that is harmful to our well-being, or that we lack-of. With this said MEMS technology has increased in sales worldwide (see Figure 1.3) it is one of the best emerging technological markets in the world. At the same time companies can thrive to create jobs and enhance people's everyday life [5,6].

Figure 1.4 – MEMS Pressure Sensor for automotive industry (left) [7] Bosch MEMS Digital Pressure Sensor (right) [8]

In electrical engineering there are many different sub-branches to study from. But the one most people are focused nowadays is the way MEMS technology proliferates by enhancing our life's day after day. This can be seen in different recent devices, which some people call 'electronic gadgets': cellular phones, Nintendo Wii, Playstation 3, computers, monitors, Projectors (DLP), printers, mp3 players, etc.

In each device there is at least a MEMS sensor implemented some way or another. We do not actually know where it is but thanks to them the device works consistently. Other important implementations of MEMS

sensors are located in the automotive industry, were pressure sensors [9] are found in seatbelts, airbag sensors, tires, etc. Figures 1.4 represent packaged MEMS pressure sensors for the automotive industry and the sensors size, respectively. In the end, it is thanks to these devices that help the driver and passengers to be safe at all times.

With this said MEMS sensors are implemented in many different ways to help the manufacturing industry in producing smaller sized devices, mass produce them, make them reliable, robust, and included in the latest technological gadgets. Similarly the cost of production is decreased because of these technological advancements. Going back to the idea of substituting our senses we can find that a relation to biology is very definitive. Researchers like to determine how to enhance solutions to problems every time new technologies are discovered. Thus the strong connection between MEMS and Biology happens to create a new branch of study named Bio medical micro electromechanical systems (Bio-MEMS).

Bio-MEMS like the name states is a relationship between biology, the study of life and MEMS, previously defined. Different applications can be seen being implemented in research in the industry of Bio-MEMS. Where there are currently two virtual ways in which the device is presented on the living body. One way of implementation is in-vitro (inside a living organism) where a sensor or device is inserted in the body being analyzed and works without harming it. Then we have in-vivo (outside the living organism) in which the sensor belongs to a contraption or device that uses the living tissue or fluid sample, removed from the body preventing from any harm, and tested in an isolated location.

1.3.0 Viscosity Sensors

Currently this project uses the device showed in Figure 1.1, a *thermally actuated MEMS viscosity sensor* [1]. The sensor is actuated by a thermal pulse, which then captures data regarding the deflection in the silicone membrane. With the data recorded, a set of mathematical equations is applied, and a computer interface is used to translate the data obtained to readable viscosity measurements. This can be seen from the read out values portrayed in the electronic portion of the sensor. The main focus on this project is the current problem with the application. It is based upon the use of non-conductive fluids, various kinds of oils with different viscosities. In order to improve this device it would be feasible to be able to use it on conductive fluids, such as milk, water, blood, etc. With this advantage the device will be able to be placed in substances that conduct electricity making it more practical to a Bio-MEMS perspective.

This device was chosen because it is a unique design and it is able to compete with other current MEMS viscosity sensors. These measuring devices are used in different ways and for many different applications. There are

various types of viscometers, most of them are created by using simple and basic MEMS technology. They can be used to measure viscosity by using cantilever beams [10] [11] [12], resonating membranes [13] [14], or through quartz crystal resonators [15] [16] technology. The method implemented in the current sensor to measure viscosity is obtained by applying a pulse to obtain the resonating frequency within the testing liquid.

To obtain viscosity values using cantilever beams a deflection has to be applied to its beam. The beam will vibrate at its resonant frequency, becoming a useful value that relates to viscosity. As the beam exerts a deflection it is recorded using resistors, the most common way is to use a wheatstone bridge setup which measures the voltage difference. This is taken into account and the result is the characteristic properties of the fluid, which will correspond to measurements of viscosity. An application in which this type of viscometer is used involves a semi-permeable membrane that encloses a vibrational cantilever beam for glucose detection [10].

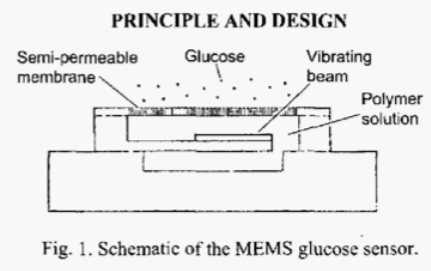

Figure 1.5 - MEMS Glucose Monitoring System [10]

In the picture above, Figure 1.5 a schematic of a MEMS glucose sensor is visible showing the cantilever beam enclosed with a semi-permeable membrane so that only the glucose solution is able to penetrate it. The polymer solution, which is located inside the chamber, contains Dextran and Con-A. Inside it cross-linking occurs between both solutions meaning that their physical properties change, forming a viscous mixture. As glucose enters the chamber through the membrane the molecules bind with Con-A since it is a glucose binding protein and this reaction weakens the Dextran – Con-A crosslinking relationship. As this occurs the mixture becomes less viscous and increases the dampening on the vibrating beam, helping determine glucose concentrations from the vibration values [10]. With the vibration characteristics it is possible to relate them to viscosity measurements. Zhao et al determined that their sensor works for frequencies under 2,000 Hz inside the solution.

Stark et al [11] researched a similar type of viscometer, which involved the use of an Atomic Force Microscope (AFM) cantilever beam. They can find resonant frequencies in the range of 1,000 Hz to 100,000 Hz

making them suitable for capturing viscosity measurements by applying the principle of vibrating plates. Some of their results are visible in different sugar solutions presented in Figure 1.6.

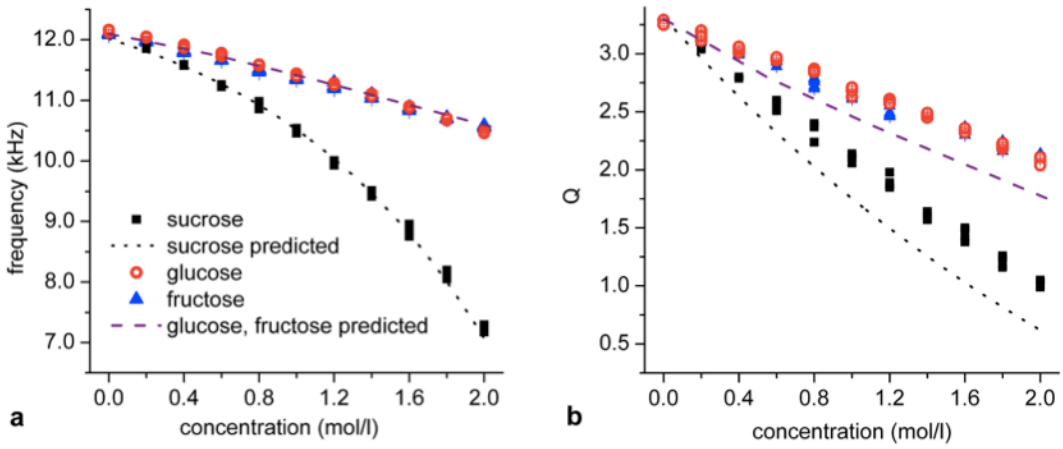

Figure 1.6 - Results from viscosity sensor of Frequency and Q Factor in different sugar solutions [11]

Vibrational type viscometers are another kind that is used in industry. In this case in order to obtain viscosity at least three different measurements are required. These are the amplitude, resonant frequency and the quality factor. By understanding how these three measurements behave a viscosity reading can be obtained.

Another way to determine viscosity is through a study that uses Lorentz force on cantilever beams or plates. [17] These devices require specific electromagnetic force actuation, which will then be read through the change in voltage by using piezoresistive resistors. Resonating micro tubes [18] are also another type of viscosity detectors, which in this case represents another type of measuring resonant frequency. In this case the tube will produce electrostatic resonance and the deflection will be measured through capacitive metal electrodes. So far various types of MEMS viscometers have been presented, with this we can understand that an improved, compact, better electrical response, cheaper and reliable device will be investigated.

2.0 Thermally Actuated Viscosity Sensor

2.1.0 Electrical Components

With the layout of the design shown in Figure 1.1, it is possible to separate the device in two processes. The first one involves a heater, and the second one a wheatstone bridge circuit.

2.1.1 Heater

The first device implemented in this sensor is the heater. Basically the heater is designed from a Polysilicon resistor. The resistance in Figure 6 is determined from the sheet resistance of the material. In this case, the material is Polysilicon, and its measurement depends on the size of the resistor, which is obtained from the length divided by the width, see Eq. 2.1.

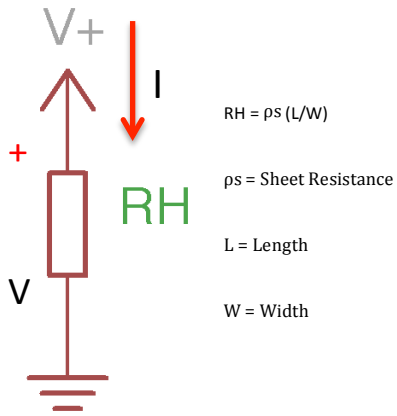

Figure 2.1 - Heater circuit schematic

$$R = \rho_s \left(\frac{\mathrm{L}}{W}\right) \tag{2.1}$$

Overall the heater works from the process of joule heating, which involves an applied current going through a resistor and releasing heat, or producing power (see Eq. 2.3). James Prescott Joule first introduced this in 1841 with an experiment involving a long wire with a specific volume of water and measured the temperature change with respect to the current that was flowing through the wire for a period of roughly 30 minutes [19]**.** Out of his experiment he was able to come up with an assumption that the heat produced, Q, is proportional to the square of the current, I, flowing times the electrical resistance, R, of the material of the wire [19]. This is known as Joule's First Law (see Eq. 2.2).

$$Q \propto I^2 * R \tag{2.2}$$

At the same time we know that due to an involvement between the voltage drop and the current traveling through, the resistor produces an amount of energy per time measured in (Joules/seconds). This output of power, also measured in Watts is able to convert the electrical energy to a thermal energy through the release of heat, which is found in the following Eq. 2.3.

$$P = VI = I^2R\ (Watts) \tag{2.3}$$

The heater will be used to activate the diaphragm and help it resonate at a given frequency in this case its natural frequency. This depends on the voltage applied to the heater.

2.1.2 The Wheatstone Bridge Circuit

We then have the second process, which involves the wheatstone bridge circuit. Sir Samuel Hunter Christie invented this design in 1833 and Sir Charles Wheatstone enhanced it and revolutionized it in 1843 [20], [21] he used the device to be able to analyze and compare the results from different soils. The main purpose of the wheatstone bridge is defined as a 'differential resistance measurer', used to distinguish the resistance for an unknown value on one of the branches. Below is an overview of a design of a wheatstone bridge circuit.

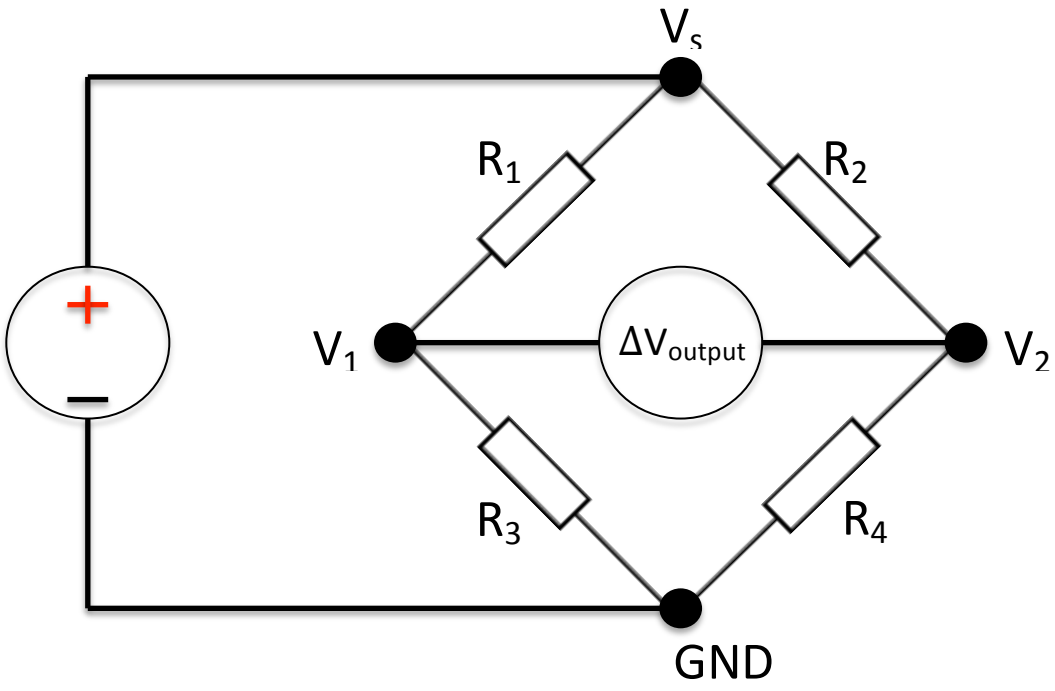

Figure 2.2 – Wheatstone bridge Design [20], [21]

Normally R_4 would be the unknown resistance value, but this depends on the users approach. In the case R_4 is the unknown value, assumptions are made, first we have to balance the entire circuit, it occurs when:

$$\Delta V = V_2 - V_1 = 0 \tag{2.4}$$

$$V_2 = V_1 \tag{2.5}$$

Then the circuit gets analyzed using Kirchhoff's Current Law (KCL), shown in Eq. 2.6 where the sum of all currents going in are equal to those leaving a node. By applying this law and assessing just like shown in Figure 2.3:

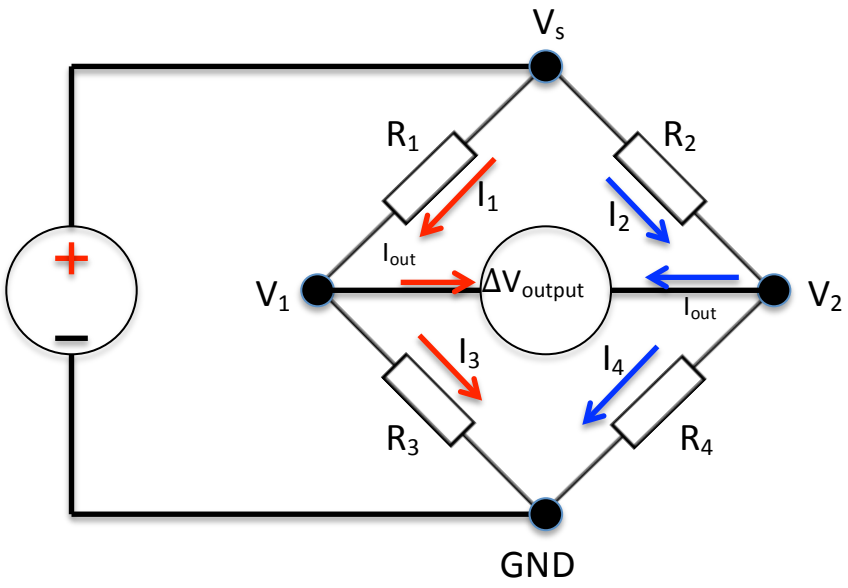

Figure 2.3 – Wheatstone bridge Design used for analysis

$$\sum_{k=1}^{n} I_k = 0 \tag{2.6}$$

where k represents the nth number of nodes, and n is the total number of currents going in or leaving the node in question. Above in Figure 2.3, by analyzing the nodes in V_1 and V_2 we find:

At Node V_1 we have: $I_1 - I_3 - I_{output} = 0$

Or $I_1 = I_3$ assuming $I_{output} = 0$ (2.7)

At Node V_2 we have: $I_2 - I_4 + I_{output} = 0$

Or $I_2 = I_4$ assuming $I_{output} = 0$ (2.8)

Now applying Kirchhoff's Voltage Law (KVL) shown in Eq. 2.9 it is possible to find a couple of voltages from every resistor and given currents. So applying this at nodes V_1 and V_2.

$$\sum_{k=1}^{n} V_k = 0 \tag{2.9}$$

Using Ohm's Law:

$$I = \frac{V}{R} \rightarrow V = IR \tag{2.10}$$

At Node V_1 we have: $(I_1R_1) - (I_3R_3) - \left(I_{output}R_{output}\right) = 0$ (2.11)

At Node V_2 we have: $(I_2R_2) - (I_4R_4) + \left(I_{output}R_{output}\right) = 0$ (2.12)

Now that the circuit is balanced, assuming the bridge gets balanced, thus $V_{output} \approx 0$, will give a $I_{output} \approx 0$ amperes. Both sets of new equations are placed equal to each other just like Eqs. 2.13 and 2.14 which satisfy the assumption from Eqs. 2.7 and 2.8:

$$(I_1R_1) - (I_3R_3) - (0) = 0$$

$$(I_1R_1) - (I_3R_3) = 0$$

$$(I_1R_1) = (I_3R_3) \tag{2.13}$$

$$(I_2R_2) - (I_4R_4) + (0) = 0$$

$$(I_2R_2) - (I_4R_4) = 0$$

$$(I_2R_2) = (I_4R_4) \tag{2.14}$$

Now look for the value of R_4 by setting Eqs. 2.13 and 2.14 equal to each other:

$$(I_1R_1)(I_4R_4) = (I_2R_2)(I_3R_3) \tag{2.15}$$

$$R_4 = \frac{(I_2R_2)(I_3R_3)}{(I_1R_1)(I_4)} \tag{2.16}$$

Using the KCL assumptions from Eqs. 2.7 and 2.8

$$I_1 = I_3 \text{ and } I_2 = I_4 \tag{2.17}$$

R_4 can be reduced to resistor values:

$$R_4 = \frac{(R_2)(R_3)}{(R_1)} \tag{2.18}$$

With the known values of R_1, R_2, and R_3 it is possible to calculate the value of R_4 when this type of electrical circuit is chosen.

On the other hand, if R_1, R_2, R_3, and R_4 are known, together with the applied voltage then the bridge can be used to obtain the voltage difference between nodes V_1 and V_2. Which is the main objective of the bridge for this

device. This can be obtained in the following form from Figure 2.2 and knowing the previous mathematical explanation:

$$V_{output} = V_2 - V_1 \tag{2.19}$$

$$At\ node\ \ V_2 = \left(\frac{R_4}{R_2 + R_4}\right) V_s \tag{2.20}$$

$$At\ node\ \ V_1 = \left(\frac{R_3}{R_1 + R_3}\right) V_s \tag{2.21}$$

Substituting the known values with their respective coefficients:

$$V_{output} = \left(\frac{R_4}{R_2 + R_4}\right) V_s - \left(\frac{R_3}{R_1 + R_3}\right) V_s \tag{2.22}$$

$$V_{output} = \left[\left(\frac{R_4}{R_2 + R_4}\right) - \left(\frac{R_3}{R_1 + R_3}\right)\right] V_s \tag{2.23}$$

Obtaining the relative voltage output at given nodes V_2 and V_1.

For purposes of this sensor, the style of circuit used is very similar to the one presented in Figure 2.2, which shows four resistors arranged as two parallel branches with two resistors in series in each branch. A voltage difference can be recorded through the use of two probes on nodes V_1 and V_2, the opposite sides from where the +5V (V_s) and ground (GND) connections are found. The main purpose for this circuit is to be able to measure the voltage difference found in the stress of the resistors as the diaphragm vibrates, this in other words is the measurement of the root mean squared (RMS) of the voltage difference.

The voltage is sensed by the resistors, which happen to be located where most of the stress occurs on a diaphragm.

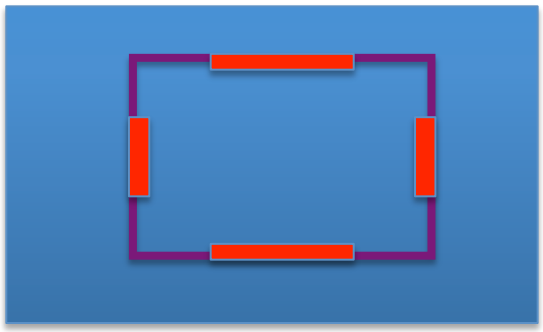

Figure 2.4 – Best Location for the Resistors on a Theoretical Membrane

The image above relates the dimensions used in the sensors. This simulates the stress locations on the diaphragm (purple) and is a suitable way to help place the resistors (red) on these exact locations where most of the stress is located, similar to various square pressure sensors.

After producing the pulse from an Agilent 33220A signal generator the voltage send from the power supply goes through the heater, activating the diaphragm and goes into a power MOSFET STP12PF06. The power MOSFET is used as a switch for the current to go through, an overview of how it is used is shown below.

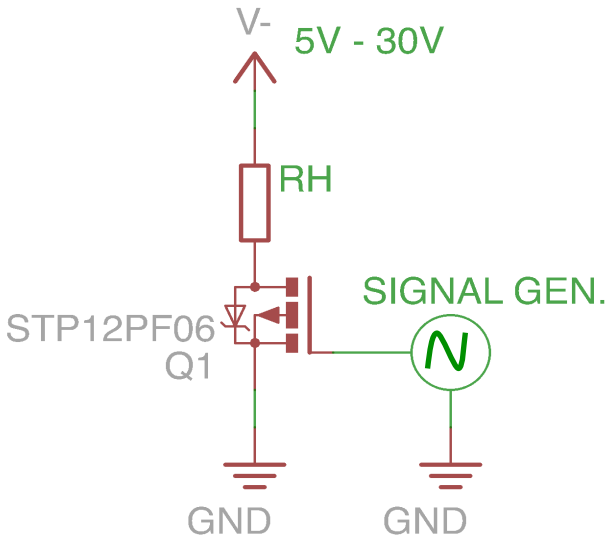

Figure 2.5 – Heater and Power MOSFET schematics

The power MOSFET is used as a switch because the power supply is feeding the heater with a voltage source of upper +5 volts. A constant signal with that amount of voltage going through the heater resistor will burn the resistor and stop it from sending pulses required for the diaphragm to resonate. Thus the switch portion behaves as follows, when the pulse is send from the signal generator it connects to the gate and the signal is normally 0V or at a OFF state most of the time. Even though the power supply is ON all the time, it is the signal generator who opens and closes the gate. The gate is activated or ON for a small portion of time from 5-50μs, depending on the sensors characteristics. With this amount of time it is possible to actuate the diaphragm and make it resonate close to its natural frequency. All of this is calculated in order to show that the device works effectively. The calculations can be seen in section 3.1.1, where the frequency is calculated according to the dimensions and material of the sensor. Then the period can be obtained from the calculated frequency, and that value is placed in the signal generator to make the diaphragm resonate.

After the power MOSFET comes the instrumentation amplifier INA101HP (see Figure 2.6), this IC is used as a signal amplification for the wheatstone bridge or strain gauge. It comes packaged in a dual in line (DIP) mode, and easy to apply to a printed circuit board (PCB). This amplifier was chosen because it contains three operational amplifiers, which are designed to obtain high-accuracy general purpose data and produce a low level signal amplification.

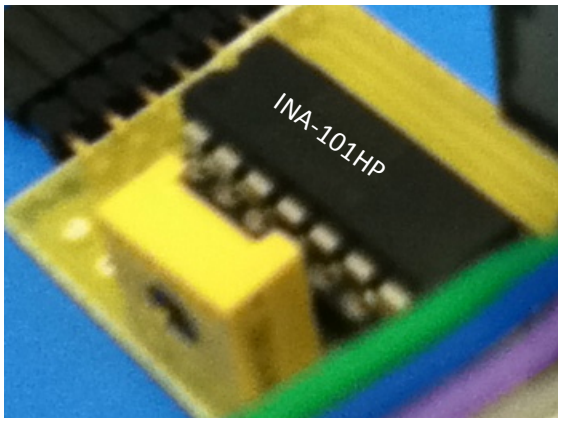

Figure 2.6 – Instrumentation Amplifier (INA-101HP)

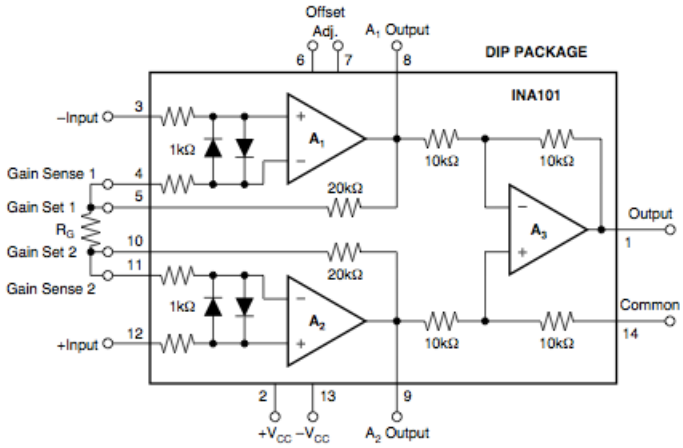

Figure 2.7 – Instrumentation Amplifier Circuitry (INA-101HP) [22]

Figure 2.7 above represents the circuit layout of the instrumentation amplifier. In the picture there is a section where a resistor, R_G is connected near the Gain Set 1 and 2 that is a potentiometer used to increase or decrease the gain from the sensors output. In order to power the IC it requires ±12V to go in to the device, applying that exact amount to pins 2 and 13 and common ground is connected through pin 14. The two input signals going into this IC are V_1 and V_2 each one goes to pins 3 and 12 correspondingly. These represent the voltages at the nodes between the resistors and due to the stress where the location of the resistors are situated it is possible to obtain a

voltage difference. Which also represents the deflection according to the voltage difference; this is calculated from a specific set of equations. Since the voltage output from the bridge is relatively small, it requires to get amplified in order to accurately obtain a specific deflection this is applied thanks to the use of operational amplifiers. The output measuring the deflection shown as a sinusoidal wave is obtained from pin 1 and it is send to the oscilloscope (Tektronix TDS 340) which portrays the signal, just as shown below in Figure 2.8.

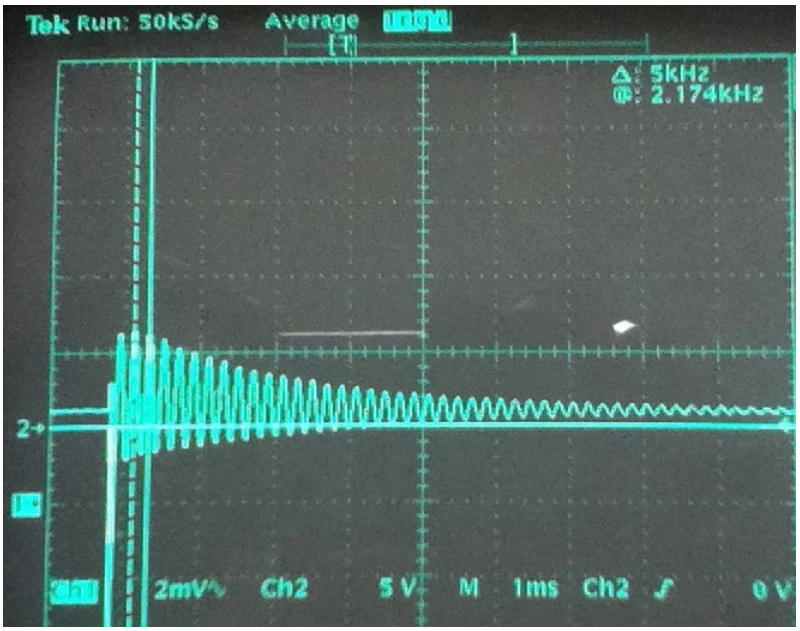

Figure 2.8 – Example of Output from a Sensor in Glycerol-Water Mixture

2.2.0 Physical Components

The thermally actuated viscosity sensor behaves like a powerful device because it can determine the *viscosity* of the liquid. The sensor is CMOS compatible and uses MEMS technology in order to achieve exceptional performances previously stated. The production price to build the device is relatively inexpensive and it can be produced in massive quantities. At the same time the device is reliable and the measurements are taken electronically in order to determine the viscosity of the fluid. This device uses the principles of vibration plates, which in turn is based upon the readings obtained and then this data is translated to values easy to understand. In order to produce a thermal signal on the sensor, a heat pulse is produced. Mathematically, what happens to the diaphragm (see figure 2.9) as it moves up and down in the Z axis can be seen in the following Eq. 2.24:

$$z = \frac{h}{2} \tag{2.24}$$

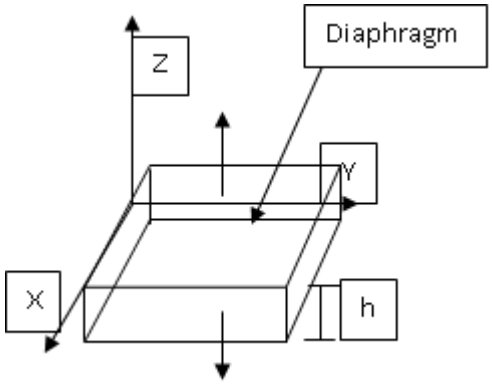

Figure 2.9 – Diaphragm on XYZ Coordinate to Define Direction of Deflection [23]

Where z represents the Z-axis found in the coordinate system of a diaphragm, and h is the thickness of the plate. With this equation we can see that after heat is applied, temperature is also applied as a side effect because the diaphragm will be in motion exerting molecules to move back and forth. Due to the side effect temperature will effectively change over time. Together with this a solution is presented in [23] where the vertical direction (z) is where most of the deflection of a square membrane occurs. Different equations were obtained in order to understand the behavior of the plate, therefore it was determined that the plate would have static and dynamic solutions that would depend on the step heat input applied. [23] In this case this direction is denoted as w and is represented in the following Eq. 2.25:

$$w(x,y,t) = w_{st} - w_{dyn} \tag{2.25}$$

Where W_{st} and W_{dyn} represent the static and dynamic terms respectively. By introducing the dynamic and static solutions as a time dependent equation we can obtain Eq. 2.26, which will be used to obtain the angular frequency of oscillation for the diaphragm, the study from [23] led to a relationship of:

$$\mathrm{w}_n = \frac{2\pi^2}{a^2}\sqrt{\frac{\left(\frac{Eh^3}{12(1-\nu^2)}\right)}{h\rho}} \tag{2.26}$$

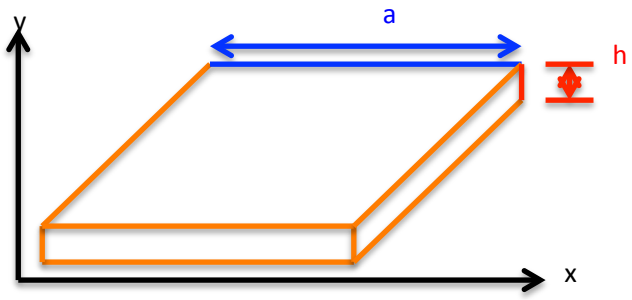

Figure 2.10 – Diaphragm on XY Coordinate

Where a is the length of the plate, h is the thickness of the plate, ρ is the density of the material, E is Young's Modulus, and v is Poisson's Ratio. Figure 2.10 gives an overview of some of the measurements required to calculate angular frequency.

With this equation it can be assumed that the sensor operates only if there is a fast enough heat pulse implemented. Without it the sensors response will be null and no output will be obtained. Luckily a heat pulse was chosen instead of step heating because this would not affect the fluids temperature. Thus it is vey important for the fluid to not change temperature while testing, because viscosity is dependent upon the temperature. With this reaction the device would act correctly and the electronics attached would obtain the data. An important point to know from this sensor is that the thermal properties do not affect the frequency of oscillations [1]; keeping the device in a more controlled environment.

Dr. Puchades also found that time is dependent upon the heat pulse produced. This can be seen on the following graph Figure 2.11 which states how temperature is affected by the pulse time.

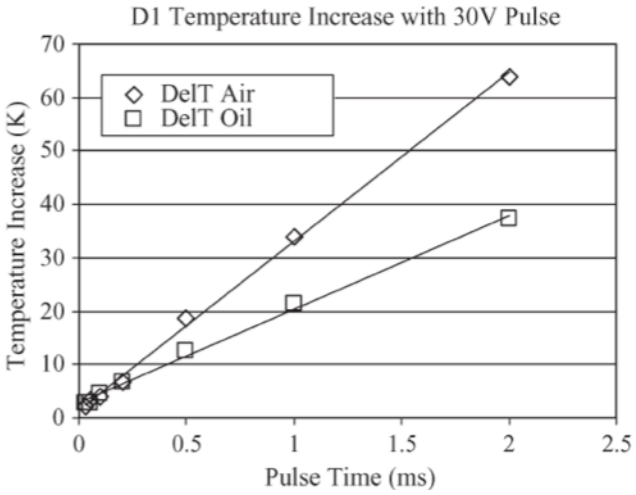

Figure 2.11 - Temperature Increase of a Membrane in Air and Oil for Pulsed Heating [1]

The data found in Figure 2.11 shows how a pulse time less than 0.2ms as temperature increases does not affect the diaphragm tested in oil with respect to water. So the time required to implement a heat pulse is less than 100μs for the sensor to operate without affecting the change in temperature. [1] After figuring out the pulse determination, the Q factor and the energy dissipation, ξ equations are obtained to determine these values [24,25] . The Q factor determines the quality of the oscillating wave and this characterizes the oscillating curves features. Visually this is done by enumerating the number of oscillations in a given time period. This is determined by the following equation [24,25,26] :

$$Q = 2\pi \frac{energy_{stored}}{energy_{dissipated_{per_{cycle}}}} \approx \frac{0.95}{\xi} \tag{2.27}$$

$$\xi = \sqrt{\frac{v}{wa^2}} \tag{2.28}$$

Where v, represents the kinematic viscosity, w is the radial frequency of vibration, and a is the radius of the membrane. With these factors the density and the viscosity of the liquid can be calculated [1]. Overall the natural frequency of vibration for a simple square thin plate in air can be determined from the following equation [27]:

$$f_{air} = \frac{19.74}{2\pi a^2}\left[\frac{Eh^3}{12\rho h(1-v^2)}\right]^{1/2} \tag{2.29}$$

Where a is the length of the plate, E is Young's Modulus, ρ is the density, h is the thickness of the plate, and v is Poisson's ratio.

As a matter of fact the overall design of the interaction between the fluid and the plates involves the density and viscosity of the fluid. It starts as an analysis by Horace Lamb in 1920, when his experiment proved that a circular plate oscillating in water produces vibrating modes that are very similar. But there is a slight variation in the frequency response from the vibrating waves, he denotes this feature as β calling it an added virtual mass [26]:

$$f_{fluid} = \frac{fair}{\sqrt{1+\beta}} \tag{2.30}$$

Lamb found that there is a relationship between the frequency of the fluid, f_{fluid}, and the frequency in air, f_{air}. They both depend upon the density of the fluid, ρ_{fluid} , the density of the material used for the plate, ρ_{plate}, the radius a, and thickness h of the plate. The outcome is that he took into account the slight variation and applied it as an equation [26].

$$\beta = 0.669\frac{\rho_{fluid}a}{\rho_{plate}h} \tag{2.31}$$

Overall in the case of MEMS devices the thickness is a factor since the size is relatively small. This was seen in another experiment by Ayela and Nicu, were they concluded that Lamb's model matches their experiment, proving that there are different natural frequencies and Q factor values present as the viscosity increases [28]. After further research on the subject itself, another researcher, Kozlovsky [25] helped enhance the topic itself by taking Lamb's idea, and take into account the viscosity of the liquid under test. By doing this he was able to modify Lamb's Eq. 2.31 to Eq. 2.32 [25] involving the virtual mass factor, β. Where ξ represents the energy dissipation of

the system that depends on the kinematic viscosity, ν, which stands for the ratio between the dynamic viscosity, η, and the density, ρ, just like previously explained Eq. 2.28.

$$\beta = 0.6538 \frac{\rho_{fluid} a}{\rho_{plate} h}(1 + 1.082\xi) \tag{2.32}$$

The electrical components that operate in this device are used to relate the data gathered to analyze and compare the expected results. The results are used to determine the Q factor. They require some signal amplification in order to analyze and understand what the collected data means. In this case the output signal is an oscillating curve that is represented from the deflection of the membrane, and the values correspond to the change in voltage of the Wheatstone bridge.

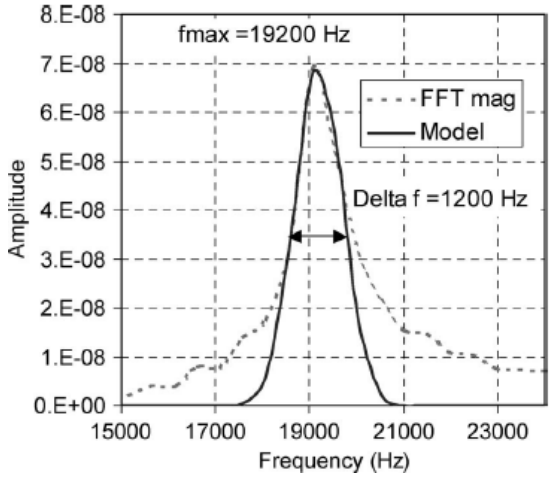

Figure 2.12 - FFT for Device 1P, Used to Determine Q [1]

A Fast Fourier Transform (FFT) is used with LabView because the graph shown with the data obtained from the signal needs to be revised and analyzed to produce a Q factor and frequency values. For the frequency the peak value is recorded from Figure 2.12, and Q is calculated using Eq. 2.33 were the values are also dependent on the signal output.

$$Q = \frac{F_o}{\Delta d_f} \tag{2.33}$$

This method is more reliable and faster in analyzing data. The sensor obtains data very accurately for non-conductive fluids. And the results obtained can be seen on Figure 2.13, as viscosity increases we can see that the amplitude of frequency decreases, the same goes for the Q factor this is because the fluid tested is thick and makes it harder for the membrane to vibrate.

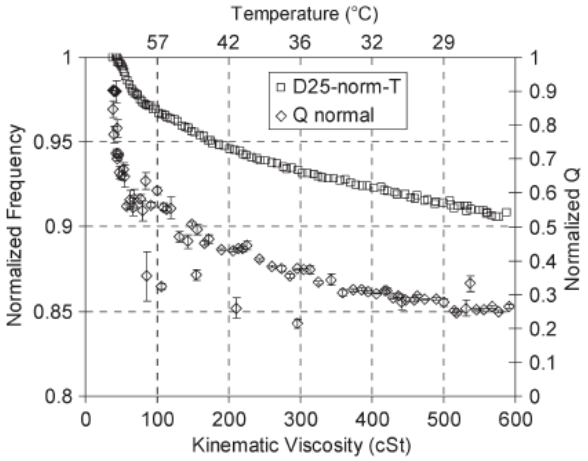

Figure 2.13 - Normalized Frequency and Q Factor Versus Kinematic Viscosity and Temperature [1]

Overall the sensor works, and is able to measure the Q factor and the natural frequency of vibration. Both values increase as temperature increases, but viscosity and density of the oil decrease. Thus the natural frequency of vibration and the Q factor decreases as the viscosity value increases. [1] These two measurements help determine the viscosity of the liquid by comparing to other known viscosity fluids.

3.0 Testing of Existing Viscosity Sensor with packaging method Version 1

Currently there are two signals used to make the sensor operate, one activates the diaphragm and the second one is the actual output the sensor produces. There are two main designs in this device; they are both previously explained in Section 2.0 Thermally Actuated Viscosity Sensor. Consequently the device is ready for testing and these are the primary results from the experiment.

3.1.0 Screening Experiment

Initially four wafers were obtained from previous testing, and devices with passivation were searched and removed from the diced wafers. This process was named the screening experiment because it had the purpose to identify all working devices. This was done very meticulously, all the new devices got named and tested to make sure they worked to specifications. All resistors were operational and the gathered devices had a properly balanced wheatstone bridge. Each die was tested under a 5V power supply to measure the voltage difference from the resistors in the wheatstone bridge. A ohmmeter was used to make sure the

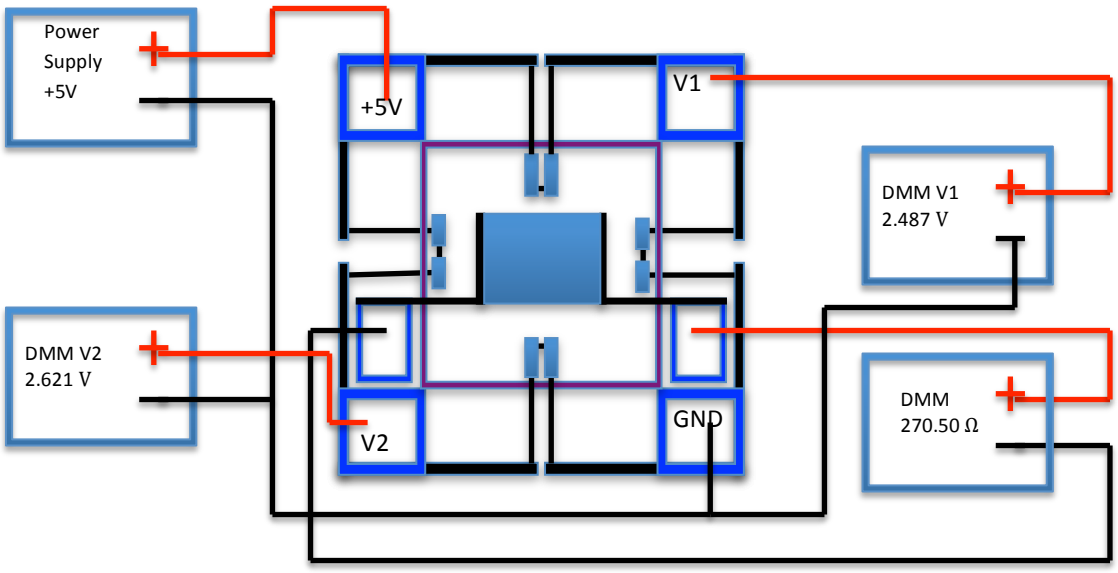

Figure 3.1 - An Overview of How the Devices were Tested

heater had a resistance value and their were no open circuits within the sensor. See Figures 3.1 and 3.2 for the visual schematics and electrical circuits of how the devices were being tested for future reference.

For these tests the Agilent 33401A was used as the digital multi-meter (DMM), and at the same time the device was placed in the testing probe to hold the device and provide a vacuum on the back to keep the device from moving from side to side as test probes were lowered. Testing probes were placed on top of the device were the

contact pads were located, at first this was hard to appreciate, but after testing a lot of devices lowering the probes to the contact pads became a habit. The DMM was connected in parallel in order to measure the resistance of the heater. On the second type of test a power supply was used providing +5 volts to the bridge in order to obtain the different voltage readings from the device, and be able to calculate the change in voltage between V_1 and V_2. At V_1 and V_2 two different DMM's were used to measure the voltage reading by connecting the negative side to ground and the positive to the corresponding pad just like shown above in Figure 3.1.

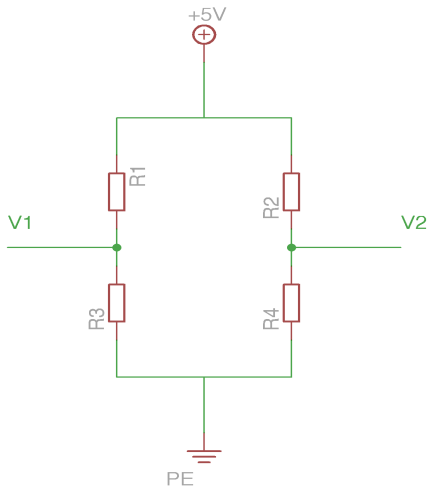

Figure 3.2 – Electrical Schematic of the Wheatstone Bridge

These measurements were compiled in a table together with the material of the resistors and the size (see Appendix for table 1A) and used later for reference. An example of the measurements taken for one device is shown in the following Table 3.1.

Table 3.1 - Example of measurements obtained from a single die from Wafer 3

Device #	**a-Size (mm)**	***Details***				
		Resistor Type (P+ / Poly)	**Resistor Size (35%, 16%, 2%)**	**Metal?**	**R_{heater} (Ω)**	**V_{Bridge} (mV)**
1	1.75	P	2%	Yes	60	78.7

Each die was placed in a new empty box container in order to choose from for later use and organize them according to the wafer each of them came from. This was very important because there were initially four wafers to choose die from. Wafers 3 and 4 contained die with a diaphragm thickness of 15µm. Wafer 5 contained devices with a thickness of 10µm and all of Wafer 6 had a thickness of 6µm. The first column defines the number given to the device, which was placed inside the box with the rest of the devices and would help differentiate them from each other.

Every numbered device had a second set of characteristics, which defined the length of the membrane or a-size ranging from 1 mm, 1.75mm to 2.5mm. At the same time each die had a specific heater resistor type and size. The material that the resistor was made out of for the heater varied between P+ Diffused or Poly. Another important factor that changed from each die was the size of the heater covering the area around the diaphragm ranging from 2%, 16% to 35%. Puchades previously analyzed the differences between each of the type of heaters in [1] concluded that the heaters with P+ diffused heaters and their respective resistor size, whether 2%, 16% or 35% bended the membrane downwards by 10 μm. If Polysilicon were used instead then the membrane would move that same amount in the opposite direction, regardless of the size between 16% and 35%. Where as for a Polysilicon heater with a resistor size of 2% would bend the diaphragm down just like a P+ diffused heater.

The other important column was the one containing Metal, even though some die had metal and others didn't the overall conclusion for the presence of metal was noticed in [1]. The different observed results shows that there is a variation in the quality factor, sensors with metal on top have a higher value. On the other hand the ones that did not have metal contained a lower value. The two last values on the table refer to the values obtained from testing both setups previously explained in this section.

All of these values were recorded in a excel spreadsheet and tabulated for later use, see Table 3.2 below for a section of the file.

Table 3.2 - Devices 1 Through 10 with Characteristics from Wafer 3

Details						
Device #	**a-Size (mm)**	**Resistor**		**Metal**	**R_{heater} (Ω)**	**V_{Bridge} (mV)**
		Type (P+ / Poly)	**Size % (2, 16, 35)**			
1	1.75	P	2%	Yes	60	78.7
2	1	P	35%	No	217	12.8
3	1	Poly	2%	Yes	46.7	35.7
4	1	Poly/P+	2%	Yes	52	11.5
5	1	Poly	16%	Yes	70	95.7
6	1	Poly	1%	No	100	-16.7
7	1	P	2%	Yes	309	30.5
8	1	P/P+	2%	No	267	1.105
9	1	Poly	2%	No	90	-50.7
10	1	P	35%	Yes	239	161

Later in the experimentation section these values would help determine reasons for failure in the underwater tests with the existing packaging. Each of these thicknesses is used in Eqs. 2.26, 2.29, and with them it is possible to calculate a different resonant frequency. Overall the device will output signals that vary depending on the material dimensions. Table 3.4 gives an overview of the calculated frequencies for the sensors in air, depending on their dimensions.

3.1.1 Calculating the frequency in Air

Just like previously stated the frequencies in air were calculated from equation 2.26 or 2.29 depending on the units, either radians per second or cycles per second correspondingly. The equation is very simple once all the variables are obtained, assuming we have a die from wafer 3 with the following parameters shown in Table 3.3:

Table 3.3 - Measurements to Calculate the Frequency in Air of a Device from Wafer 3

h, thickness of membrane	***a***, length of membrane	***E***, Si Young's Modulus	***v***, Poisson's Ratio	***ρ***, Density of Si
$15x10^{-6}\ m$	$1.75x10^{-3}\ m$	$1.9x10^{11}\ \frac{N}{m^2}$	0.3	$2330\ \frac{Kg}{m^3}$

$$f_{air} = \frac{19.74}{2\pi * 1.75^2}\left[\frac{E * 0.000015^3}{12 * 2330 * 0.000015 * (1 - 0.3^2)}\right]^{1/2} \tag{3.1}$$

$$f_{air} = 42{,}050\ Hz \tag{3.2}$$

With this said, this assumes that the measurements are all perfect and nothing went wrong during fabrication or packaging processes. Thus a sensor with these characteristics will output a response of 42,050 Hz in air. Similarly this can be done to the rest of the devices that have different characteristic properties and Table 3.4 shows the output response expected from them. Consequently a column gets added to the data in Table 3.1 for the calculated value of the frequency in air of each device and look just like Table 3.5.

Table 3.4 - Calculated Frequencies in Air at a Given Thickness and Length Size, *a*

	Calculated F_{Air} (Hz)	***a*** (mm)		
		1	**1.75**	**2.5**
h (μm)	**15**	128,779	42,050	20,605
	10	85,853	28,034	13,736
	6	51,512	16,820	8,242

Table 3.5 - New Column Added to Table 1 with Calculated Frequency in Air Value

Device #	*Details*						
	a-Size (mm)	Heater		Metal	R_{heater} (Ω)	V_{Bridge} (mV)	Calculated F_{Air} (Hz)
		Resistor Type (P+ / Poly)	Resistor Size (35%, 16%, 2%)				
1	1.75	P	2%	Yes	60	78.7	42,050

With the value of the calculated frequency a time period can be deduced, and this information will be used to determine the heat pulse applied to the sensor. Sending this pulse to the device causes the membrane to vibrate at its resonant frequency producing an oscillating wave. The oscilloscope will be able to view this output, which in turn is recorded by the computer interface, in this case LabView. As the device changes medium from air to a fluid a variation will be witnessed. A frequency change is expected as the medium changes and the Q factor varies with the frequency accordingly. This can be seen in Eq. 2.29, which contains information regarding air, and Eq. 2.30 has a different calculation for the frequency in a fluid.

3.1.2 Calculating the frequency in a Fluid

To be able to determine the frequency of the device on a given fluid a different equation was applied. In this case Eq. 2.30 previously described in Section 2.2.0 is used to be able to determine the frequency, this equation is completely different because it involves the previous Eq. 2.29 to determine the frequency in air with another term, which is previously explained in Section 2.2.0 as β. Consequently the new term involves the density of the fluid, the length of the membrane, the density of the material of the diaphragm, and the thickness of the membrane. With all of these values it is possible to find the frequency of the fluid assuming all measurements are accurate enough to be used for the simulations.

From previous calculation for the frequency in air of a sensor we are able to solve the first part of the equation. As for the second portion we input the next set of parameters:

Table 3.6 - Parameters to Calculate the Frequency of the Sensor in a Fluid

h , thickness of diaphragm	***a*** , length of membrane	***E*** , Si Young's Modulus	***ν*** , Poisson's Ratio	***ρ*** *of plate* , Density of Si	***ρ*** *of fluid*, Density of DI water
$15x10^{-6}m$	$1.75x10^{-3}m$	$1.9x10^{11}\ \frac{N}{m^2}$	0.3	$2330\ \frac{Kg}{m^3}$	$1000\ \frac{Kg}{m^3}$

With these new parameters it is possible to calculate the frequency of the sensor in a given fluid, in this case we are using distilled water as the fluid. The calculations goes as follows for a device with an ***a*** = 1.75 mm, and an ***h*** = 15 μm:

$$fair = 42{,}050\ Hz$$

$$\beta = 0.669\frac{(1000 * 1.75x10^{-3})}{(2330 * 15x10^{-6})} = 33.497854$$

$$f_{DI\ Water} = \frac{42{,}050}{\sqrt{1 + 33.497854}}$$

$$f_{DI\ Water} = 7{,}159.3\ Hz$$

A sensor with these measurements will theoretically produce a resonant frequency of 7,159 Hz inside a vial of de-ionized water.

3.1.3 Determining the L2T and Pulse Time for good output

A way to determine the best die for this project is to choose the correct diaphragm thickness and side length for the sensor. This will allow calculating a ratio between both values. This ratio will then be used to determine the best die that will provide the correct dimensions and avoid any side effects from the materials used. In a study by Brand e.t. al, it was proven that sensors with a ratio higher or lower than 166 would produce non-linearity effects, and tend to limit the output produced by the sensors. This ratio is used to avoid any non-linearity effects found from material stiffening, membrane buckling from compressive stress [29]. The sensors tested would not be working to their full capability and this value was used to compare the different expected results from different thicknesses and side lengths. The approximate value used to achieve the perfect ratio is ≈166 [29,14], which means that the critical thickness to length ratio calculated should be close to 166.

If the hand calculations agree with the pre-determined value of 166, then it is possible that there will be fewer side effects present as the membrane vibrates for the provided dimensions. These values can also be found on a modified Table 3.1, shown in the last column length to critical thickness ratio (L2T) as seen below.

Table 3.7 – Length to Critical Thickness Ratio Column

Device #	*Details*							
	a-Size (mm)	Heater		Metal	R_{heater} (Ω)	V_{Bridge} (mV)	Fair (Hz)	L2T Ratio
		Resistor Type (P+ / Poly)	Resistor Size (35%, 16%, 2%)					
1	1.75	P	2%	Yes	60	78.7	42,050	116.7

As for the length to critical thickness ratio, there are die with similar and dissimilar dimensions meaning there will be different values that are higher and lower than 166, while others would contain similar ratios. This operation is done by applying Eq. 3.3 from [29], where ***a*** is the length size of the membrane, and ***h*** is the thickness of the membrane, these measurements can be seen in Figure 2.9.

$$Length\ to\ Thickness\ Ratio = \frac{a\ (mm)}{h\ (\mu m)} \tag{3.3}$$

With Eq. 3.3, the best die can be chosen from the screening experiment and this helps by determining the best device in our samples. This is also very important because it can avoid non-linearity or buckling effects [14]. From this explanation each device from their corresponding wafer was evaluated and the best ones were chosen for testing. Wafers 3 and 4 contain the same membrane thickness, ***h*** of 15µm. Even though each wafer had many devices with different lengths, an ***a*** of 2.5mm was chosen because the calculated ratio was 166.7 which matches the desired thickness to length ratio. Just like previously stated, a value ≈166 is the best value for non-linearity effects. The same approach was taken to determine the best die in wafers 5 and 6. For wafer 5 it was established that the best length size was 1.75mm for a thickness of 10µm, since the ratio obtained from these measurements was of 175. Even though it was off by a value of 9 units from the target value, this was close enough to the desired value, compared to the rest of the calculations. For wafer 6, the best die was determined to be those with a thickness of 6µm and a length size of 1mm, giving a value of 166.7. But this would also mean that it is the smallest length size available and diaphragm thickness, thus it should be harder to see the oscillations produced by the sensor. Table 3.7 explains the different calculations for each of the sensors according to their ***h*** and ***a*** values.

Table 3.8 - Information on L2T Ratios for all the Different Devices

Wafer	***h*** (µm)	***a*** (mm)	**L2T**
3, 4	15	1	66.7
		1.75	116.7
		2.5	166.7
5	10	1	100.0
		1.75	175.0
		2.5	250.0
6	6	1	166.7
		1.75	291.7
		2.5	416.7

	Too Far from desired L2T
	Near desired L2T
	Close or perfect match for L2T

Desired Length to Thickness Ratio for less non-linearity effects
h = 15µm → ***a*** = 2.5mm (Wafers 3, 4) ***L2T*** = 166.7
h = 10µm → ***a*** = 1.75mm (Wafer 5) ***L2T*** = 175
h = 6µm → ***a*** = 1.0 mm (Wafer 6) ***L2T*** = 166.7

After the screening process, each device was tested in air. This was done to show that the device would work close to an expected calculated value and produce the output signal. The calculated frequency obtained from Eq. 2.29 would help find its resonant frequency by applying the value to the following Eq. 3.4 to find the time period.

$$f = \frac{1}{t} \tag{3.4}$$

$$f_{calculated} = \frac{1}{t_{calculated}} \tag{3.5}$$

where $f_{calculated}$ is the frequency calculated in air, and $t_{calculated}$ is the calculated time period

$$t_{calculated} = \frac{1}{f_{calculated}} \tag{3.6}$$

Once the time period is found, this value would be applied to the heater. This would help determine the pulse required for the membrane to resonate at its natural mode of vibration. Sometimes the calculations did not provide an adequate time, and caused delays in obtaining the results by requiring a trial and error approach. One of the main reasons for this to occur was due to the fabrication steps. Depending on the pre-determined times of RCA cleans and wet etch baths, the step could be done under the given amount of time, right at the spot, or a little over. There is always some space for error, and while fabricating these devices, these changes are taken into account because it can always damage the end product. Table 3.8 shows the time required for the heat pulse to be ON in order for the sensor to vibrate at its resonant frequency.

Table 3.9 - Time Required for Heat Pulse to Activate Sensor

Device #	***Details***								
	a-Size (mm)	**Heater Resistor**		**Metal**	**R_{heater} (Ω)**	**V_{Bridge} (mV)**	**Fair (Hz)**	**L2T Ratio**	**Time (µs)**
		Type (P+ / Poly)	**Size (35%, 16%, 2%)**						
1	1.75	P	2%	Yes	60	78.7	42,050	116.7	23.8

As for the trial and error approach it is very simple, but takes quite a long time. This is because one has to start seeking for a signal, especially when you have at least three different ways to obtain a signal. It starts by generating the pulse, changing the amount of voltage to the heater, and increasing or decreasing the gain. The pulse requires two important values the frequency of the pulse and the pulse width. The frequency is pre-determined by the user, in this case a negative pulse at 5 Hz or at every 0.2 seconds, using Eq. 3.6.

Next is the pulse width, which is determined from the frequency in air calculation or Eq. 2.29. This value is used to determine the time period required to input the pulse from Eq. 3.6. In this case the pulse is applied using an Agilent 33220A Signal Generator. With this device it is possible to input a pulse at a frequency of 5 Hz, this also means that the signal send is always OFF and it will be ON only for a short period of time, with a range from 0V - -5V. Figure 3.3 explains the signal generators output.

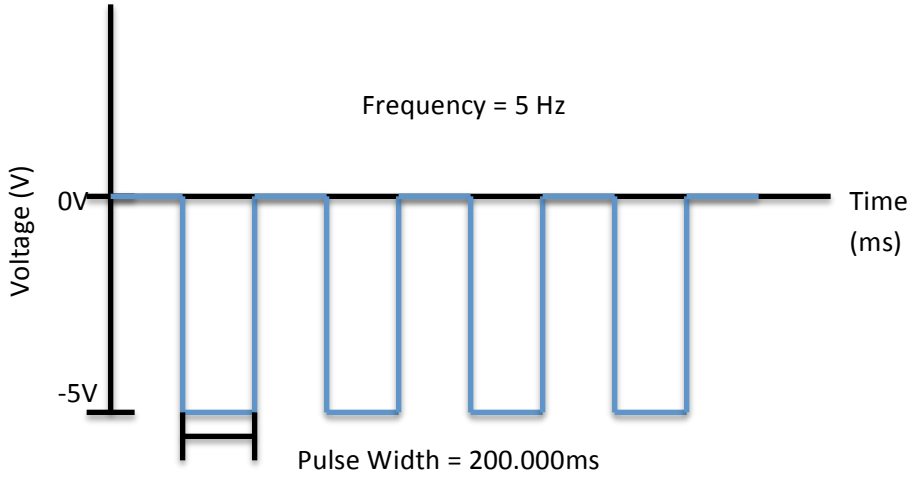

Figure 3.3 - Graph Showing Pulse from Signal Generator

After the frequency and the voltage range has been input into the device, now the pulse width can be manipulated from the frequency in air calculation. With the value calculated it is now possible to input the amount of time into the signal generator. Table 3.10 shows the information of the calculated time from the frequency in air calculations, Table 3.4, using equation 3.6.

Table 3.10 - Time Required for Sensor to Activate Membrane According to their Characteristics

	Pulse Width Calc. time (µs)	***a* (mm)**		
		1	**1.75**	**2.5**
***h* (µm)**	**15**	8	24	49
	10	12	36	73
	6	19	59	121

Now that the time has being calculated it is possible to subtract from the time period previously given to the device, meaning that the calculated value needs to be subtracted from the original time. As an example calculation for a $\boldsymbol{h}$ = 15µm and $\boldsymbol{a}$ = 1.75mm the calculated time comes to be around 24µs using Eqs. 3.7 – 3.9. This new calculated time is the input value for the signal generator in order to send the correct pulse to activate the membrane.

$$Pulse\ Width = \ Original\ Pulse\ Width\ Time - Calculated\ Pulse\ Width\ Time \qquad (3.7)$$

$$Pulse\ Width = 200.000ms - 0.024ms \quad (3.8)$$

$$Pulse\ Width = 199.976ms \quad (3.9)$$

3.1.4 Determining Heater voltage and gain

First a value for the time period was obtained from the previous calculations, and then a voltage is applied to the heater starting at +5 volts to see if there is a signal. If nothing were observed through the oscilloscope then it would seem it would require more voltage applied to the heater. On the other hand if the oscillations were still weak and no output was observed, the time period would have to change. This in turn would have to balance out with the amount of power being input to the device. So every time the pulse width changes the voltage is set to change from +5V up to +30V in search for this signal. Similarly the gain was increased in case a result was obtained and required for the signal to be stronger, meaning the amplitude was too small it needed some "amplification", increase the signal strength seen on the oscilloscope.

Most of the time the devices would work with values further away from their calculated measurements due to many reasons. Some of them were due to the sensitivity of the resistors, and the material they were made out of. Other times it meant it was due to packaging process of the device. In order for the sensor to provide accurate readings for the membrane deflections, the best sensitive material has to be picked adequately. Sometimes during the packaging process, epoxy or nail polish would stand in the way of the membrane, adding mass to the overall picture. This would cause the device to either not work at all or partially produce the output signals expected. Another reason for these sorts of problems were also found in the manufacturing process of the devices, since they followed the MEMS Bulk process at RIT. While following the flow chart, either the processing times were under or over by a fraction or fractions of seconds, which are vital to be able to create the correct end products.

Before testing the devices in air, the packaging method is implemented to test the sensor using the pin connections between the oscilloscope, the signal generator, and both power supplies. There are many ways to implement packaging methods to a die added to a printed circuit board (PCB). But the one used in this project is the die level packaging, a term taken from [30]. Wang acknowledges this method, which is a similar process to those found in the IC industry by combining IC and MEMS together in one.

3.2.0 Steps for packaging die to PCB

Various trials were attempted before obtaining a working procedure for the packaging of a device on to a PCB. First is the cleaning of the PCB itself, using a wool made out of iron, this will clean the board and the copper lines from any impurities. At the same it removes the "oxidized" or aged copper from the mixture of air particles.

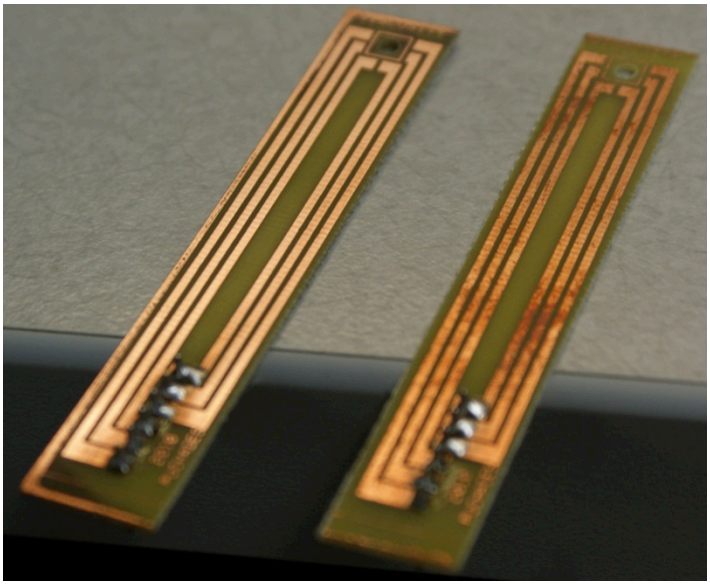

Figure 3.4 – Before (right) and After (left) Cleaning Impurities from PCBs

Then holes are drilled for the copper line connections to the die itself, and a top hole where the die will be placed on top. Solder the 6 pins that go underneath the PCB. Afterwards use a wipe with isopropyl alcohol (IPA), which is used to smoothen everything and remove some impurities if not all, the die is also cleaned with IPA. Epoxy is used to hold the back of the die to the PCB by applying with a paper clip, this is a very delicate step, because any slight miss to the perimeter and the membrane gets glue too. Since the sensor depends on membrane movement, there has to be no epoxy on the back or on top of the die where the diaphragm is located. The die is then placed on top of the PCB and sits for 15 - 25 minutes to make sure that the epoxy has attached the die to the PCB, or place it in the oven for 5 minutes at a temperature of close to 100°C.

After this step wire bonding is applied, this is an extremely small wire (<1 μm) connecting the die to the PCB, creating a bridge between both pads. For this process the wire bonder located in the Characterization Laboratory at RIT was used. This tool requires a lot of patience and determination, because placing the wire at the right location with the exact amount of power to bond it perfectly to the pads is not an easy task. Afterwards epoxy is used to cover the wire bonds to prevent them from breaking loose and disrupting the connections. Especially when the final test requires placing the sensor in a conductive fluid. The wire will be sending electrical currents and the conductive fluid is not a suitable medium for them. More epoxy is applied to prevent the die from moving around, this is done by adding epoxy to the surrounding perimeter of the die and moving in towards it, where the contacts

are located. This is a very important step, because covering the contact pads is critical since that is where most of the electrical currents are going to be exerting their power. The only visible traces are the ones near the membrane.

Figure 3.5 – PCB packaged and ready for testing

Finally the PCB's copper connections get covered with epoxy or nail polish to isolate them from spreading electrical currents to the fluids and short out the sensor. Subsequently the device is ready for testing. Below are images (see Figures 3.6, 3.7, 3.8) of the PCB board layouts and the sensor in its location. The biggest remark on this protective layer is that the device itself is left with an opening on top of the membrane. This occurs because epoxy and nail polish are too heavy, adding quite a lot of mass to the membrane. The layer they provide is thick or thin depending on the amount applied. This in turn will invalidate the membrane from creating any deflections, as neither of them are flexible materials.

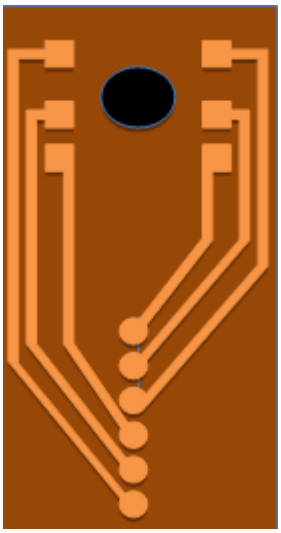

Figure 3.6 - PCB Layout with Drilled Holes and Top Hole for Diaphragm Placement

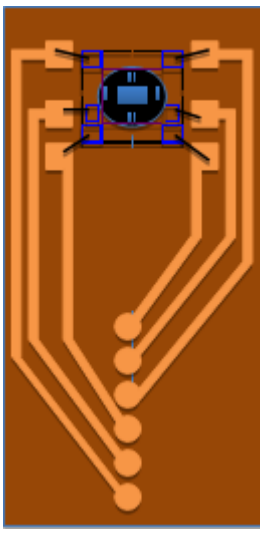

Figure 3.7 - PCB Layout with Sensor and Wire Bonds

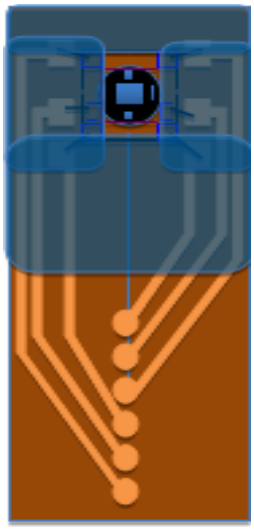

Figure 3.8 - PCB Layout with Sensor and Epoxied for Protection

3.3.0 Testing of Sensor with Version 1

After packaging the devices and figuring mathematically all the required inputs for the sensors they were ready for testing. All the previous steps before packaging were noted because if anything went wrong it would be

easier to look at the problem and analyze it. This section explains the setup for testing the device and how the data was gathered. At the same time it contains the results from testing the devices and the different tests done to be able to obtain the optimal results for the sensors while applying the protective layer version 1.

3.3.1 Test Setup

The device is tested using an oscilloscope (Tektronix TDS 340), a signal generator (Agilent Technologies 33220A), and two dual power supplies in order to find the required signal produced by the thermal vibrations on the sensor. After the heater activates the diaphragm, it will start deflecting and this will be sensed by the wheatstone bridge, detecting the deflection through the small voltage differences. The block diagram (see figure 3.9) below will explain how the sensor records the data.

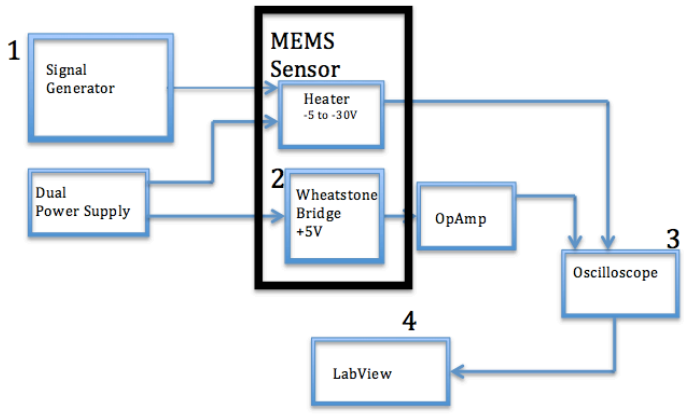

Figure 3.9 - Block Diagram of Viscosity Detection

It all starts from block 1, the signal generator sends a pulse to the heater; this will activate the membrane and make it vibrate at its resonant frequency. Once the membrane starts moving, the wheatstone bridge, Block 2 is able to detect this deflection, but since it is too small for the data to be read, its signal is amplified through a differential amplifier. The values used for the signal generator are explained in section 3.1.1, which talks about the use of the value of frequency in air and the time period, together with the amount of voltage required for the heater from section 3.1.3.

Both signals from blocks 1 and 2 are sent to Block 3, the oscilloscope, they are used to view the pulse (input), and the oscillation (output). Both signals are seen in the oscilloscope and an oscillation is obtained (see figure 3.10), this represents the expected output. The data is recorded using block 4, LabView, connecting the oscilloscope and the signal generator to the computer through a GPIB (General Purpose Interface Bus) data cable connection to the computer. The program is then able to replicate the data and show it in a computerized graph.

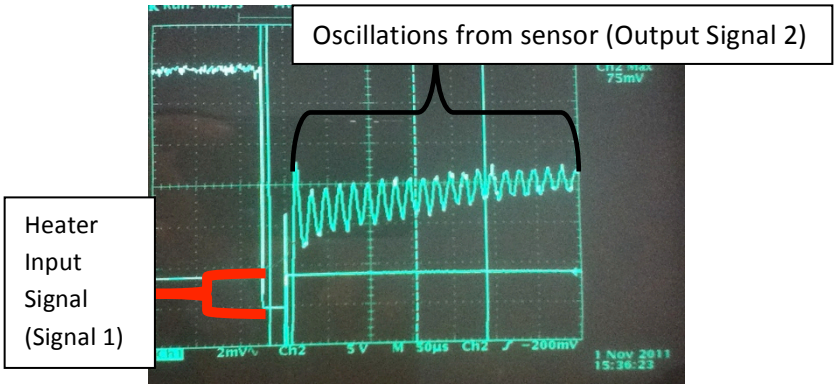

Figure 3.10 - A view of the oscilloscope with the 2 required signals

3.3.2 Test Results

Various devices were packaged using version 1 specifications, some used epoxy, while others used nail polish as the protective layer against conductive fluids. Overall both materials passed the test for covering the copper lines on the PCB to prevent them from releasing any electrical shortages while submerged in a conductive fluid. The nail polish and epoxy used are presented below see Figure 3.11.

Figure 3.11 - Nail Polish (left) and 5 minute Epoxy (right)

The nail polish chosen was from Sally Hansen, and it stated that it contained nylon as part of the chemistry used to make the nail polish. Even though it seems nail polish is meant for a different application, it acts like epoxy. Meaning that it can be used as a layer of protection for encapsulating the sensor. This lacquer is much easier to apply and it requires less time to dry at room temperature, it is much faster than regular epoxy. It is also easier to apply compared to epoxy, since it uses a brush to add the lacquer and it is a one-part mixture. On the other hand applying epoxy requires using a clip or a wooden stick to mix the hardener and resin parts before applying on to the PCB since there is no brush as it can get sticky pretty fast. The big difference between the actual device and this test

was making sure the membrane was not covered. This was a very important feature because the membrane requires movement, and having a big mass on top of it would prevent it from deflecting. This was not taken into consideration at the time, and using this method only alleviated protecting the copper lines.

3.3.3 Observations from testing devices in Air

Various devices were tested in air to comprehend how the sensor behaved before placing them in a fluid. At the same time it would help determine how accurate the sensor was with respect to the theoretical calculations previously explained in Section 3.1.1. Most sensors were tested in air before placing them in a fluid, this test was used to compare and be able to find trends in order to understand how the sensor reacted with the different mediums.

In this case sensor I3 was tested in air with the following parameters:

Table 3.11 - Sensor Characteristics for Device I3

Device Name	*Details*								
	a-Size (mm)	Heater Resistor		Metal	R_{heater} (Ω)	V_{Bridge} (mV)	Fair (Hz)	L2T Ratio	Time (µs)
		Type (P+ / Poly)	Size (35%, 16%, 2%)						
I3	2.5	P	2%	Yes	271	33.59	20,605	166.7	49

Applying 15 volts through the heater, with a time period of 20µs, and pushing a constant 5 volts to the wheatstone bridge. The calculated frequency for this device with the previous measurements using Eq. 2.29 give a theoretical frequency in air of 20,605 Hz. Unfortunately the result was close enough to the theoretical calculations leading us to understand that there is always a margin of error during the fabrication steps and this will need to be taken into consideration. Even though they are calculated values, in theory every result obtained from the measurements should be close to the calculated values. The results are presented in Figures 3.12, 3.13, 3.14. Red squares represent the calculated frequency in air for sensor I3 and the blue dots are the measured data points. These measurements were taken for 5 minutes and the average values were a frequency of 23,056 ± 24 Hz and a quality factor of 19 ± 1. With a variation of about 2,500 Hz or a 10.6% change between measured and calculated values.

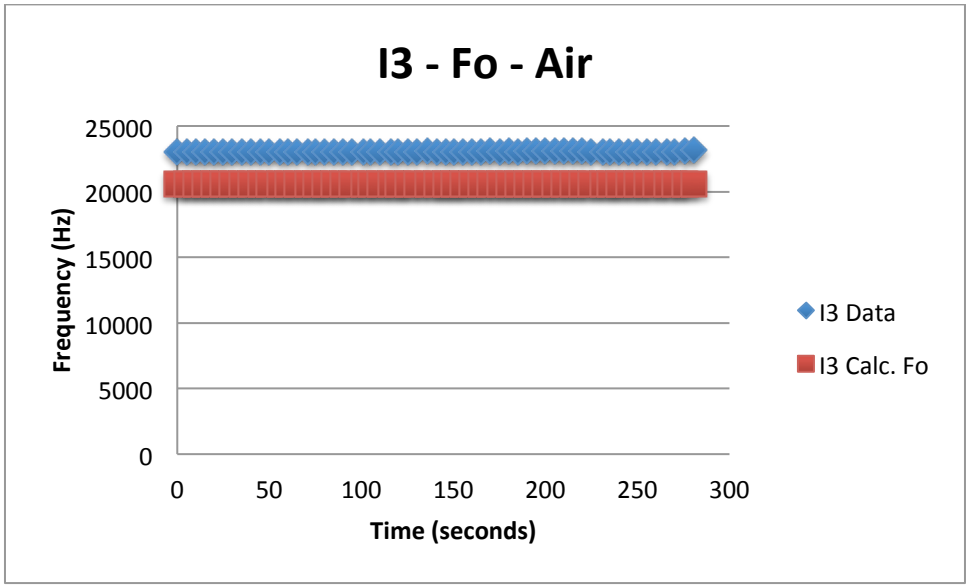

Figure 3.12 - Frequency Response of Sensor I3 in Air

The outcome of this sensor represents an output found similarly in different sensors, depending on the sensors characteristics, which are described in Sections 2.2.0, 3.1.1, and 3.1.3. Their frequencies, and Q factor values will vary accordingly. With all the required measurements and calculations these results are obtained.

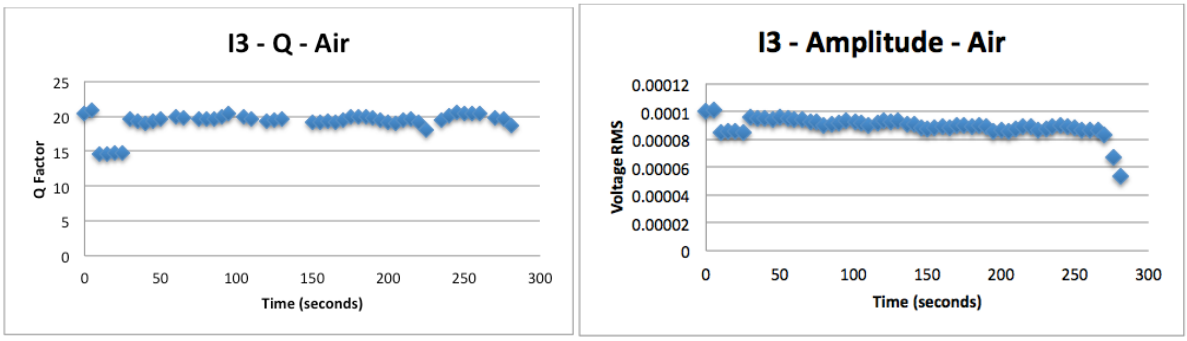

Figure 3.13 – Quality Factor (left) and Amplitude (right)

3.3.4 Nail Polish Selection (Nail Aid or Sally Hansen)

Two different brands of nail polish were used to determine which one was the best for the current application to protect the copper lines from touching the conductive fluids. This was an important test because there was nothing protecting the copper lines from touching the conductive fluid. Both of them were applied on the sensor in the following locations:

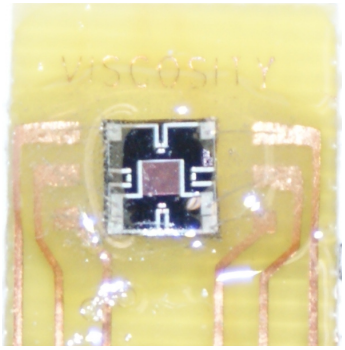

Figure 3.14 – Application of Nail Polish on to the PCB Board (see Figure 3.5) and Near the Sensor

With this new setup it would help prove that a combination of epoxy and nail polish could be applied to the sensor to prevent it from shorting out when placed under a conductive fluid. At the time nail polish was chosen as a protective layer because it was much easier to apply on the PCB than epoxy. For testing purposes two PCB's were picked and each had nail polish covering the copper lines. With this layer of nail polish we were aiming to prevent the conductive fluid from touching the copper lines and shorting out the sensor. After covering the sensor with nail polish the PCB would be connected to a power supply in series with a current meter and placed inside a beaker with a conductive fluid, de ionized water. The setup is shown below in Figure 3.15.

Luckily both setups worked without a problem. There were no electrical shortages present while testing the copper lines covered with nail polish inside a conductive fluid. Visually there were a couple of differences between the Sally Hansen and Nail Aid. Both liquids inside the nail polish were less viscous compared to the mixture of epoxy. Nail Polish 1 (SH), Sally Hansen Hard as Nails with Nylon and Nail Polish 2 (NA), Nail Aid grow tougher growth + hardener + ridge filler, see Figure 3.16.

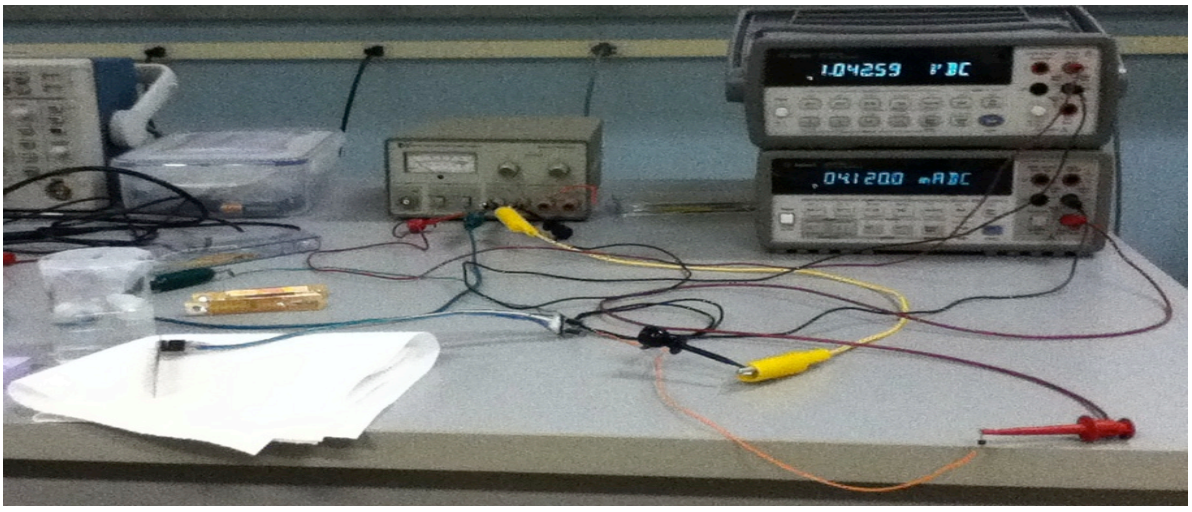

Figure 3.15 – Electrical Testing of a PCB with Nail Polish Inside a Beaker with De Ionized Water

Figure 3.16 - Nail Polish Containers Sally Hansen (left), Nails Aid (right)

Physically there were no shorts seen on the device while they were tested, SH solution after curing contained no bubbles and the layer was thinner than NA. The NA solution created more bubbles and made a thicker layer. At the time having more bubbles seemed more problematic because it contained air gaps and it was desired to have a clearer solution to be able to see through to the copper connections. As a matter of fact the copper lines withstood 100 volts through them without producing any actual shorts over a period of one full hour. With that test, out of the two nail polish provided, SH was chosen because it had a more clear consistency after the curing process and produced less bubbles. Below Figure 3.17 represents the physical observations of the lacquer or nail polish after the curing process.

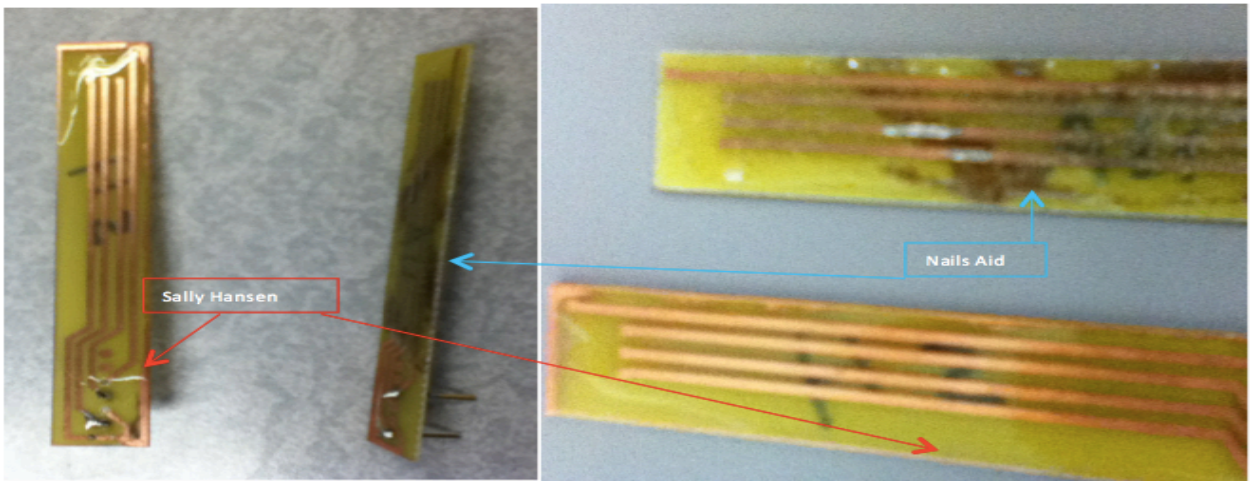

Figure 3.17 - NAIL POLISH SH Clear and Thin Layer (left) and NA Bubbles with Thicker Layer (right)

After being able to choose the nail polish on which to work it was time to compare to the epoxy solution. There are many kinds of epoxy, but the one used in this comparison was of a high strength grade, 5 minute epoxy. It

is a non-flammable mixture, which can withstand 1,500 lbs/in^2, and the most important fact is that it *can* resist water. This epoxy just like previously stated uses two different parts, the resin and the hardener. In order to mix the solution both parts have to be exactly the same amount. Otherwise a coloring effect would occur, and bubbles would start to grow while mixing.

Figure 3.18 - NAIL POLISH SH Clear (left) and EPOXY Bubbly (right)

Material 1, Sally Hansen nail polish was very useful because it was very clear and much easier to apply compared to epoxy. This did not require mixing two parts and obtaining a solution. In order to apply nail polish it just required a one-part mixture, making it much easier to apply straight from the container. Another important difference is the clearness in the cured layer of nail polish compared to epoxy, there are more bubbles present in the epoxy finish rather than the nail polish. But that also changes with the way the mixing is done, it is suppose to be a 50% – 50% from each part in order to create the correct mixture. Another difference between epoxy and nail polish was the amount of time required to cure, after mixing both parts it took 15-25 minutes to fully cure at room temperature. As for nail polish, the curing time would be much less in order to dry and become hard. While applying the solution it came very noticeable that nail polish was less viscous compared to epoxy. When adding the layer near the sensor location it was much easier to use nail polish, it seemed to be much cleaner than using epoxy.

These two materials were used to cover the sensor and the PCB board, this helps prove that the sensor could be placed in conductive fluids and be tested for electrical shortages. Both the nail polish and epoxy survived the test for a given period of time. At first the PCB lasted 5 minutes with current flowing through the circuit, and no

open circuits were observed, as the PCB remained underwater. This test was undergoing past the first 5 minutes, reaching a total time of one complete hour underwater.

3.3.5 Observations from testing devices in a conductive fluid

At the time, packaging the first set of sensors was a hard task, because it was not specified how thick of a protective layer was required and how much should be added. It was a trial and error, some devices contained a thicker layer while others did not, to help withstand the electrical conductivity against the conductive fluids. Primarily testing started with bottled water as the conductive fluid, and then as tests progressed different conductive fluids with different viscosities would be used to test the device. Below we can see Figure 3.19 showing a cross-section of the sensor with the different layers of protection.

Testing results varied from sensor to sensor, the devices gave good and bad readings as they were tested. This can be seen in the overall outcome of the results presented in Table 2 (see Appendix). Most devices failed over time, some of them did not provide any results at all. This was due to the reason of non-linearity effects, because they were not close to the desired ratio (≈166) this would agree with Brand et Al [14] suggesting the given ratio. But some devices with a desired ratio of 116.7, & 175 were chosen to work adequately just like a 166 since they were not that far from the given ratio.

At the same time the passivation layer, was not thick enough to help prevent the conductivity of electricity through the metal lines. With these results it was possible to find that

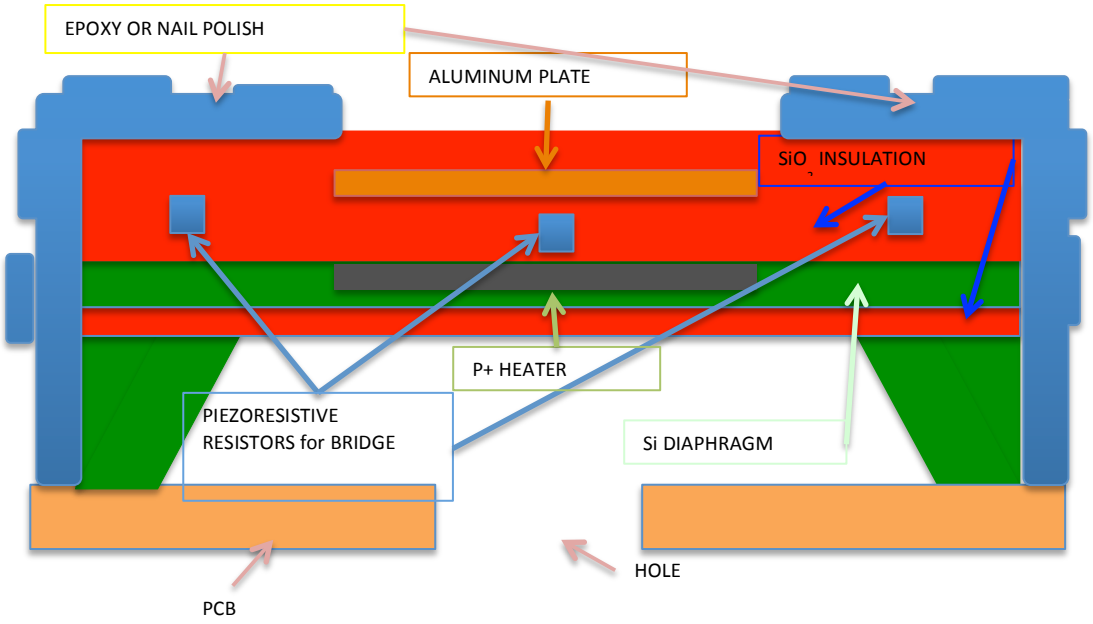

Figure 3.19 - Cross Section of Sensor with Protective Layer Version 1 (Epoxy or Nail polish)

epoxy and nail polish both helped the device control the conductive fluid as it is placed underwater. But the evidence suggests that some bubbles are created during the curing process of both, the epoxy and nail polish material. This was taken into account for creating air pockets between the protective layer and the copper connections, and the device itself. Having air pockets within the insulating layer, can cause space for water vapor to creep, and thus creating a chemical reaction causing the pocket to contain water vapor and affecting the sensors performance.

Another problem obtained from the results was discovered by analyzing the devices under the Bausch & Lomb microscope located in the Characterization Laboratory at RIT. This can be seen in the following images (see Figure 3.20).

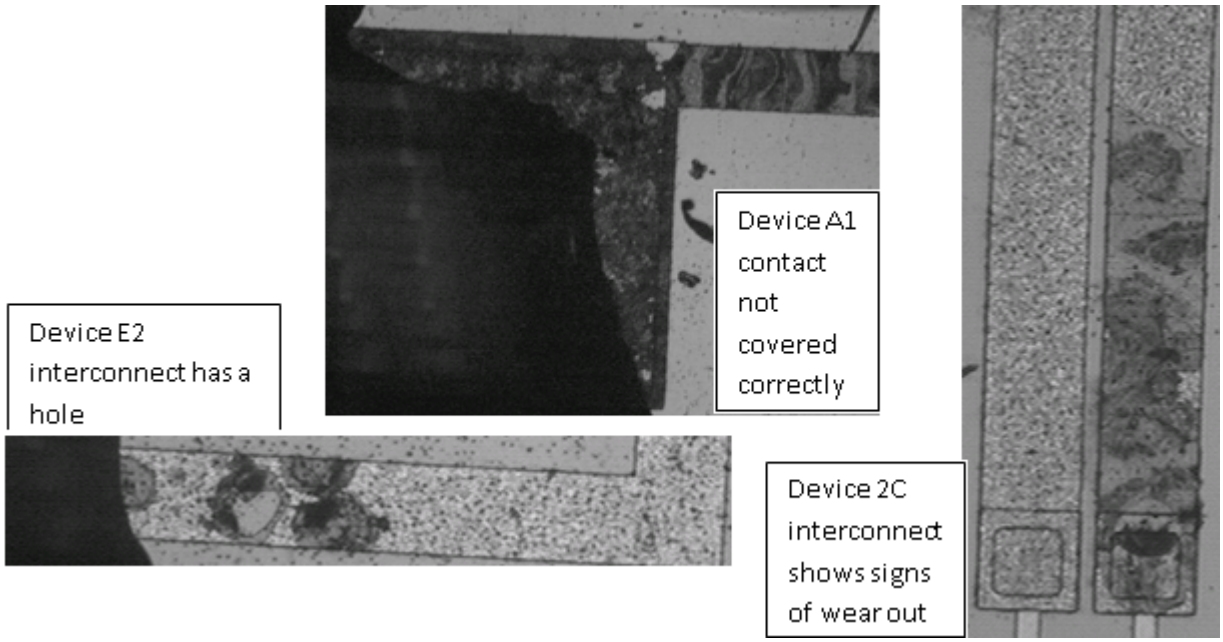

Figure 3.20 - Overview of Some of the Visible Problems Using a Microscope Occurring to the Sensors

From these observations made, new problems arose, some of them clearly seen in the previous pictures relates to cracks due to pinholes. Another reason why the device would fail is shown above when the protective layer does not fully cover the contact pad with epoxy or nail polish. At the same time interconnects show a clear response to the conductive fluid because some of their sections are not fully covered. These sections are the ones where the microscope can visually detect the problems occurring in the devices. It is due to the relationship between the water and electricity that cause reactions within the particles when the device is placed underwater.

At first it can be seen that there are small cracks present on the traces. With these small cracks and a combination of water and electricity causes the device to have problems. Due to this, the protective layer does not do

its job correctly. This in return makes the device to stop working properly and ruins the normal operation of the sensor. The small cracks previously stated are present in an extremely small scale, thus a more powerful microscope was used, RIT's Amray 1830 Scanning Electron Microscope (SEM) helped discover the problems on the device. The images are presented below (see Figure 3.21). They clearly show cracks occurring on actual metal lines, meaning that there could be a couple of things occurring. Either the current density is too high, for the aluminum to withstand it, or the water is actually going through the passivated layer and affecting the contacts.

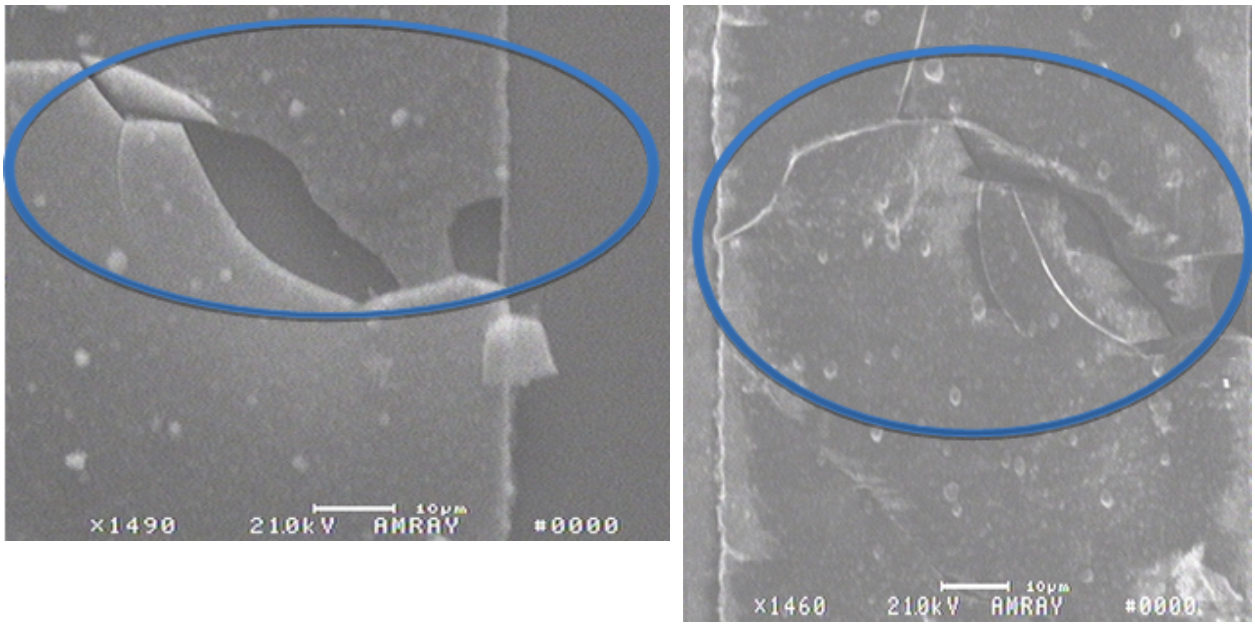

Figure 3.21 - SEMs @ 1490X of Broken Interconnects

At the same time the data was recorded through LabView and compiled to produce the following outcomes. The following graphs (see Figure 3.22) show the results from sensor 5B, one of the best devices tested and producing acceptable signals while testing underwater.

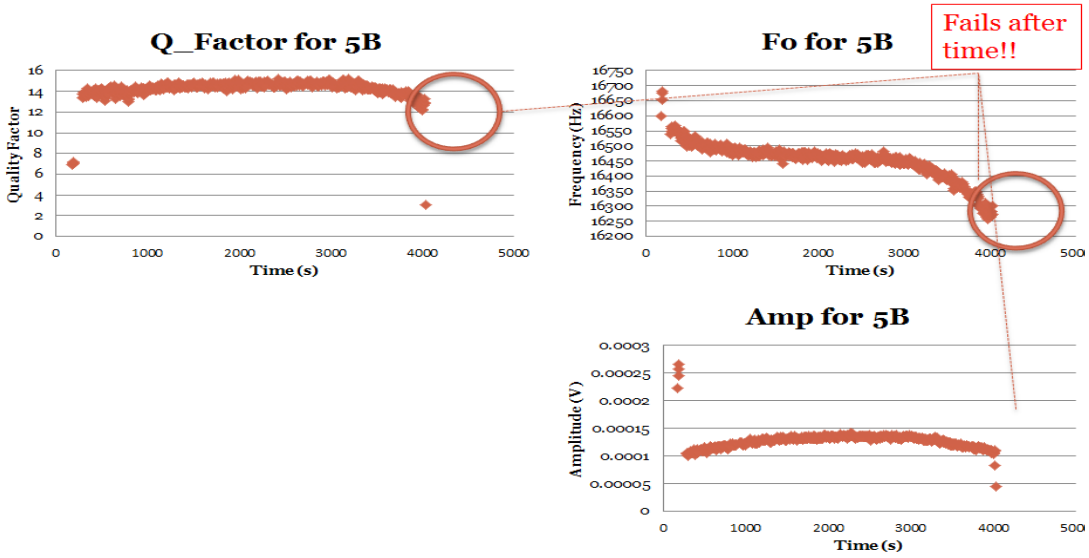

Figure 3.22 – Underwater Testing Results from Device 5B

The device contained a diaphragm thickness, ***h*** of 15µm and a length size, ***a*** of 1.75mm. The heater and the bridge resistors are made out of Polysilicon. Even though the thickness to length size ratio was not found to be optimal (116.7 compared to 166) the results from the device were very optimistic. The image (Figure 3.23) below shows one of the first tests done to a sensor underwater.

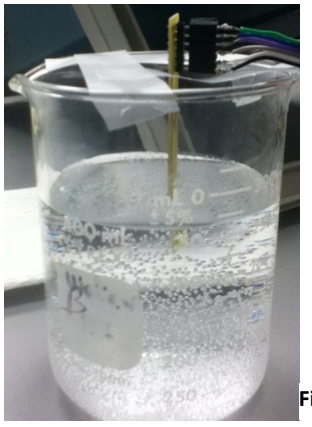

Figure 3.23 - Sensor 5B Testing in De Ionized Water

The device survived water conditions for an average of 67 minutes, producing results of an average Q factor of 14, and a fundamental frequency of 16 kHz. These values were compared to those obtained in air, and it clearly shows that as the medium in which the sensor is placed in changes, the sensor will detect a change in oscillation. This is due to the change in mass present on the top and bottom of the sensor. See Table 3.12 below for reference. Thus providing good information that the sensor works underwater as hypothesized, but due to time the sensor fails.

Table 3.12 - Test Results for Sensor 5B

5B	Fo (kHz)	Q Factor
Air	59.52	32
H2O	16.452	14

Overall the test results helped define the problem by providing a visual problem and giving an understanding of the devices functionality. The epoxy and nail polish compounds were used accordingly to show that they are good candidates used to cover the copper connections. Even though nail polish has a clearer and thinner layer of protection, epoxy seems to have a tougher layer. With this said the sensor completely packaged works underwater, but time defines its fate.

3.4.0 Problems to Current Sensor with packaging Version 1

Now that the sensor has been summarized, the problems will be re-defined in the next paragraphs. This sensor works according to its specifications, so far the problem stated is that the device works for non-conductive fluids (i.e. Oil). But this new approach is trying to surpass that problem and be able to use it on conductive fluids (i.e. water, milk, blood, etc.). Another important feature observed is the modification to reduce the amount of voltage used to send the heat pulse. The device uses “high” (5V - 30V) voltage source in order to produce the required signals, thus it would be applicable to reduce this amount. These low power consumption requirements are very important for the device to be packaged in small dimensions.

Similarly the data obtained from the sensor is required to have a more dynamic range, meaning that the device needs to be focused on specific applications. Previously stated, it depends on the application this sensor will be used for to analyze the fluid, which leads to choose a specific packaging method. In reality the major change made to this sensor is to be able to obtain results for a wider set of applications.

Another very important feature, which is definitely required for this device, is to optimize the production of sensors with improved sensitivities. In most applicable sensors used nowadays there is a separate knob embedded to the device which helps regulate their sensitivity. This is very important for the user of the device and the application in which it will be used for. The sensitivity issue can be identified to be a part of the problems found in the thickness of the membrane. It is the material which the resistors are made out which depends on how sensitive they are to change.

An important problem found while the devices were tested underwater are the interconnects, these are more visible under a microscope because they are so small. To the human eye they appear as lines and it is hard to analyze if it is missing a trace or not. But it is due to the combination between the conductive fluid and the electricity applied that help the small pinholes within the interconnects to corrode the material faster and lead to a complete failure of the device over time. Together with these cracks, the device fails by affecting the heaters traces causing it to stop working due to an open circuit. And the wheatstone bridge will have its resistance values drift, due to the previous stated effects, the bridge is not able to measure the deflection and makes the sensor unreliable and unoperational because it is not working to its specifications.

As a matter of fact the main reason all of this problems occur is the main reason explained in section 3.3.2 where the device is not fully covered with a protective layer from conductive fluids where the membrane is located. The main reason is due to the material used for coating the section where the membrane is. It might be too fragile for such a "thick" coating from either epoxy or nail polish and none of them are flexible enough as thin layers. Thus leaving it without protection against the conductive fluids as the entire device is submerged.

3.5.0 Proposed Solutions to Current Sensor

In order to solve all of these problems other researchers have tested different attempts. Some groups have applied basic packaging methods by adding epoxy and parylene in a post fabrication step. Passivation is applied to the device to enhance its contact against other fluids around the sensor. This term refers to a formation of a hard non-reactive surface layer that prevents corrosion to a certain extent. Some of the most common passivation methods involve the use of nitrides [31,32] or oxides. With these materials one is able to cover the sensor with a thin layer, x nm thick, of the substrate for protection. The actual sensor holds 1,000 Å or 1 μm of SiO_2 as the layer of passivation.

The solution for this problem is basically trial and error because the sensor requires testing. This will help understand the duration of the sensor submerged in a liquid that conducts liquid compared to those that do not, such as oil. With this trial the device can also be tested for other symptoms, which will help determine how to prolong the duration it can withstand underwater. Therefore it is imperative that the packaging chosen for the sensor depends on the application in which it will be used for.

A very common material used for passivation by some researchers is Parylene [33,32,34,35,36]. This is a material, which is added as a thin layer, and it can measure up to X nm in thickness. The material itself is flexible, and depending on the kind used, it can be dark or clear. Huang et. Al [37] while researching a glucose detection

sensor realized that a viscosity difference could be assessed in glucose determination. This sensor is based using MEMS technology, carrying two magnetic vibrating diaphragms placed inside a micro chamber. He was able to create an in-vivo and in-vitro system to continually test for glucose using a protective layer of parylene.

In order to create this device that withstands all human acids and bases in the body, the layer of protection has to be extremely durable and impermeable. Therefore during his fabrication process, Figure 3.24, he adds 3 different layers of parylene for passivation to ensure the safety of his electrical connections. Overall his sensor was tested inside a laboratory rat for a duration of 3 hours. This helps understand how effective a layer of parylene can help as a passivation layer as a pre-fabrication step.

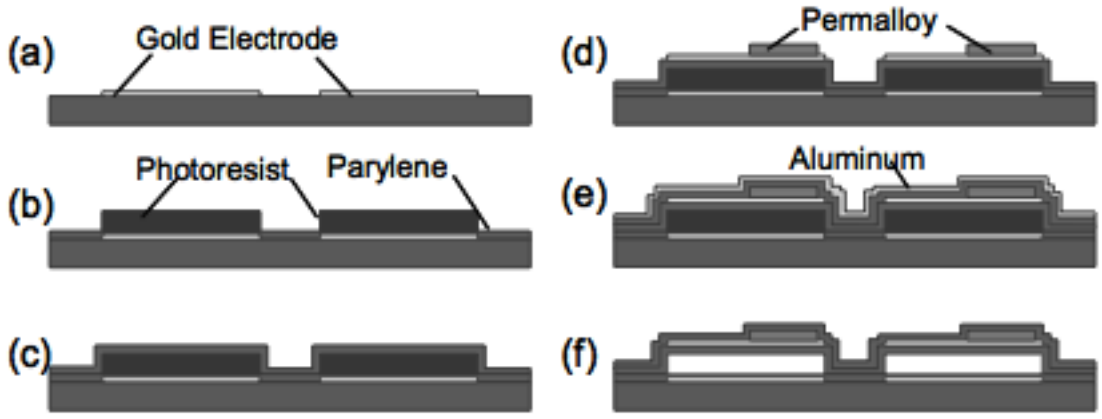

Figure 3.24 - Fabrication Process for Continuous Glucose Detection [37]

Another method is by using silicon nitrides and/or silicon oxides as part of the fabrication process. In this case Riesch et. Al [17] developed a viscosity sensor, which is set to enhance the measurement of the quality factor. They added a suspended plate, which adds a mass to the moving sensor, and due to this addition the quality factor of the resonance is "enhanced". They managed to produce a plate that resonates in a frequency of 12.7 kHz - 9.4kHz in viscous fluids. The device overall uses distinctive fabrication steps which increase the overall thickness of the device, leading to work different. This option seems very feasible, but because there are a lot of sensors already diced up from previous testing, it seems reasonable for this project to use the existing sensors and apply post fabrication steps to them.

From all the papers gathered the best option for a post fabrication step without altering the sensors performance is the use of parylene C as the coating material. Even though there are many ways to solve this problem, currently there are a lot of sensors available for post processing. Therefore the best choice is to use those

devices and implement the protective layer using Parylene C. The new device will look the same as in Figure 1.1, but the cross-section and the overview of the device on the PCB will look different. The images below (see Figures 3.25, 3.26) represent the addition of the parylene coating. Table 3.11 shows a comparison of some of the materials properties [38] [39] [40]. The emphasis is on the Tensile Strength and the Yield Strength which describe how much force is required to break, and the amount of stress it can withstand without deformation. At first sight, Parylene C has much higher yield strength, and comes 3rd to best in the tensile strength. But the biggest factor seen is the

Table 3.13 - Physical Properties from Different Sources Regarding Materials for Encapsulation

Properties	Parylene C	SiO_2	Si_3N_4	Polyimide
Melting Point (°C)	290	1500	1900	400
Linear Coefficient of Thermal Expansion at 25°C (ppm/°C)	35	0.5	0.8	4.5
Thermal Condutivity at 25°C (W/(m*K))	0.084	1.1-1.4	21.3	0.12
Secant (Young's) Modulus (GPa)	2.76	75	0.97-1.03	3
Tensile Strength (MPa)	69	48.3	1,440	72
Yield Strength (MPa)	55	8.40E-06	1.40E-06	-----
Elongation to Break (%)	Up to 200	----	----	> 10
Yield Elongation (%)	3	----	----	4
Water Absorption (% after 24 hrs)	< 0.1	----	----	0.4-2.5
Flexible?	Yes	Yes	Yes	Yes

water absorption, compared to polyimide, Parylene C has a much better property, where as SiO_2 and Si_3N_4 would require different multiple layers in order to encapsulate the device without any problems.

Some of the main points why parylene C is a very powerful thin film is because it is one of the best coating materials used for medical applications. Thus it fulfills the idea of applying this sensor to a bio-medical application. Similarly this coating is insoluble to all inorganic solutions up to a high temperature of 150°C, if the sensor is implanted inside the body should withstand most of the acids. One of the most impacting facts comparing it to epoxy is that Parylene C has a low permeability to moisture, chemicals and other kind of gases. It is a flexible thin film layer that is very useful to this application since the sensor has a heater that requires deflections to the membrane. The coating as it gets added to the sensor is conformal which means that it adheres to the sensor just like shown in Figure 3.25 it follows the shape of the previous layers. This is very useful for the current application and it defies the way epoxy is added to the sensor. You can also see this comparison in Figure 3.25.

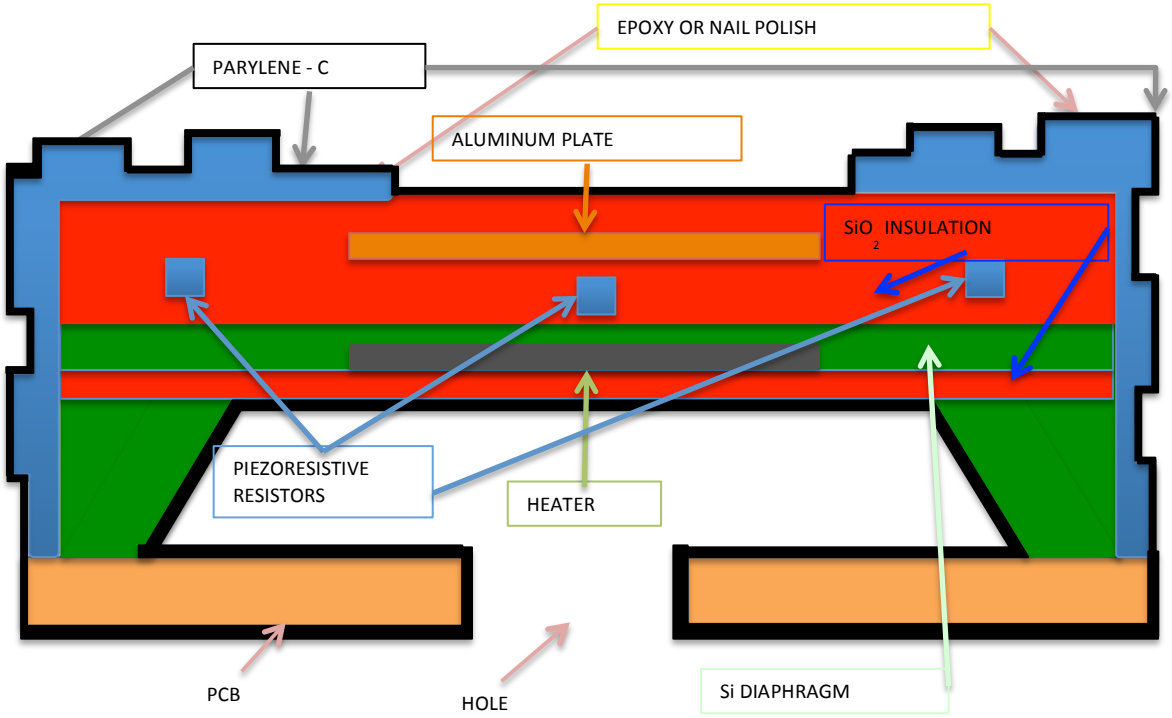

Figure 3.25 - Cross Section of Device with Protective Layer Version 2 (Parylene C)

The new protective coating is the first line of defense that the conductive fluid will fight against to get to the electrical currents. Thus it is imperative that this flexible layer of parylene be used and placed on top of the membrane and its surroundings. An advantage of using parylene-C compared to epoxy or nail polish is that adding this on top of the device adds protection to everything. This can be seen from the previous layer version 1 (see Figure 3.19) and compare it to the new protective layer version 2 (see Figure 3.25). With this comparison it is clear that the device will be fully covered and hopefully those images previously presented with the cracks (see Figure 3.20, 3.21) will not be visible.

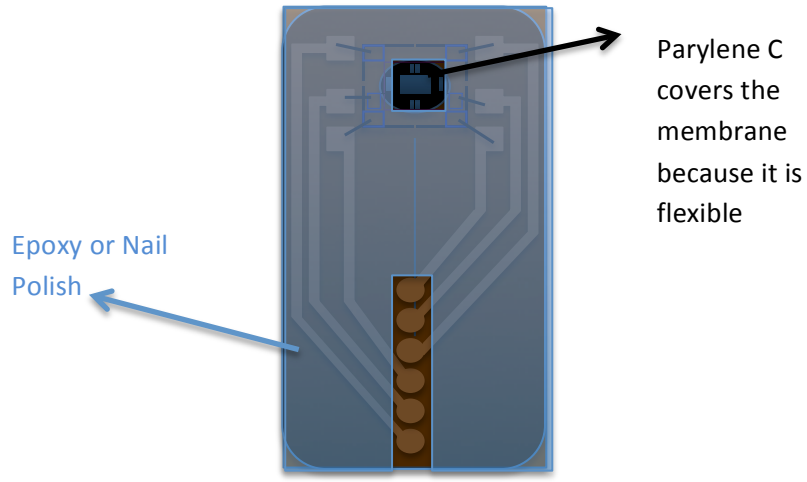

Figure 3.26 – Protective Layer Version 2 - Top View of PCB + Die + Parylene Coating + Epoxy

At the same time applying parylene on the entire device will be useful because it will be covering the membrane. It is one of the major things that seem to lack from previous trials, because the previous coating left the membrane section unprotected. Thus this will fight hand on hand with the conductive fluids and make sure the device will still work while being underwater. Parylene-C is added on top of the membrane because it is an extremely thin layer and it is flexible, meaning the membrane will be able to deflect even though this layer is on top.

Epoxy or nail polish will be added after adding parylene-C for precaution and add more layers of protection to the device. This other layer will be added just like in Figure 3.19 and will be an extra layer to make sure that the conductive liquids will have to fight two different shields before getting to the electrical currents.

With this new protective layer it is important to say that the device will withstand all the problems previously presented. This also agrees with the decision to choose a post fabrication process that helps use of all available sensors, and it is a cheap option. Another advantage of using the current sensors and not altering the fabrication steps is that Parylene C can be added at room temperature not affecting the PCB or the sensor. At the same time it will show that it is a reliable option because it will help the sensor withstand all the problems the sensor is already suffering from the conductive liquids. Luckily after this new layer is applied all the sensors will work according to specifications and this might have been the solution as the best choice given the current problems presented.

4.0 - Testing of Sensors in OIL before adding protective layer and after adding protective layer

Viscosity measurements were obtained by using the current sensors on commercial standardized oils. On table 4.1 you can find the different oils used for testing from Koehler Instrument Company Inc. which have provided their viscosity and density quantities at different temperatures ranging from 20°C - 100°C. All of their measurements have been recorded using long capillary Master Viscometers at all temperatures according to the ASTM D 2162 standard with an uncertainty between 0.7% and 0.15%.

Table 4.1 - Viscosity and Density Values for Standardized Oils at Room Temperature

Oil	Viscosity (25°C)		Density (25°C)
	Kinematic (mm^2/s or cSt)	Dynamic (mPa*s or cP)	(g/mL)
S3	4.035	3.262	0.8085
N10	17.01	14.43	0.8484
N35	65.07	55.43	0.8519
5W30	132.91	117.76	0.886

The different devices tested with all of these oils are found in Table 4.2 and Table 4.3, they were chosen from a list according to their characteristics, previously described in Sections 3.1.1 – 3.1.4.

Table 4.2 - Sensors Characteristics

ID	*Details*											
	h (µm)	a (mm)	Heater		Metal	Measured			L2T Ratio	Calc. Fair (Hz)	Calc. Time (s)	Meas. Time (s)
			Resistor Type (P+ / Poly)	Resistor Size (35%, 16%, 2%)		Heater	Bridge	PMOS				
5B	15	1.75	P	2	Yes	30	5	12	116.7	20,605	48.5	20
I3	15	2.5	P	2	Yes	30	5	12	166.7	20,605	48.5	20
J1	15	1.75	Poly	2	Yes	22.5	5	12	116.7	42,050	23.8	30
J5	15	1.75	P	2	No	18	5	12	116.7	42,050	23.8	30
K1	10	1.75	P	16	Yes	30	5	12	175.0	28,034	35.7	10

The information on table 4.2 has a clear description for each of the sensors with their corresponding ***h***, diaphragm thickness, ***a***, length of membrane, heater resistors type and size, if it contains metal or not, the calculated values frequency in air, the calculated time for the pulse and also the measured voltages for the heater, bridge and PMOS, and the measured time required for the given pulse.

The oils used are presented in Figure 4.1, each vial is labeled with their respective name. The main reason to use these vials is because of the repeatability factor for each test. In order for the different sensors to behave in a similar manner, the same testing procedure has to be followed. Therefore the sensors location and position should always be the same. This improves the sensors reliability and also makes the testing procedure repeatable and takes into account the discrepancy of the PCB from touching the sidewall. If the sensor or PCB where to touch the sensor sometimes would make the vibrations in the sensor behave differently, outputting some kind of noise from the sensor. Similarly the vials are used because it helps prevent the pins from touching the liquid as the diameter of the lid is small compared to the length of the pins, this can be seen in Figure 4.2, shows a sensor inside a vial ready for testing.

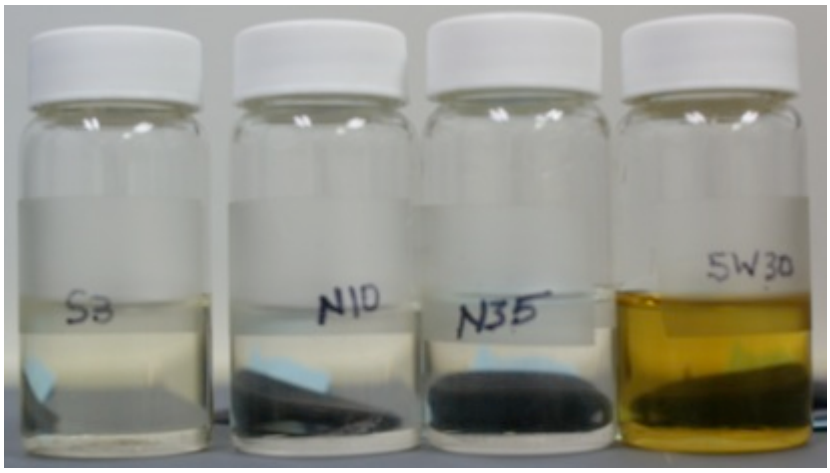

Figure 4.1 – Oils S3, N10, N35, 5W30 in their Respective Vials

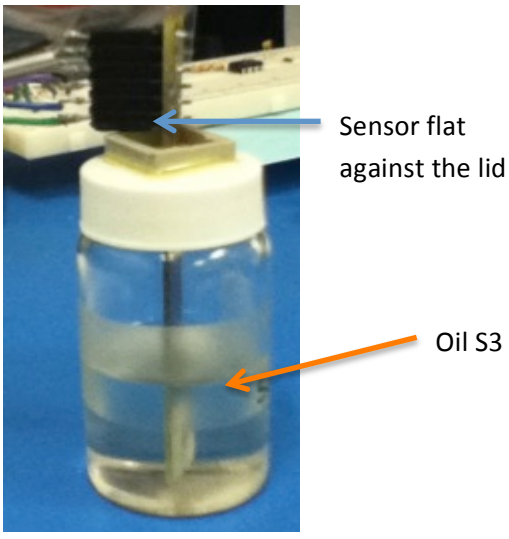

Figure 4.2 – Sensor Placed Inside a Vial Ready for Taking Measurements

Each of the sensors was tested for their frequency, amplitude and quality factor for 20 minutes inside each vial of oil.

4.1.0 Output Signal

For each of the sensors tested only those that produced good results were taken into consideration, because some gave false output signals. Producing frequencies in the range of 100 - 300kHz. Comparing these values to the calculated values would seem unreasonable since the highest frequency in air measurement for all thicknesses that were good enough for the L2T ratio was of 42,050Hz. This is a device with an $\boldsymbol{h}$ = 15μm, and an $\boldsymbol{a}$ = 1.75mm.

The L2T ratios are previously explained in Section 3.1.3 this device gives a ratio of 116.7. Meaning the value is less than the study done by Brand et. Al. of 166.7 stating that even though it is not the same ratio it will still work, but behave with some problems. These problems have been previously stated in Section 3.1.3. Most sensors chosen were in the range for the L2T ratios of 116.7, 166.7, 250. These sensors would have different $\boldsymbol{h}$ and $\boldsymbol{a}$ values according to their ratios.

When sensors actually worked, it was easy to tell because the output signal would be close to the output, Figure 4.3 shows the oscillation from a sensor working in air. Once this reference was obtained testing the following sensors in air were easy to obtain measurements from. Inputting the calculated values to the signal generator was an ordeal of its own because sometimes the sensor would not produce a given output. In turn this would require changing the input value by either 5μs or 10μs.

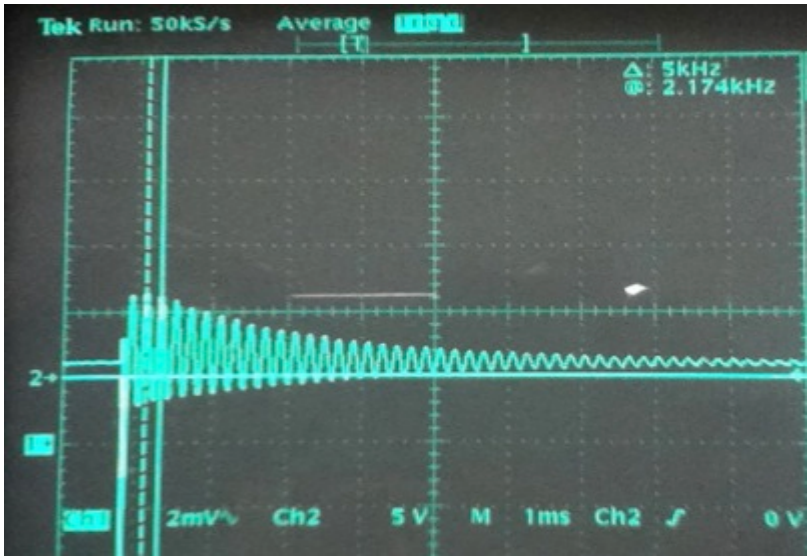

Figure 4.3 - Sensor Output in Air

As a matter of fact finding the right amount of time in μs required for the pulse is also important because that helps increase the signals output. This would also be dependent upon the users judgment of what is a good signal output. Some devices would output a signal and the amplitude of the oscillations would be twice the height than the one shown in Figure 4.3.

4.2.0 Sensor Oils Test Before Parylene C protective layer

Various sensors were chosen to determine their frequency in different oils by using Eqs. 2.29, 2.30, 3.31 together with the data from Table 4.1. With these values it is possible to understand that there is a trend as viscosity increases. Even though each device produces a dissimilar frequency, theoretically the trends show a distinctive power law fit. All values were normalized to be able to place them in the same scale on a graph. The different sensors that were used for this test have been defined according to their characteristics with calculated values of frequency, and response time and are presented in Table 4.3.

Table 4.3 - Sensors Characteristics with their Corresponding Values

Device	h (μm)	a (mm)	Metal	Heater		Bridge Resistor	a/h	Calculated for Air		Calculated for Oil
				Type	Size (%)			Frequency (Hz)	Time (μs)	Frequency (Hz)
I1	15	1.75	Yes	Poly	35	Poly	116.7	42050	23.8	7159
I3	15	2.5	Yes	P	2	Poly	166.7	20605	48.5	2948
5B	15	1.75	Yes	P	2	Poly	116.7	42050	23.8	7159
J1	15	1.75	Yes	Poly	2	Poly	116.7	42050	23.8	7159
J5	15	1.75	No	P	2	Poly	116.7	42050	23.8	7159
K1	10	1.75	Yes	P	16	Poly	175.0	28034	35.7	3916
L1	15	1.75	Yes	Poly	2	Poly	116.7	42050	23.8	7159
L2	15	1.75	Yes	P	2	Poly	116.7	42050	23.8	7159
L3	15	2.5	No	P	35	Poly	166.7	20605	48.5	2948
L4	15	2.5	No	P	16	Poly	166.7	20605	48.5	2948
L6	15	1.75	Yes	Poly	35	Poly	116.7	42050	23.8	7159
L7	10	1.75	Yes	Poly	35	Poly	175.0	28034	35.7	3916
L8	10	1.75	Yes	P	2	Poly	175.0	28034	35.7	3916

The theoretical results for the chosen sensors are presented below in Figure 4.4, which shows a representation of the trend previously stated. As viscosity increases there is less movement in the liquid for the membrane to deflect back and forth. Thus the sensors output will produce a reduced frequency response, together with a lower quality factor and amplitude. These values were calculated at room temperature for each given sensor. With the different results a power law fit was obtained from each set of points and they all agreed to have the following equation:

$$y = ax^b \tag{4.0}$$

where ***a*** represents the scalar, and ***b*** is the slope of the equation.

$$y = 1.014x^{-0.011} \quad (4.1)$$

$$y = 1.3721x^{-0.221} \quad (4.2)$$

In Figure 4.4 the legend only shows three different shapes, the reason for this is that for the theoretical calculations according to Lamb's and Kozlovsky's equations we are able to categorize them according to their L2T ratios. Thus representing the different ratios of 116.7, 166.7, and 175. With these ratios it is possible to categorize them accordingly just like shown below, where the blue diamond and orange circle represents the ratio of 116.7, the red square and purple x is the 166.7 ratio and the green triangle and light blue x contains information on the 175 ratio.

Equation 4.1 represents the hypothesized power law fit relationship between the viscosity and the normalized frequency using Lamb's equation where as Eq. 4.2 talks about Kozlovsky's approach. After calculating the theoretical values of frequency for each of the 13 sensors at each of the oils, the actual collected data results were analyzed. Figure 4.5 shows a representation of the normalized data points for all sensors and their respective theoretical calculations.

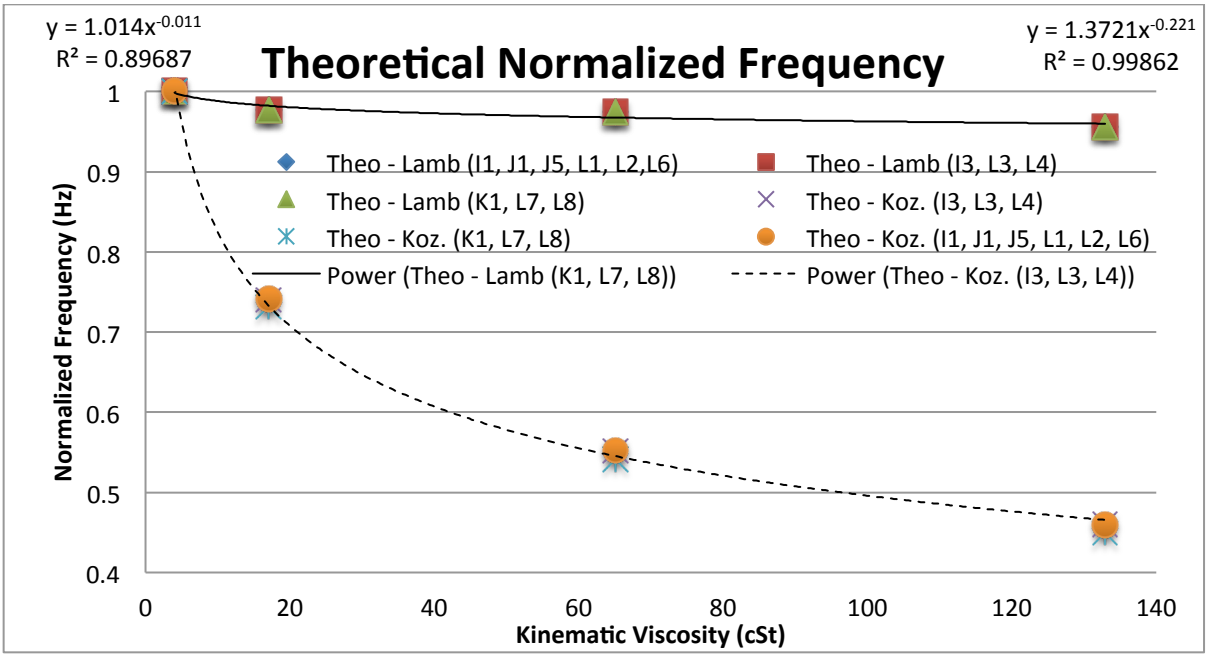

Figure 4.4 - Theoretical Calculations of Normalized Frequency for Different Viscosity Values

With these results we can see that the trend still follows, as viscosity increases there is a decrease in frequency. First we can see in Table 4.3 there are many devices, they were chosen in a random manner from Wafer

4 and 5. Following the L2T ratios previously specified to understand why it was that Brand et. Al. [14] decided to use the 166.7 ratio in terms of having non-linearity effects.

The devices also varied in length of membrane from 1.75mm to 2.5mm. Since we are aiming to test the sensors in conductive fluids, all devices had passivation on them. Some sensors varied their design by containing a metal layer of aluminum on top of the diaphragm to create a bimetallic effect. This provided an added mass, enhancing the deflection of the membrane through the change in thermal expansion coefficients between the membrane and the metal layer [1].

Looking at the different characteristics of each sensor the two furthest points represented by the red dash line, L3 and the green dash line, L4 show a similar response as oil samples vary in

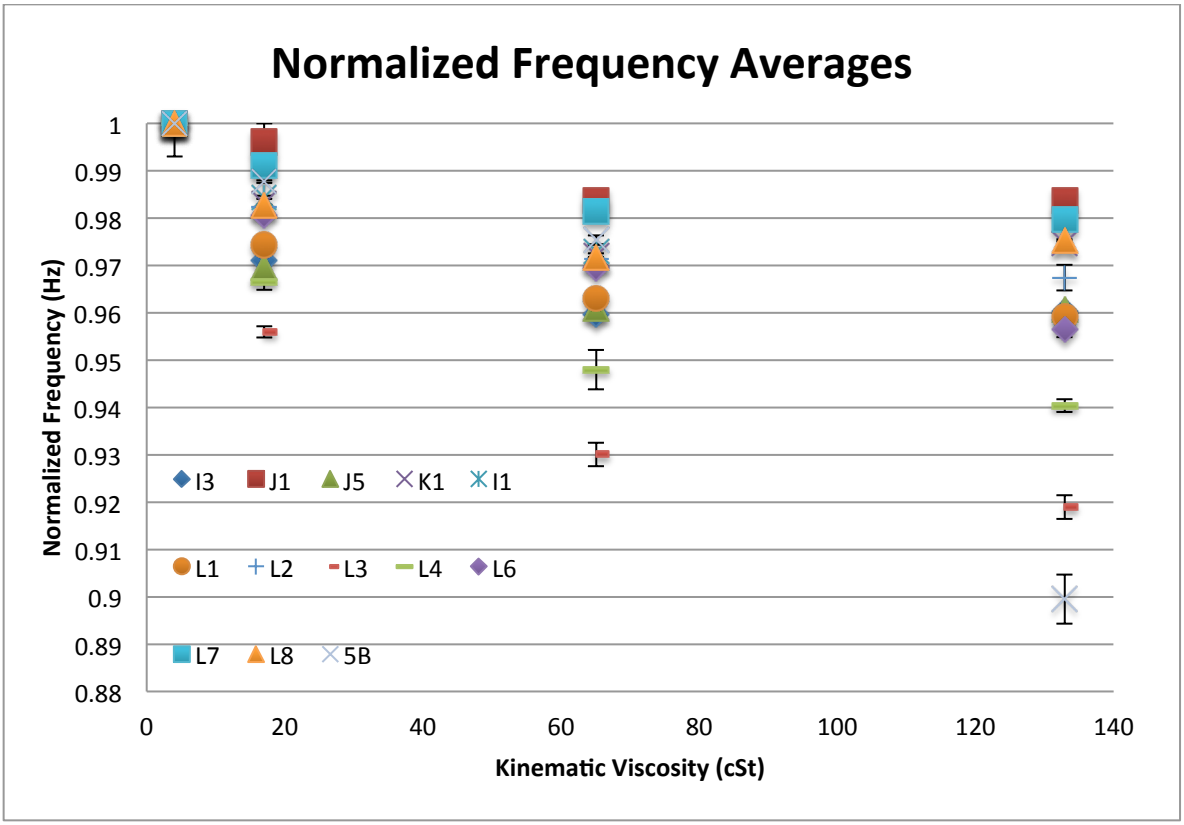

Figure 4.5 - Normalized Frequency Variation in Different Oil Samples

viscosity. Both had similar L2T ratios of 166.7 which agrees with Brand et. Al. assumption of having less non-linearity effects, and shows a bigger range between each oil sample. Where as if we look at the results from sensors L6, L1, J5 and I3 their ratio is 116.7 except for I3 having a ratio of 166.7. They all have similar outputs with different oil samples.

Overall the main sensors that did not follow a similar trend were I3, K1 and L8. Comparing their L2T ratios, L8 and K1 share the same value of 175 where as I3 has a 166.7. Though that does not proof why they would act differently in the 5W30 oil sample. It seems that the reason for the frequency to rise in thicker oil is the cleaning procedure changing from sample to sample. Cleaning is also a very important factor, because leaving a small particle of oil on the device will change the outputs reading.

Table 4.4 - Power Law Fit of Normalized Frequency Averages

Device Name	a size (mm)	Heater Size	Heater Type	Metal	Y =	R^2
I1	1.75	35	Poly	Yes	$1.0133x^{-0.01}$	0.9954
L7	1.75	35	Poly	Yes	$1.0083x^{-0.006}$	0.9877
L6	1.75	35	Poly	Yes	$1.0167x^{-0.012}$	0.9851
L3	2.50	35	P	No	$1.03x^{-0.024}$	0.9828
L2	1.75	2	P	Yes	$1.0116x^{-0.01}$	0.9796
L4	2.50	16	P	No	$1.0213x^{-0.018}$	0.9766
L1	1.75	2	Poly	Yes	$1.0132x^{-0.012}$	0.9494
J1	1.75	2	Poly	Yes	$1.0085x^{-0.005}$	0.9247
K1	1.75	16	P	Yes	$1.0083x^{-0.008}$	0.8975
I3	2.50	2	P	Yes	$1.0115x^{-0.012}$	0.8899
L8	1.75	2	P	Yes	$1.0079x^{-0.008}$	0.8701
J5	1.75	2	P	No	$1.0104x^{-0.011}$	0.8655
5B	1.75	2	P	Yes	$1.0497x^{-0.025}$	0.6694

The results on Table 4.4 represent the power law fits to each of the sensors normalized frequency response. With the given results the equations show a negative slope with a good sensitivity average compared to that from the theoretical Eq. 4.1, where the slope is negative and shows a value of -0.011. Even though the added trend line does not sit right on top of the points, Eq. 4.1 represents an overview of what it should look like. As viscosity increases there is a decrease in normalized frequency following the actual trend seen on [1]. But this is not a very good way to determine how accurate the response should be as shown by device J5 which has the same predicted negative slope. Showing a lower R^2 value compared to those in the 90% range.

On the same table it is possible to see the R^2 values, which represent the simulated calculations analyzed by the recorded data using Microsoft Excel. In theory the value of R^2 determines how accurate the predicted model made by Excel's calculations can be compared to the actual data. Sensor I1 shows a very awesome output according to the R^2 value, but in reality that sensor did not finish testing since it got burned halfway through testing. The next devices, L7, L6, L3, L2, L4 show a very good approach to the calculated value and theoretically provide a positive output. But as seen in Figure 4.5 all those sensors show a very good output response. The sensors highlighted in

yellow in Table 4.4 show a similar response but their range is not that drastic compared to the green highlighted sensors. It seems N+ Polysilicon heaters containing a bigger heater size area have a much accurate response.

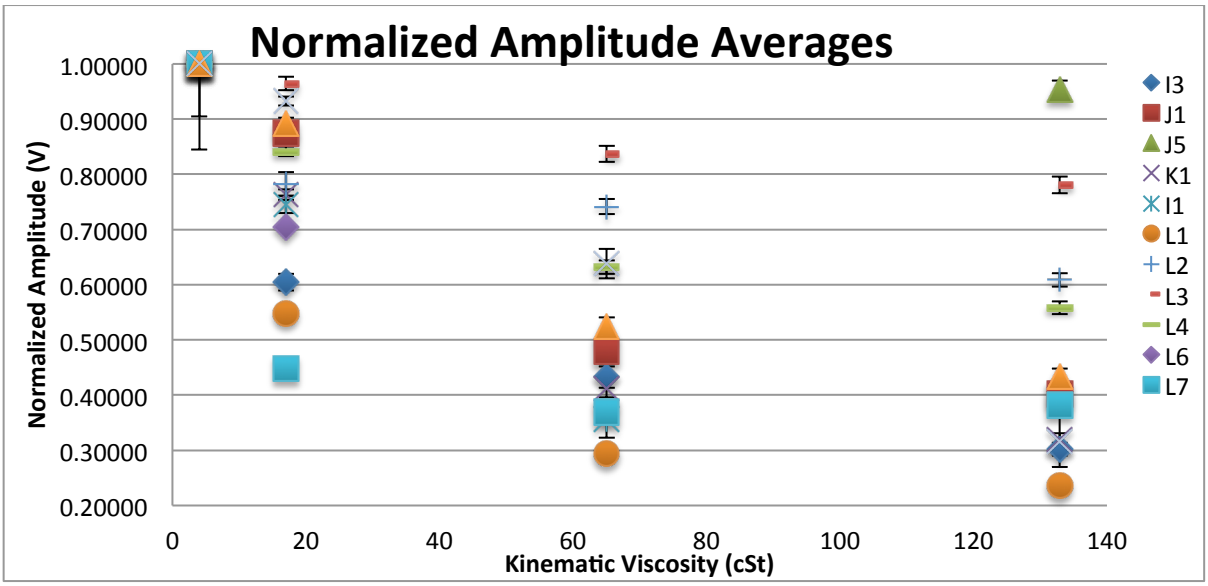

Figure 4.6 - Amplitude Variation with Different Sensor Characteristics in Different Oil Samples

In Figure 4.6 the normalized Vrms results shows a similar output. This measurement explains the deflections that the membrane is outputting referring it as the "amplitude" of vibration. Due to the increase in viscosity and the fluid being "thicker" causes the vibrations to decrease in theory and this is seen in the results with a negative slope. There is a little of controversy in some devices like J5, green triangle, L7, light blue square and L6, purple diamond. They do not follow the trend, the main reason for these errors are due to cleaning procedures which require removing the device and using wipes to remove the oils. Also the location of the sensor inside the vial is very important, as you place it inside the vial and keep it perpendicular to the table. Figure 4.7 shows a representation of how the sensor is badly position inside the vial.

Table 4.5 shows the predicted excel equations for each of the sensors and their R^2 values. The outcome of the R^2 values shows most of them have a 90%, which follows the predicted trend. Taking into account that the sensors that did not follow the actual trend are highlighted in red. They show a completely different response, showing increasing amplitude as viscosity increases. Sensors L6, L7 and J5 seem to have had a problem while recording the data at the time.

Table 4.5 - Predicted Excel Equations for Amplitude Results

ID	a size (mm)	Heater Size	Heater Type	Metal	Y =	R^2 =
L1	1.75	2	Poly	Yes	$1.7950x^{-0.422}$	0.99726
I3	2.5	2	P	Yes	$1.5763x^{-0.328}$	0.98747
L4	2.5	16	P	No	$1.3027x^{-0.171}$	0.98505
K1	1.75	16	P	Yes	$1.7282x^{-0.337}$	0.96782
I1	1.75	35	Poly	Yes	$1.8075x^{-0.369}$	0.93222
L3	2.5	35	P	No	$1.1358x^{-0.073}$	0.93099
L2	1.75	2	P	Yes	$1.1786x^{-0.128}$	0.93075
J1	1.75	2	Poly	Yes	$1.6176x^{-0.279}$	0.92798
L8	1.75	2	P	Yes	$1.5529x^{-0.252}$	0.92561
5B	1.75	2	P	Yes	$1.7935x^{-0.301}$	0.77725
L7	1.75	35	Poly	Yes	$1.2510x^{-0.275}$	0.82215
L6	1.75	35	Poly	Yes	$0.6402x^{0.1995}$	0.32553
J5	1.75	2	P	No	$1.0402x^{-0.006}$	0.0249

Figure 4.8 shows the variations in quality factor as viscosity changes from different sensors. Just like the predicted values, a negative slope is expected from each of the sensors since this measurement values the characteristic of the oils. This value can be used to compare the quality of the oils, and possibly rate them according to a specific standard. The measurements were very consistent in all the different sensors tested, showing that as viscosity increases the quality factor decreased. This shows that with increasing viscosity the value of Q largely decreased due to the properties of the liquid being more viscous. Most of the variations are seen in sensors L1, L2, L6, 5B and I3. Showing a bigger change in quality factor at each oil sample. They all have metal, and they are predominantly P+ diffused. But L1 and L6 both have a Polysilicon heater and similar to Puchades findings these types of heaters have a higher response of Q. In Table 4.6, the overall overview is that all sensors show a good result in terms of quality factor.

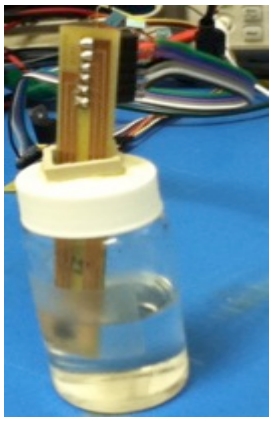

Figure 4.7 - Sensor Placed Inside the Vial in Wrong Position

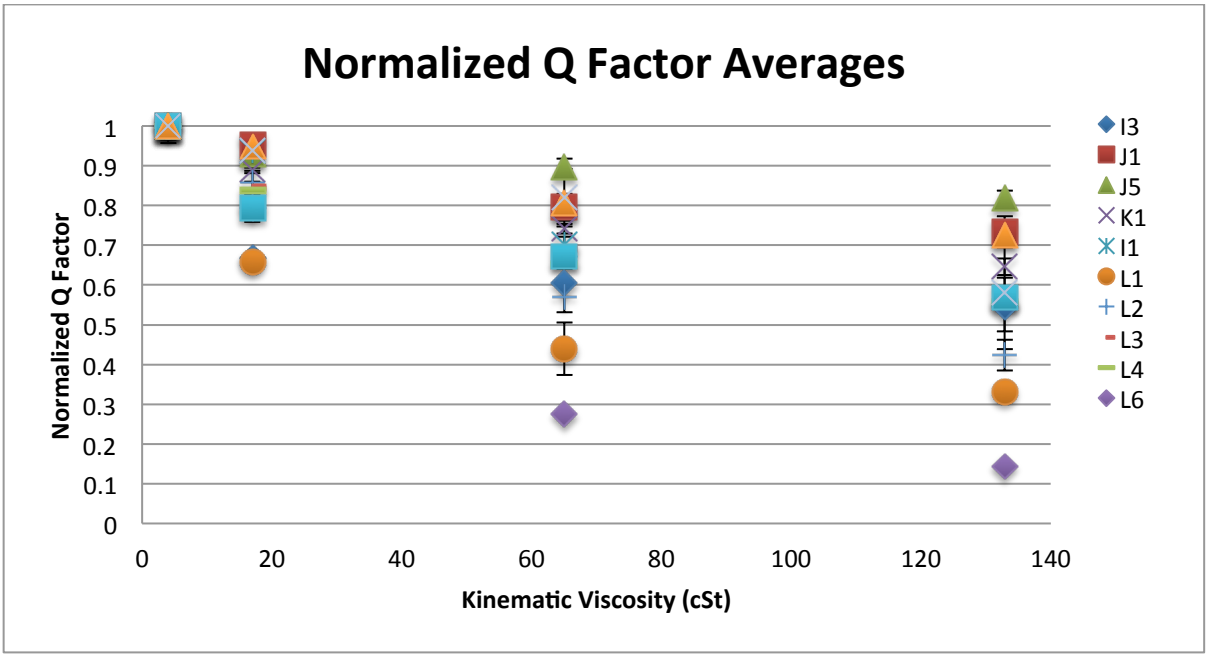

Figure 4.8 - Normalized Quality Factor with Sensor Variation Characteristics

Table 4.6 - Q Factor R^2 Theoretical Calculations

ID	a size (mm)	Heater Size	Heater Type	Metal	Y =	R^2 =
L1	1.75	2	Poly	Yes	$1.5677x^{-0.311}$	0.99677
L7	1.75	35	Poly	Yes	$1.2451x^{-0.156}$	0.99103
L4	2.5	16	P	No	$1.2969x^{-0.168}$	0.98471
K1	1.75	16	P	Yes	$1.2176x^{-0.123}$	0.97207
L3	2.5	35	P	No	$1.2965x^{-0.163}$	0.95724
L2	1.75	2	P	Yes	$1.5244x^{-0.245}$	0.93564
J1	1.75	2	Poly	Yes	$1.1727x^{-0.092}$	0.9341
L8	1.75	2	P	Yes	$1.1731x^{-0.092}$	0.93483
J5	1.75	2	P	No	$1.0797x^{-0.052}$	0.92785
I3	2.5	2	P	Yes	$1.1884x^{-0.166}$	0.92521
L6	1.75	35	Poly	Yes	$2.7400x^{-0.564}$	0.91294
I1	1.75	35	Poly	Yes	$1.2383x^{-0.126}$	0.86994

With the different results it is evidently that all sensors show an accurate response of their functionality.

The sensors utilized were also analyzed in different manners to find any other trends. Some showed very interesting results when comparing the L2T ratio with frequency. Figure 4.9 shows the described trend. With this it can be seen that besides splitting the sensors with their corresponding L2T ratio, the size of the heater also affects the results. According to the tests with the 4 different oils it is possible to find out the following results seen on

Table 4.7. Devices with the ratio of 116.7 and 175 show a higher output in frequency close to 10kHz – 13kHz. But the big difference between both ratios is the size of the heaters. For the 116.7 as you increase the size of the heater the higher the frequency output. On the other hand for the ratio of 175, as the size increases your frequency output decreases.

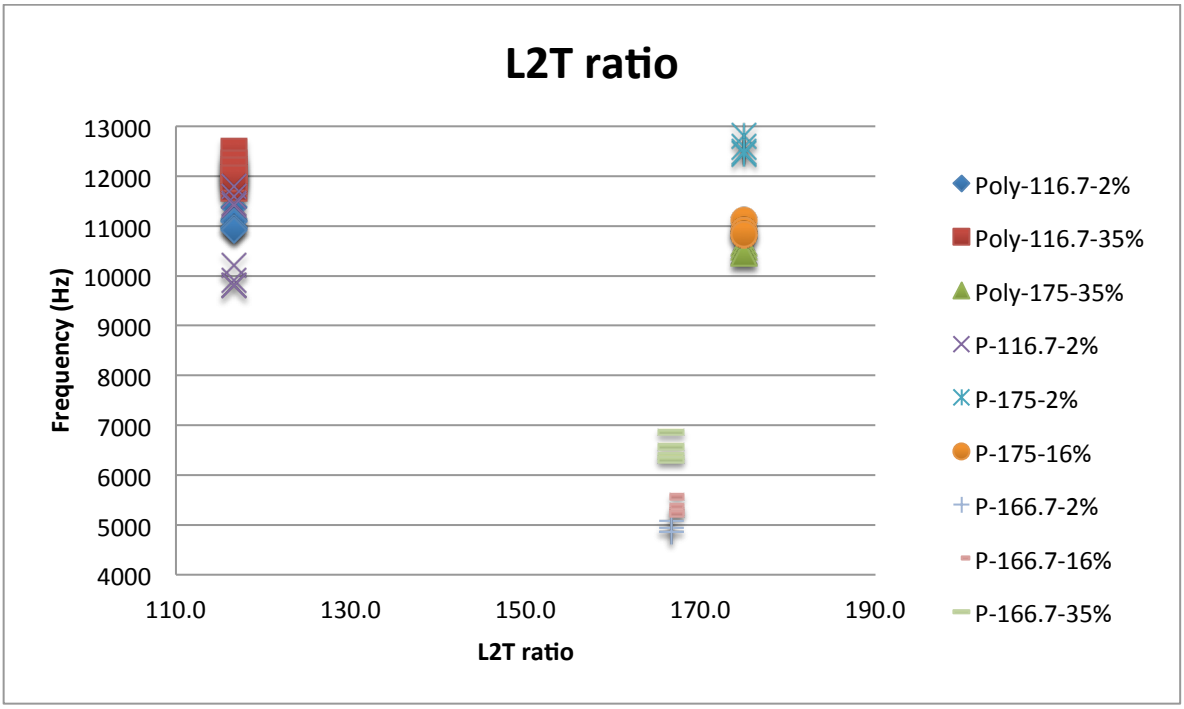

Figure 4.9 - L2T Ratio Versus Frequency

Table 4.7 - L2T Ratios Corresponding to the Heater Size

L2T Ratio	116.7	166.7	175
Heater Size	35%	35%	2%
	2%	16%	16%
		2%	35%

Frequency (Hz)

4.3.0 Parylene Coater Tool (Version 2)

With the results from the different sensors in oil, that proofed that the device works just like [1] explained. Finding similar trends like Puchades did, this work corroborates his findings. The next step for this sensor is to place it in a conductive liquid and see if it can work in the fluid.

Using the concept idea from Section 3.5.0, parylene C is chosen as the protective layer to cover the sensor and withstand the electrical currents from spreading inside the fluids under test. Some sensors were chosen to add a thin film of parylene C. A parylene coater made by Dr. Alan Raisanen and his team created a similar device like the

one from Specialty Coating Systems. This tool is found in the Chemical Mechanical Planarization Laboratory (CMP) in the basement of the Micro Electronic Engineering Building. With this tool it is possible to add a thin layer of the protective coating in order to prevent it from releasing its electrical currents to the fluid and causing the device to fail.

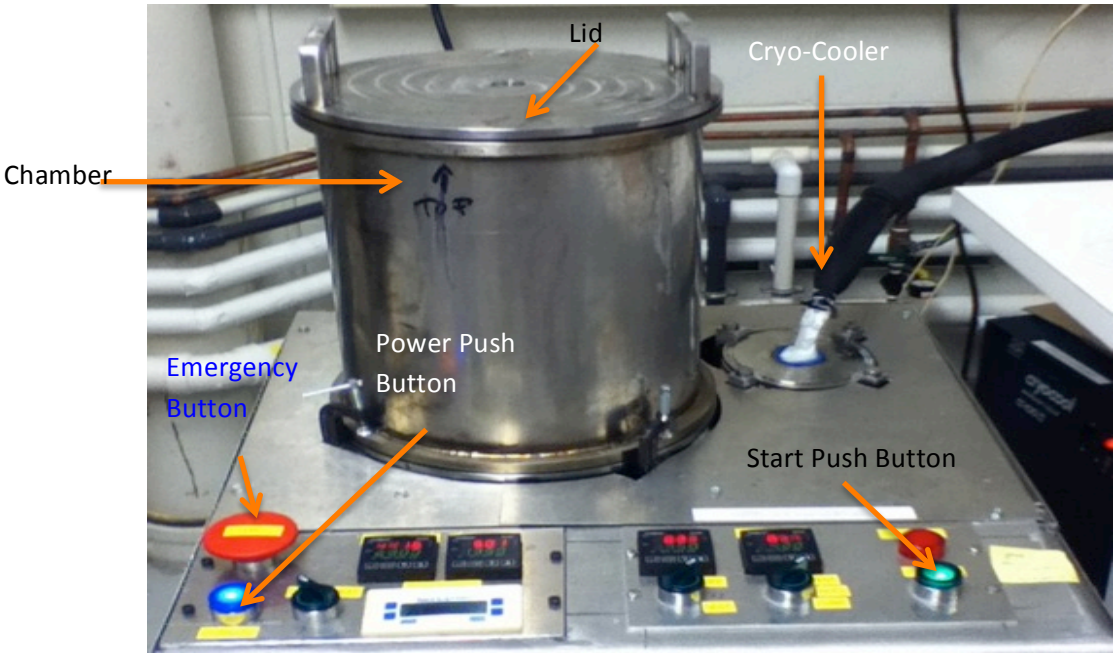

Figure 4.10 - Parylene Coater Tool Made in House by Dr. Alan Raisanen and his Team at RIT

The coating material Parylene – C it comes as a dimer substance from Specialty Coating Systems (SCS). It spreads as a conformal coating, meaning that it can adhere to any shape and it can be easily applied at room temperature as a vapor deposited polymer. This coating is widely used in the electronics industry, as it can withstand chemicals and has a very low water vapor transmission rate (WVTR) compared to conventional epoxy and other coating materials [41]. This is a very important factor for this project, because with such a low WVTR the device with such a thin film layer can theoretically withstand fluids, and not worry about the moisture produced from the heat and water content.

Figure 4.11 - Parylene C Dimer (Specialty Coating Systems)

The parylene coater is an easy tool to utilize, because it contains three different major steps throughout the entire process. The chemical aspect of this process involves the vaporization of the dimer (Di-Para-Xylylene) into a gas like substance at a temperature of 175°C. After this step is achieved the gas pyrolizes in vacuum, meaning that the dimers gas initializes a thermochemical decomposition of the material at a very high temperature (695°C) without the presence of oxygen. At this point the gas molecules have broken apart from being together as a couple to a single molecule or a monomer (para-xylylene). These gas molecules are kept at high temperatures so that it does not immediately polymerize with anything it touches due to the change in pressure and temperature through a free radical process. Which then leads to the final step of applying the monomer onto the device and produce a thin film layer added at room temperature (25°C) in vacuum. As the gas touches the device it produces a conformal thin film, which chemically changes the monomer to a polymer (poly (para-xylylene)). Figure 4.12 summarizes the different chemical steps as the dimer goes through the tool.

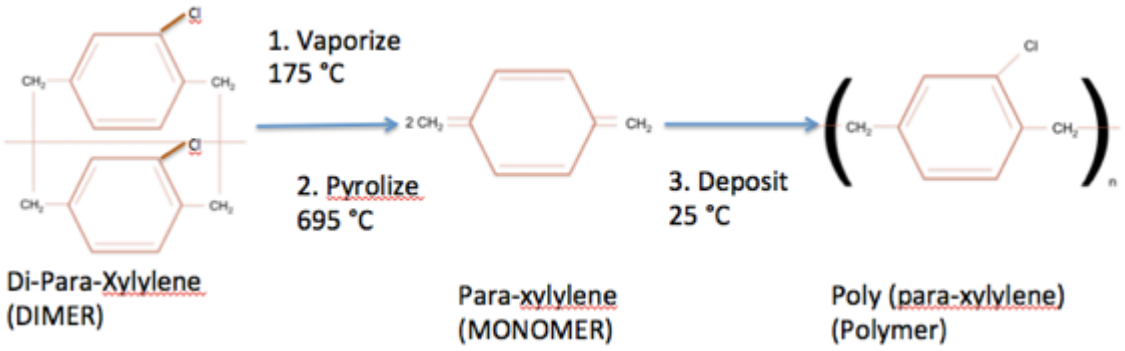

Figure 4.12 - Chemical Process Inside Parylene Coater Tool with Parylene C

In the Appendix section it is possible to find the instructions to use the Parylene Coater in the CMP laboratory.

4.3.1 Quick steps to operate the parylene coater tool

The tool requires to be cleaned thoroughly before putting the wafer or sensor inside the vacuum chamber. A re-agent, called Micro-90 is used which prevents the thin film from sticking to anything it comes in contact with. The chamber and the lid are presented in Figure 4.10, both the inside of the chamber and the bottom part of the lid, which faces the inside of the chamber have to be cleaned with a wipe and micro-90, see Figure 4.13. The evaporation chamber, which is covered with aluminum foil, also requires to be cleaned with a wipe and the reagent, see Figure 4.14.

Figure 4.13 - Micro 90, Reagent used to Prevent Thin Film from Sticking to Any Surface

After cleaning the lid of the evaporation chamber, a boat (Figure 4.15) is hand made from aluminum foil long enough to push through so that it reaches the end of the evaporation chamber. The parylene C container is taken into the SMFL to use the scale and weigh the mass of the dimer to later determine the thickness of the film.

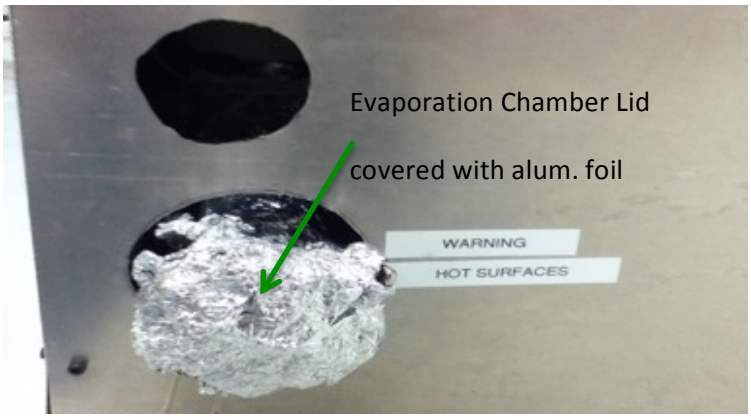

Figure 4.14 - Evaporation Chamber Covered with Aluminum Foil (Location for Boat with Parylene C dimer)

Smaller boats (Figure 4.16) are used on the scale, because of the space constraint compared to the actual size of the boat. And that is something very important to have in mind, a couple of times when measuring the dimer, the boat would flip over

Figure 4.15- Boats Hand Made from Aluminum Foil to Hold Parylene C Dimer Pellets

and the weight would change. This would make the user re-weight the same boat with the dimer because there would be pellets everywhere around the scale.

Figure 4.16 - Smaller Boat used to Weight Parylene C Inside Scale

One very important step not to skip before placing the wafer or the sensors inside the chamber is covering them with some adhesion promoter. Figure 4.17 shows the box of A-174 Silane, this helps parylene C adhere to the substrate. The sensors are placed inside a beaker with the solution, so that

Figure 4.17 - A-174 Silane, Adhesion Promoter (left), Sensor Inside Beaker with A-174 (right)

it evaporates at room temperature over night, like seen on right side of Figure 4.17. Then the sensor is taken out of the beaker, and placed inside the chamber together with a glass slide to be able to measure the thickness of the film and obtain an average, Figure 4.18.

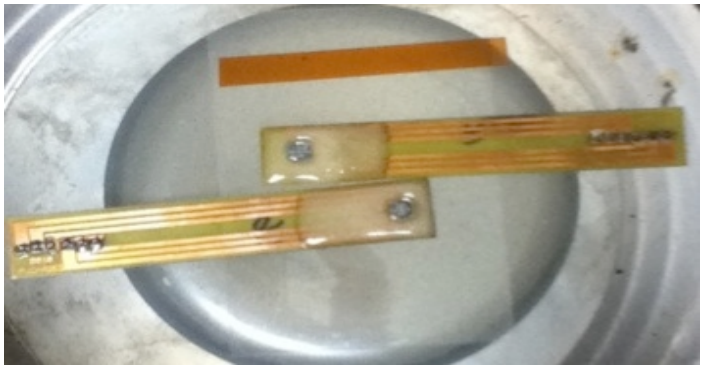

Figure 4.18 - Sensors Inside the Chamber Next to a Glass Slide

4.3.2 Determining thickness of Parylene C from 1st trial

The parylene coater tool uses x grams of Parylene C dimer in order to produce a thin film. Dr. Raisanen made a sample on March 17th, 2009 to have a reference value. He used 1.0 grams of Parylene C dimer at a pressure of 42 mTorr and produced a thin film coating measuring 0.8 µm. He also made a remark that it is very important to keep the surface area constant, at the time he used a 6" wafer. This value was used as a suggestion, and it was possible to calculate a thickness from the amount of grams used. The unlucky portion of this was that this was a sample made in 2009, but 3 years later the tool was down for many different reasons, thus a new calibration had to be ran.

With this in mind, a couple of runs were done in order to figure out the desired thicknesses, see Table 4.8. Keeping in mind that the pressure should remain constant, and also the number of samples placed inside the chamber itself. With the first run about 1.059 grams of Parylene-C dimer at 42 mTorr were used to create a thickness of 1.93µm. Since there is a relationship between the mass and the thickness a ratio was used, this can be seen in the following Eqs. 4.3 – 4.5.

$$\frac{1.059\ g}{x\ g} = \frac{1.93\ \mu m}{h_{desired}\ \mu m} \tag{4.3}$$

With a desired thickness of 0.3 µm.

$$0.3177 = 1.93x \tag{4.4}$$

$$x = 0.1646\ g\ of\ PAR - C \tag{4.5}$$

Once the ratio was established, it was possible to calculate the desired thicknesses of 0.3 µm, 0.6 µm, and 0.9 µm. These three values were chosen to help figure out the best thickness for the sensor to be submerged in the conductive fluid, also assuming that a maximum of 1.0 µm of Parylene C might not change the way the sensor

behaves. As a matter of fact adding a layer to the device would change the sensors operation. But the main question was if it would change its sensitivity and lead to drifting the results.

At the same time two other tests were run and Table 4.8 has the other measurements.

Table 4.8 - Testing Measurements for Thickness of Thin Film

M of Dimer (g)	*t* (µm)
1.095	1.93
0.476	0.526
0.317	0.3068

4.3.3 Measuring film thickness using Tencor P2

After applying the coating it was required to measure the thickness of the thin film, this was done by using the Tencor P2 Profilometer. This tool was located inside RIT's SMFL and just like the name states it is a profilometer. This means that a profilometer stylus inside the machine is used to detect the surface as it moves a long a given distance and measures the step heights. The tool can scan lengths up to 200mm and has a total step height of 100 Å up to 300 µm. For purposes of this project, this was enough because the maximum height expected from the thin film was about 0.3 µm – 1.0 µm. In order to be able to measure the thin film a special tape located in the materials box of the CVC 601 was used to help create a step height by removing this tape after the deposition of the thin film. Figure 4.19 and 4.20 show the tool and the film ready to measure thickness.

Figure 4.19 - KLA Tencor P2 Profilometer

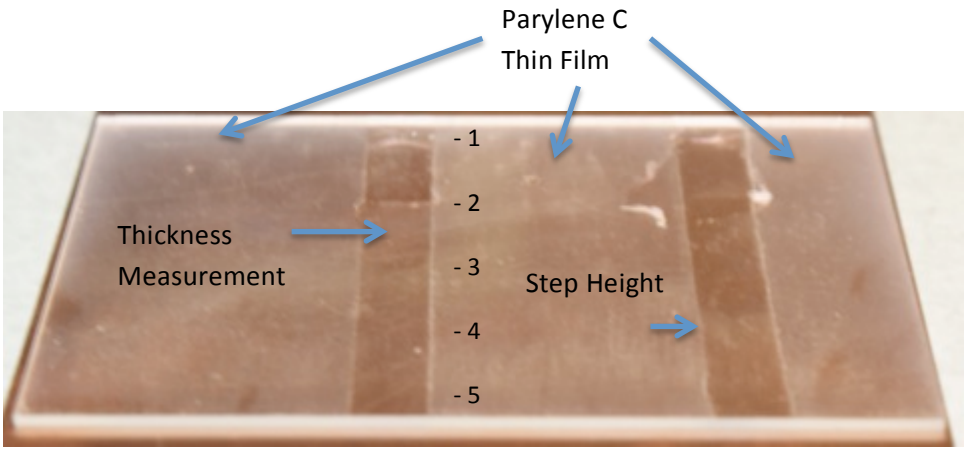

Figure 4.20 - Glass Slide for Thickness Measurements of Parylene C Runs

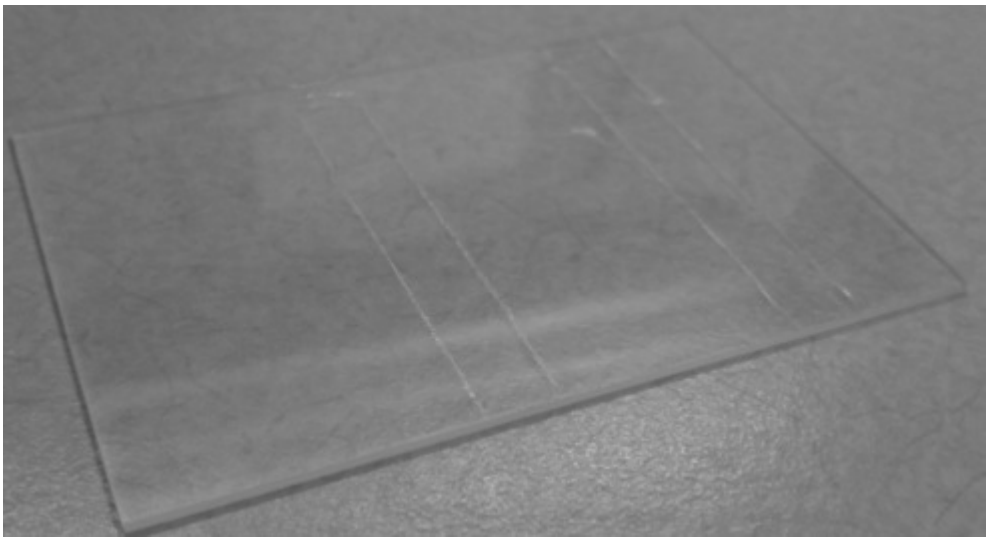

Figure 4.21 – Another Glass Slide for Thickness Measurements of Parylene C

After measuring the thickness of the film in at least 5-10 different locations along the step height. An average is obtained from all the values and it is possible to create a table with the information regarding the mass of the dimer, just like seen in Table 4.8. This method of measuring the thickness of the glass slide is the only possible way to be able to determine the actual thickness of the parylene coating on the sensor, otherwise it would be hard to measure the step height on the sensor because it would require to remove some of the added layer.

4.3.4 Determining Mass of Dimer required for specific thicknesses

Once the different trials were achieved, the results from Table 4.8 were taken into consideration and a theoretical equation was obtained applying a linear fit to the recorded data points using Excel. Figure 4.22 shows the measured results, and the equation used to determine the mass of the Dimer required, Eq. 4.6 which x represents the mass of Parylene C required to produce the desired thin film thickness, Y.

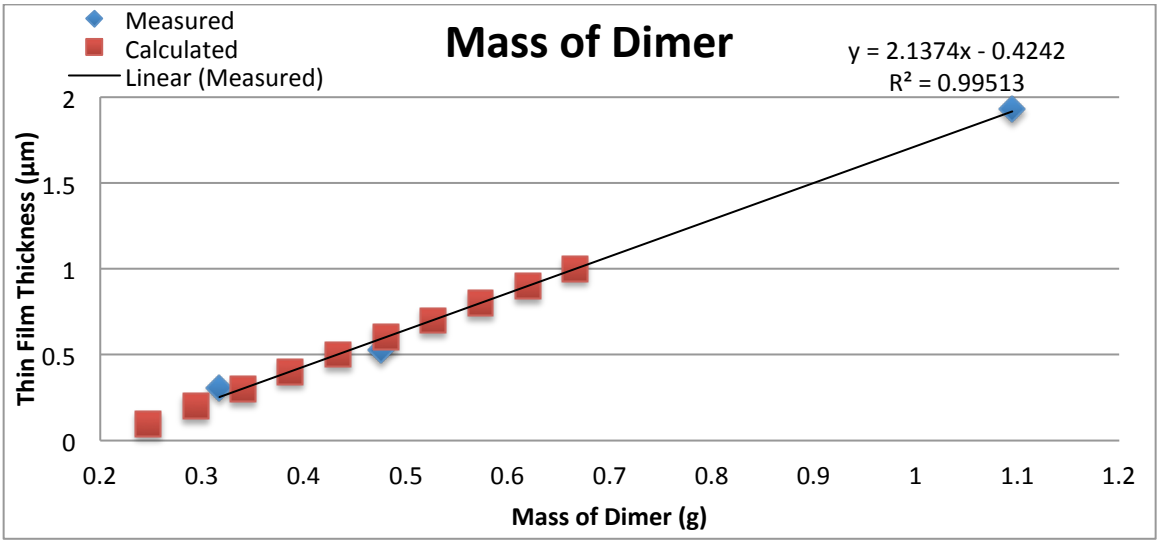

Figure 4.22 - Determining Mass Required of Parylene C for Desired Thin Film Thickness

$$Y = 2.1374x - 0.4242 \tag{4.6}$$

Calculations were done with equation 4.6 to figure out the mass of the dimer for the three different thicknesses. Table 4.9 shows the calculations and on Figure 4.22 the calculated values are also shown to hypothesize the required mass of parylene C. With equation 4.6 it is possible to assume that as long as the pressure is kept at 42mTorr on the tool, and the number of devices inside the chamber remains the same a desired thickness of 0.3 µm, 0.6 µm, and 0.9 µm can be achieved by using the required amount of mass pre-determined shown on Table 4.9.

Table 4.9 - Mass Required to Produce Desired Thickness of Thin Film

Desired Thickness (µm)	Required m (g)
0.1	0.247
0.2	0.294
0.3	**0.340**
0.4	0.387
0.5	0.433
0.6	**0.480**
0.7	0.527
0.8	0.573
0.9	**0.620**
1	0.666

4.3.5 Strength Test of Parylene C Thin Film

Now that the film can be added to the sensors, and a couple of runs have been made to provide feedback information on how to correctly add this layer, it is important to test the thin film and see its future points of failure. Especially when the sensor will be subject to various testing methods, it requires for the thin film to go through a very scrutinous strength test process.

The viscosity sensor undergoes different cleaning procedures, thus it is important to understand if the film will withstand them. The cleaning steps for the sensor done between each of the tests includes using a wipe and Isopropyl Alcohol (IPA). This soft wipe is also used together with water and an extra wipe with more IPA. This helps remove the oil residues on the sensor and makes the sensor ready for testing for the next oil test. The glass slide undergoes a similar clean up procedure, first IPA is added to it and a soft wipe is used to remove any impurities (aka oil residues), then water is used on top to clean it. Similarly the oil is seen to dissipate from the film itself and can now be re used for testing. If there is still some residue left, redo the previous step as many times as you can until there is no more oil visible.

Thus cleaning the thin film of parylene C does not get affected from the cleaning procedure, as long as there is no crack visible. If there is a crack just like seen in Figure 4.23, then the film is expected to fail, and the sensor will stop working.

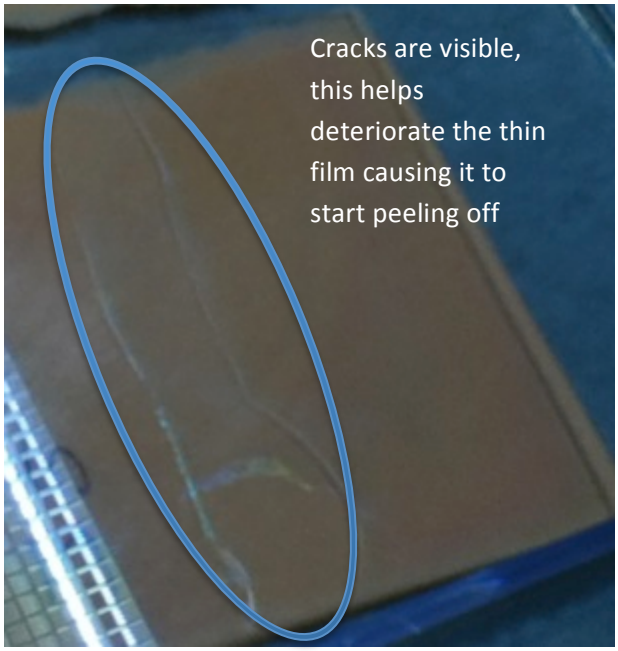

Figure 4.23 – Visible Crack Causes Cleaning Problems

4.3.6 Testing protective layer on a different sensor in a conductive fluid

Different sensors were chosen to test the protective layer of parylene C in order to prevent damaging the actual viscosity sensors. They are resistors and similarly with the same concept from the heater of the viscosity sensor, a current is produced from the voltage applied to the resistor. In this case a voltage is applied to the resistor

to produce a current. This will help determine how much heat the film could withstand and if there would be any problems if the sensor were tested in different oils.

These sensors are shown in Figure 4.24, which are made on glass and they are designs from a different research project. The main idea taken from these sensors is that they have a resistor design on them made out of nickel, with a little bit of chrome as an adhesion promoter. The design involved steps of evaporation and lift off in order to make these sensors. There were two designs the device on the left sensor 15 had a resistance of 6,121 Ω, where as sensor 13, on the right had a value of 72,114 Ω. With this if voltage is applied to the resistor then current is created. Assuming this worked it would be possible to simulate the heaters reaction to the thin film of Parylene C.

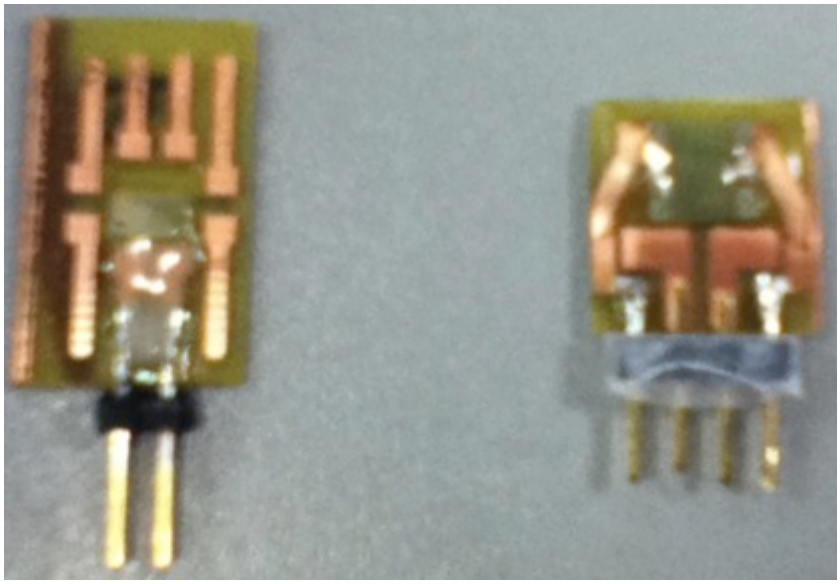

Figure 4.24 - Resistor Design from Nicholas Liotta

A protective thin film layer of Parylene C was added to both of them, their thickness measured 0.7311 μm, Figure 4.25 shows the two sensors before adding the protective film inside the chamber. This would help determine whether the protective layer would dissipate the water vapors from the electrical currents present on the device. An overview of how the electrical schematics would look like for this sensor looks just like Figure 4.26.

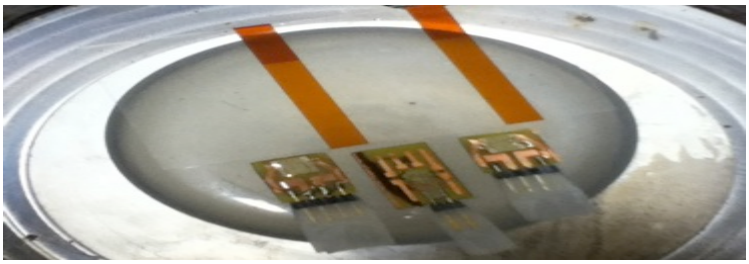

Figure 4.25 - Three Dummy Sensors to Test Thin Protective Film

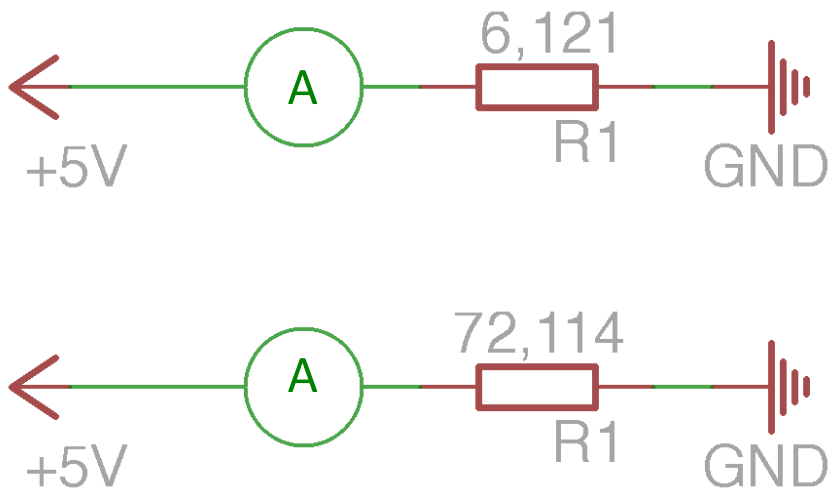

Figure 4.26 - Electrical Schematics for Testing Heater like Devices in Deionized Water

The previous electrical schematics shows the power supply connected to the resistor and an ammeter in series to measure the current going through the circuit. The resistor is where the sensor would be going and that would help determine whether the thin film is helpful or not. If the ammeter gives a reading of zero current then the sensor is touching the water and electrical currents are spread throughout the liquid, invalidating the circuit.

Each of the sensors were placed in each of the oils for a period of 5 minutes per oil and they worked fine, this was already previously proven since oil does not really conduct any electricity. On the other hand de ionized water was used as a conductive fluid sample and a 1 volt was applied every ten minutes. The results are shown in Table 4.10, the test setup and test trials can be seen in Figure 4.27.

Table 4.10 - Test Results of Sensors with Parylene C in Oils and Deionized Water

R = 6,121 Ω			
15	V (V)	I (mA)	Time (min)
Liquids	1.00792	0.1649	5:00
S3	1.00792	0.1649	5:00
N10	1.00735	0.1647	5:00
N35	1.00708	0.1646	5:00
5W30	1.00676	0.1645	5:00
DI H2O	1.03505	0.1698	124:00
DI H2O	2.00110	0.3265	10:00
DI H2O	3.00140	0.489905	10:00
DI H2O	4.00670	0.654937	10:00
DI H2O	5.01430	0.818303	12:05

R = 72,114 Ω			
13	V (V)	I (mA)	Time (min)
Liquids	1.00749	0.0139	5:00
S3	1.00745	0.0139	5:00
N10	1.00729	0.0139	5:00
N35	1.0072	0.0139	5:00
5W30	1.00671	0.0138	5:00
Air	1.0223	0.1665	2:00
DI H2O	1.00572	0.1644	10:00
DI H2O	1.01745	0.1665	13:05
DI H2O	2.0281	0.3315	10:15
DI H2O	3.0514	0.4982	10:05
DI H2O	4.0828	0.6666	10:15
DI H2O	5.0179	0.8183	10:25

Sensors worked in deionized water, a current is present in the circuit and sensor 15 was tested for about 2 hours without having any problems with the conductive liquid. This proves that the protective coating film works for underwater purposes.

Figure 4.27 - Sensor 15 with Parylene C Coating Testing in Deionized Water

4.3.7 Theoretical Calculations of adding a layer of Parylene C

Adding a layer of parylene C changes the sensors thickness, thus producing a different value for frequency, q factor, and amplitude. Eq. 4.7 shows a relation of radian frequency, Wn ($\frac{rads}{sec}$) is equal to the stiffness of body or spring constant ($\frac{N}{m}$), k divided by the mass, m in kg. This equation will show a relationship and help prove whether the mass or the spring constant help determine the angular frequency.

$$W_n^2 = \frac{k}{m} \tag{4.7}$$

As a matter of fact a better relationship found within the natural frequency, f is determined if we combine Eqs. 4.8 and 4.9 we are able to use the term of $\frac{1}{2\pi}$ to discard the radian units and obtain Eq. 4.10.

$$\omega = 2\pi f \tag{4.8}$$

$$f = \frac{1}{2\pi} W_n \tag{4.9}$$

$$f_n = \frac{1}{2\pi}\sqrt{\frac{k}{m}} \tag{4.10}$$

With these equations it is possible to theoretically find the changes to the diaphragm as the thickness and weight change with the addition of the protective layer. Eq. 4.10 can be used to obtain a relationship between the mass and the spring constant, see Eq. 4.11.

$$f_n \propto \sqrt{\frac{k}{m}} \tag{4.11}$$

$$k = \frac{AE}{L} \tag{4.12}$$

Within Eq. 4.12 the spring constant, k we are able to find a more detailed analysis of what is going to change the value of frequency. Were A, is the cross sectional area, E is Young's Modulus, and L is the length of the sensor. Figure 4.28 shows a description of all the values involving the changes according to the spring constant and the layer of Parylene C.

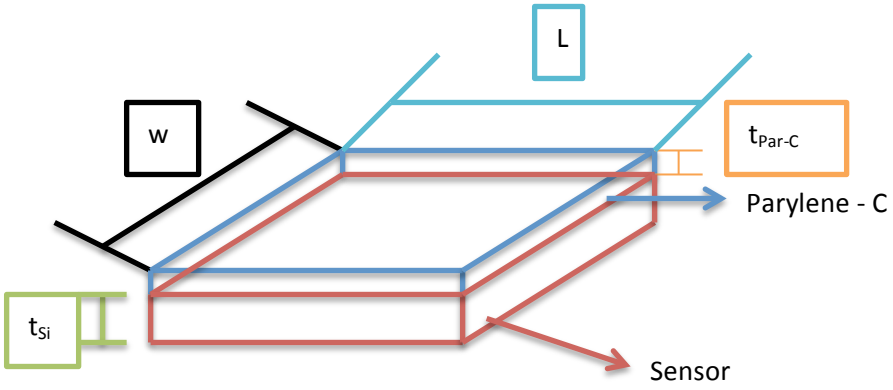

Figure 4.28 - Sensor View After Adding a Thin Layer of Parylene C

With Eq. 4.12 we also get A, the cross sectional area of the device, which in this case is represented by Eq. 4.13.

$$A = tw \tag{4.13}$$

where t, is the thickness of the diaphragm, and w the length of the area is multiplied by each other. As a matter of fact in order to obtain the mass for the sensor it is required to define the different materials, one is the mass of parylene C, $m_{Par\text{-}C}$ and the second one is the mass of silicon, m_{Si}. For this it is required to involve volume, because of the space it takes, where this represents the length by the width by the height. Since we are using a square diaphragm

we can assume that length and width are both the same values. The next set of equations 4.14 - 4.19 will help understand the relationship behind the spring constant and the mass.

$$V = L\ x\ w\ x\ h \tag{4.14}$$

where *L*, is the length of the diaphragm, *w* is the width, and *h* represents the thickness of either silicon or Parylene C, just like seen in Figure 4.28. Once the concept of volume is established, the mass can be related to density with Eq. 4.15 where *m* is the mass of the layer, *V* is the volume of the area, and ρ, is the density of the material.

$$m = V\rho \tag{4.15}$$

$$m = At\rho \tag{4.16}$$

With Eq. 4.16 it is possible to calculate the mass for the silicon and the parylene with their corresponding density and Young's Modulus values found in Table 4.11.

Table 4.11 – Density and Young's Modulus of Silicon and Parylene C

	Si	Par-C
ρ (g/cm^3)	2.32	1.29
E (Pa)	1.50E+11	2.76E+09

At the same time the spring constant has its own relationship between its values, using Eq. 4.13 and substituting to Eq. 4.12 it is possible to equate Eq. 4.17 and reduce it to a relationship of Eq. 4.18 assuming *w* and *L* represent a equal sided square.

$$k = \frac{twE}{L} \tag{4.17}$$

$$k = tE \tag{4.18}$$

Using the proportionality previously found in Eq. 4.11 we can now say that it can be read like Eq. 4.19 where we take into account the two different materials added.

$$f_n \propto \sqrt{\frac{k}{m}} \approx \frac{k_{Si} + k_{Par-C}}{m_{Si} + m_{Par-C}} \tag{4.19}$$

Using Eqs. 4.13 – 4.18 it is possible to start calculating the mass and the spring constant to figure out which one will be the one affecting the frequency change. Focusing on two types of sensors with lengths 1.75mm, 2.5mm and thicknesses of 10μm and 15μm.

Table 4.12 - Volume Calculations for Relation with Mass

Length (mm)	Area (cm^2)	Volume Si (cm^3)		Volume Par-C (cm^3)			
		10µm	15µm	0.3µm	0.6µm	0.9µm	1.0µm
1.75	0.030625	3.06E-05	4.59E-05	9.19E-07	1.84E-06	2.76E-06	3.06E-06
2.5	0.0625	6.25E-05	9.38E-05	1.88E-06	3.75E-06	5.63E-06	6.25E-06

Table 4.13 - Mass Calculations Using Data from Previous Table

Length (mm)	Mass Si (µg)		Mass Par-C (µg)			
	10µm	15µm	0.3µm	0.6µm	0.9µm	1.0µm
1.75	71.050	106.575	1.185	2.370	3.556	3.951
2.5	145.000	217.500	2.419	4.838	7.256	8.063

Table 4.14 - Spring Constant Calculations

	K for Si (Mega N/m)		K for Par-C (Mega N/m)			
	10µm	15µm	0.3µm	0.6µm	0.9µm	1.0µm
K (N/m)	1.50	2.25	0.000828	0.001656	0.002484	0.002760

With Tables 4.11 and 4.12 it is possible to calculate the information presented in Tables 4.13 relating the amount of mass added in silicon compared to parylene C. With those theoretical calculations it is possible to see that adding a thicker layer will add more mass. As for the spring constant, Table 4.14 shows that the calculated values vary slightly. This comparison can be seen in Tables 4.15 and 4.16, which show a percent (%) change difference between Silicon and Parylene C.

Table 4.15 - Mass Percent Change According to their Lengths and Thicknesses

		% Change for m @ 1.75mm		% Change for m @ 2.5mm	
		10µm	15µm	10µm	15µm
Thickness of Parylene	0.3µm	1.7	1.1	1.7	1.1
	0.6µm	3.3	2.2	3.3	2.2
	0.9µm	5.0	3.3	5.0	3.3
	1.0µm	5.6	3.7	5.6	3.7

Table 4.16 - Spring Constant Percent Change with Respect to Thickness of Parylene C

		% Change for K	
		10µm	15µm
Thickness of Parylene	0.3µm	0.055	0.037
	0.6µm	0.110	0.074
	0.9µm	0.166	0.110
	1.0µm	0.184	0.123

Overall the m_{Si} and $m_{Par\text{-}C}$ correspond to the biggest factor changes with respect to the frequency. Thus using Eq. 4.19 the denominator has the biggest variation, meaning that as a thin layer of Parylene C is added to the sensor the thickness of the diaphragm changes and mass gets added. With these factors it is possible to understand that there will be a frequency variation due to the mass, and not the spring constant.

4.4.0 Testing Sensors with Parylene C in Air

This section compares output values of frequency and quality factor from viscosity sensors without a thin layer of Parylene C to the same sensors with the protective layer version 2. Before placing the sensors in a conductive fluid, the sensors were tested in air an environment that would not require damaging their functionality, assuming the protective coating does not behave as expected. The sensors characteristics are compared in Table 4.17.

Table 4.17 - Information on Sensors with Parylene C

ID	Wafer	h_{Si} (µm)	a (mm)	Metal	t ParC	Heater		Calc Fo Air (Hz)	Calc FoP Air (Hz)
						Type	% Size		
I3	4	15	2.5	Yes	1.93	P	2	20,605	23,256
K1	5	10	1.75	Yes	0.526	P	16	28,034	29,508
J1	4	15	1.75	Yes	0.3068	Poly	2	42,050	42,910
J5	4	15	1.75	No	0.4091	P	2	42,050	43,197
L6	4	15	1.75	Yes	0.662	Poly	35	42,050	43,906

Only 5 sensors are tested in air to understand how adding a thin film of parylene C affects the output. Table 4.18 shows the results obtained from the sensors output in terms of frequency and quality factor.

Table 4.18 - Information on Output of Sensors

ID	Air @ Room Temp					
	No ParC		With ParC		% Chng Fo	% Chng Q Factor
	Fo (Hz)	Q_Factor	Fo (Hz)	Q_Factor		
I3	30601	11	28274	13	7.60	-18.18
L6	63343	12	62777	19	0.89	-58.33
K1	77582	15	78546	22	-1.24	-46.67
J1	58247	35	58583	23	-0.58	34.29
J5	51260	16	52172	20	-1.78	-25.81

Decrease
Increase

After adding Version 2 of the protective layer, sensors I3 and L6 show a decrease in frequency with a change of 7.6% and 0.89% correspondingly. I3 seems to have the biggest % change, but that seems because it has the thickest thin film from all sensors tested. At the same time it has a small sized resistor but it is the biggest in terms of length of the diaphragm, *a*. Comparing Table 4.17 and 4.18 we can see that the theory suggests that the frequency should increase. In this case it shows the opposite, the only two reasons in mind are during the fabrication

steps the values can vary slightly and change the theoretical thickness and length size of the diaphragm. Also when packaging, placing the sensor right on top of the hole of the PCB and adding epoxy to the surrounding areas can affect the sensors output. Sensors K1, J1 and J5 show the opposite, their frequency increases slightly this is shown on the second to last column as a negative change.

The quality factor changes are all relatively similar by which they increase in value, showing a negative % change presented in the last column of Table 4.18. But for the exception of J1 the % change is positive and the value decreases instead.

Overall the protective layer definitely changes the sensors characteristics due to the influence of the mass just like previously explained in Section 4.3.7. At the same time parylene C is known to be flexible, but also adds a stiffness factor that reduces the frequency of vibration. So far the thickest coating added to the sensors measures 1.93μm and the sensor operates without any problems.

4.5.0 Comparison between sensors before and after Parylene C layer

In this next section the sensors previously tested in air, presented in Section 4.4 were used with the new protective coating to measure the four different oil standards. These tests were done to compare the sensors output before and after adding the protective layer. There will be obvious changes seen on the output, like previously seen from the tests in air. Therefore some calculations were applied to the main equations to see what is expected from the changes in oil. This is where Eq. 2.30 from Section 2.2.0 is used to determine the frequency of the sensor inside the fluid.

In theory in terms of the virtual mass, β, they vary slightly since Lamb's does not take into account the use of viscosity while Kozlovsky's does. This factor is very important, because it helps compare a different range of viscosities. In theory using Lamb's equation helps understand the changes in frequency for viscosities of less than 10cP [Ayela & Nicu]. On the other hand Kozlovsky's theoretical equation is better applied to those above 10cP [Kozlovsky Paper]. The main reason is that once the liquid passes that value Lamb's model starts to shift away from the trend and the factor of viscosity is taken into account because membrane in the MEMS industry are extremely thin.

The four standard oils tested, vary from 3.3cP – 117.8cP thus Lamb's and Kozlovsky's equations will be used accordingly. The results are observed in Figure 4.4 showing the different sensors theoretical calculations with both theories applied to them. Table 4.19 shows the sensors characteristics used for comparison of the before and after the protective layer with the measured thicknesses, thus changing the total thicknesses.

Table 4.19 - Information on 3 Sensors with Protective Layer Version 2

Device	h_{Si} (µm)	a (mm)	Metal	Heater		Bridge Resistor	L2T	t PAR-C (µm)	New L2T
				Type	Size (%)				
I3	15	2.5	Yes	P	2	Poly	166.7	1.9300	147.7
5B	15	1.75	Yes	P	2	Poly	116.7	0.8917	110.1
K1	10	1.75	Yes	P	16	Poly	175.0	0.5260	166.3

A similar procedure was done to obtain these results, just like previously done to obtain the viscosity measurements from sensors without Parylene C. Every sensor was placed in each vial for 20 minutes to obtain the corresponding data. With this the values were gathered, analyzed and the values were normalized.

Figure 4.29 shows the comparison between sensors I3, K1, and 5B before and after adding parylene C. Each sensor is separated between red and blue lines, they represent the devices without parylene C and devices with parylene C respectively. The red lines show a higher normalized value compared to those with Parylene C (blue lines), thus it clearly shows that devices with a layer of Parylene C will decrease the outputs frequency at different viscosities.

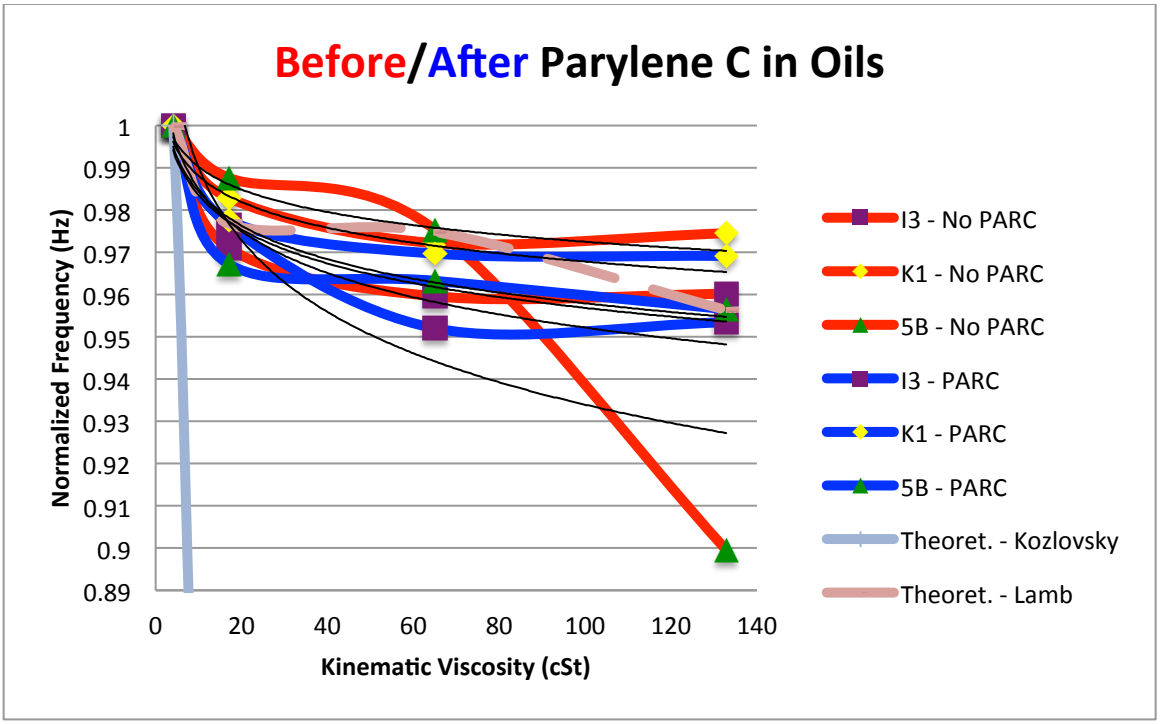

Figure 4.29 – Normalized Frequency Response of Sensors Before and After Parylene C

Theoretical calculations for the sensors have been applied using Lamb's and Kozlovsky's theories. For each of them the values increase in their frequency respectively, as the devices add a protective layer of Parylene C. But at the same time in Section 4.3.7 it is possible to see that the mass is the value that influences in the frequency variation, thus a thicker layer of Parylene C will definitely involve in affecting the results.

A similar analysis is applied to the results presented, in comparison with the theoretical results. Where a power law fit is applied to the results, to analyze and understand any trends. Table 4.20 contains information on an applied trend line using excel to theorize an equation relating to the power fit. This seems to be the best choice to theoretically approach the results because as the normalized frequency decreases viscosity increases. Thus the table is represented by a negative curve and depending on the characteristics of the sensors its frequency value will change. They all have a trend that shows a similar negative slope, it has a range between 0.008 – 0.025.

Together with the results presented in Figure 4.29 it is possible to see that for the four different oils the best-fit line achieved through both theories, is Lamb's approach. The different values of R^2 help understand how close data was to Excel's calculations, it shows that sensor 5B has a varied response. This can be seen in Figure 4.29 and Table 4.20 by showing a value of .669, this is pretty low in comparison with the rest of the results. Sensor 5B varied quite a lot in frequency response between N35 and 5W30. This helps comprehend that the oils viscosity are definitely not alike, and the liquid definitely became more viscous. This causes the sensor to produce fewer vibrations as it is placed inside the vials with increasing viscosities.

Table 4.21 shows the sensors with Parylene C and their corresponding power law fit. The negative slopes on both tables do not vary that much, and they seem to be on the same range. Also comparing the R^2 values the results from 5B definitely improved its response when adding the protective layer of Parylene C. This proves that it is very important to keep the testing setup as similar as possible every time it is tested. Similarly the sensors output seems to change with the increase in diaphragm thickness, which varies its output response.

Table 4.20 – Normalized Frequency Power Law Fit Applied to Data in Oils to Devices with No Parylene C Layer

ID	Y =	R^2
5B	$1.0497x^{-0.025}$	0.66941
I3	$1.0115x^{-0.012}$	0.88994
K1	$1.0083x^{-0.008}$	0.89748

Table 4.21 – Normalized Frequency Power Law Fit Applied to Data in Oils to Devices with Parylene C Layer

ID	Y =	R^2
5B	$1.0109x^{-0.012}$	0.86908
I3	$1.0189x^{-0.015}$	0.95281
K1	$1.0087x^{-0.009}$	0.89382
Theory Lamb	$1.014x^{-0.011}$	0.89687

With the V_{rms} results it is possible to see the trend with bigger variations throughout the different oils as it shows a measure of the amount of energy dissipated by viscosity, Eqs. 2.27, 2.28. The trends are similar to those previously discussed, and show a common result through out the power law fit equations presented in Tables 4.22 and 4.23. As the devices are submerged in the different oils, and the amplitude is recorded, it shows all sensors regardless of their characteristics with Parylene C have a higher energy dissipation compared to those without the protective layer. This can be seen as more mass gets added to the diaphragm there is that change which affects the frequency, shown in Section 4.3.7. With changes occurring to the frequency, similar changes can be seen occurring to the sensors quality factor and V_{rms} amplitude.

Also when gathering data for sensor K1, an issue appeared when testing it in 5W30 oil, which relates to the straight curve presented in Figure 4.30. This result does not follow the trend, because of the wrong data point for that oil, which relates back to the position of the sensor in the vial and the cleanliness of the sensors area. It does show a decrease of amplitude as viscosity increases which definitely agrees with the theory and overall trend.

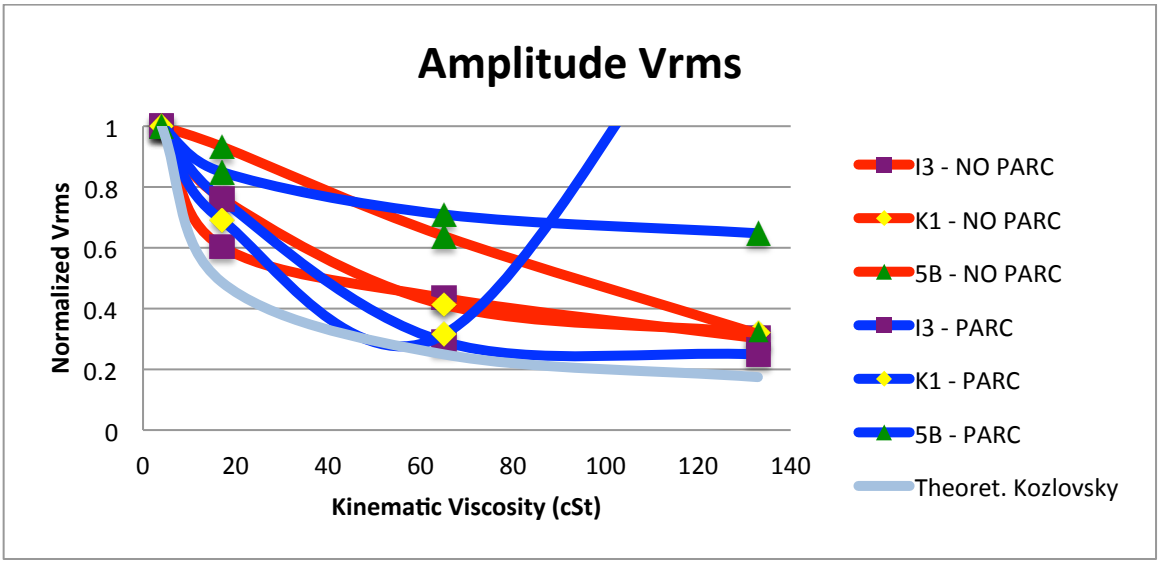

Figure 4.30 - Normalized V_{rms} of Sensors Before / After Parylene C

Table 4.22 – V_{rms} Power Law Fit to Data on Sensors with No Parylene C

ID	Y =	R^2
5B	$1.7935x^{-0.301}$	0.77725
I3	$1.5763x^{-0.328}$	0.98747
K1	$1.7282x^{-0.337}$	0.96782

Table 4.23 - V_{rms} Power Law Fit to Data on Sensors with Parylene C

ID	Y =	R^2
5B	$1.1978x^{-0.125}$	0.99859
I3	$2.0458x^{-0.434}$	0.93817
K1	$0.7678x^{-0.0051}$	0.00012

For results pertaining quality factor, a similar result was seen as different oils were tested, the quality factor change would be more spontaneous. For sensors I3 and K1, the values of Q would increase after adding the layer of Parylene C. This relates to the mass added to the device, as more mass is present on top of the diaphragm, Q is enhanced due to the flexibility of Parylene C. On devices with a value L2T > 166.7 show a increase in Q, on the other hand devices with a value L2T < 166.7 have a decrease.

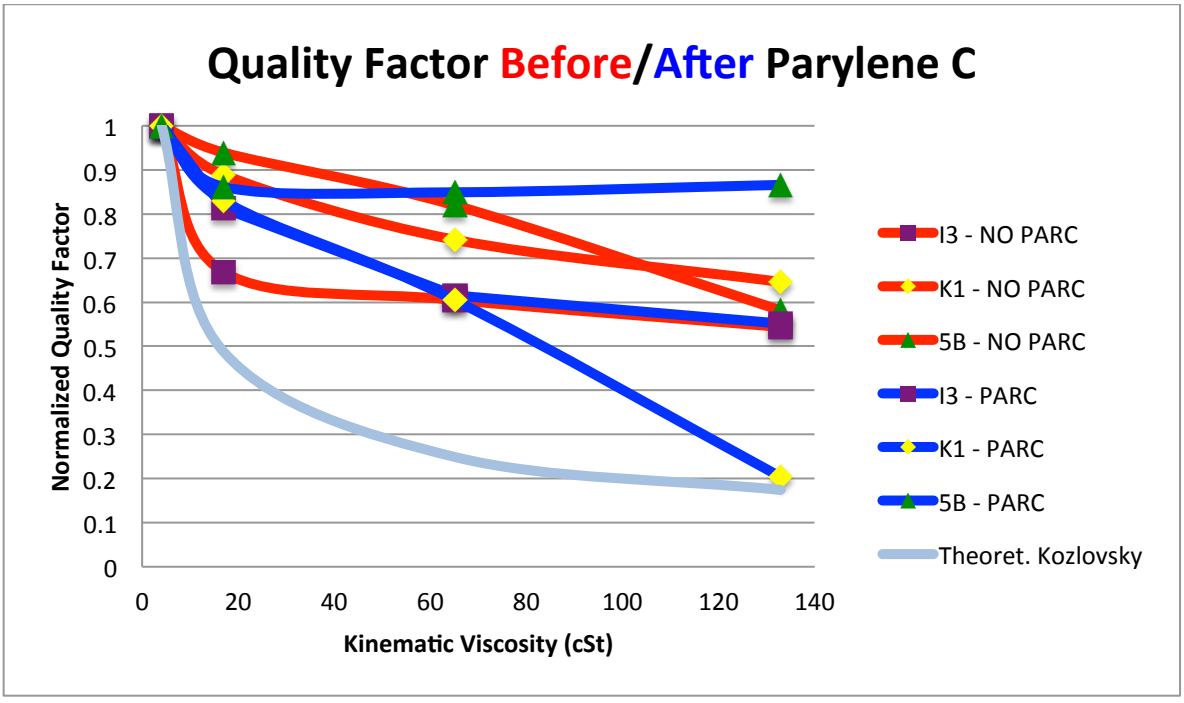

Figure 4.31 - Normalized Q Factor of Sensors Before / After Parylene C

Tables 4.24 and 4.25 show the power law fit equations for each of the sensors with no parylene C and the same sensors with parylene C with respect to their Q output response. In Table 4.24 the slopes show a similar negative trend, since all the sensors have a P+ diffused resistor for the heater and they all have aluminum metal on top of the diaphragm. This has been previously shown to help the outputs response in [1] were a comparison between devices with metal have a better Q than those without them.

Table 4.24 - Normalized Q Power Law Fit to Sensors with No Parylene C

ID	Y =	R^2
5B	$1.2956x^{-0.138}$	0.77712
I3	$1.1884x^{-0.166}$	0.92521
K1	$1.2176x^{-0.123}$	0.97207

Table 4.25 - Normalized Q Power Law Fit to Sensors with Parylene C

ID	Y =	R^2
5B	$1.0218x^{-0.041}$	0.67728
I3	$1.2938x^{-0.174}$	0.994
K1	$2.1104x^{-0.396}$	0.73847

Table 4.26 shows the frequency percentage change with respect to the devices without Parylene C to the results with Parylene C. This gives an overview that sensors I3 and K1 had a positive change, which resulted in a decrease with respect to the sensors having a layer of Parylene C. On the other hand sensor 5B with the addition of parylene C had a negative change, increasing the sensors frequency response. Every single sensor has different characteristics, but their differences are seen in their L2T ratios.

Table 4.27 shows the opposite response compared to that from frequency change. Sensors I3 and K1 show a negative percentage change which is an increase in quality factor values, where as sensor 5B shows a positive change showing an actual decrease in Q values. Overall all devices show a percent change of about 50% in the negative or positive direction.

Table 4.26 - Frequency % Change with Increasing Viscosity for Sensors with and without Parylene C

	Fo (Hz)			
Oil	Kin. Visc.	I3 % change	K1 % change	5B % change
S3	4.035	3.47	0.78	-14.24
N10	17.01	2.92	1.32	-11.87
N35	65.07	4.23	1.04	-12.82
5W30	132.91	4.15	1.33	-21.48

Table 4.27 - Quality Factor % Change with Increasing Viscosity for Sensors with and without parylene C

	Q Factor			
Oil	Kin. Visc.	I3 % change	K1 % change	5B % change
S3	4.035	-56.74	-51.65	46.76
N10	17.01	-90.81	-41.53	51.16
N35	65.07	-59.41	-23.62	44.83
5W30	132.91	-58.91	52.17	20.70

With these tables it is also possible to see the effect of adding parylene C to the sensor, it changes its length to thickness (L2T) ratio. Just as seen in Table 4.19 were the ratios have completely changed, as seen on the last column. Depending on the thickness of the thin film, the ratios change accordingly. All of the sensors present in this test show a decrease in their ratios compared to the original values. Most of them seem to be further away than the theoretical 166.7 by Brand et. Al. [16]. But the sensors still show a very good output, regardless of their L2T ratio. This new factor is very important, as it was used to determine the non-linearity effects, now that the thickness has changed, the ratio changes too.

Overall the devices with parylene C are affected by the increase in thickness and mass on the diaphragm. This causes the frequency to decrease for most sensors, where as others will increase. At the same time we are able to see that the overall quality factor also gets enhanced with a protective layer of parylene C due to the increase in mass. This effect is also due to the inertia of the device, as mass varies and the acceleration of the diaphragm is kept constant, the force will vary. Similarly devices with aluminum metal on top of the diaphragm show a better response in terms of its quality factor.

5.0 Protective layer Version 2 tests in conductive fluids

The protective layer of parylene C has been added to different sensors, they will be tested in conductive fluids. This section will test the sensors with parylene C to see if they are functional in conductive fluids for more than 24 hours. Using the same setup by placing the sensor in deionized water and not letting the sensor touch anything but the oil in order to not alter the data recorded. This section also contains information on testing the sensors in conductive fluids with varying viscosities, or different glycerol water mixtures. This last portion will provide information to proof the sensor can distinguish varying viscosities in conductive fluids.

5.1.0 Sensors with Parylene C in 24Hrs Test

Different sensors have an additional protective layer of Parylene C, and they are ready for testing in conductive fluids. This second test uses sensors with parylene C, they will help determine whether the sensors will function in conductive fluids for a prolonged period of time. Various sensors were tested in deionized water, placed inside a vial with the conductive fluid and data was recorded using LabView to see if there were any fluctuations between the results.

Table 5.1 - Information on 3 Sensors with Parylene C for Deionized Water Tests

ID	Wafer	h_{Si} (µm)	a (mm)	Old L2T	New L2T	Heater Type	Resistor Area	PARC t (µm)
K1	5	10	1.75	175	166.3	P+	16%	0.526
J1	4	15	1.75	116.7	111.1	N+ Poly	2%	0.7508
I3	4	15	2.5	166.7	147.7	P+	2%	1.93

The sensors chosen for this test are presented in Table 5.1. They were chosen according to their L2T ratio to understand what would happen to the sensitivity of the device, and also see if different ratios would still function appropriately, regardless of the non-linearity effects [14].

5.1.1 Procedure test setups

There were three different test procedures to experiment the devices for 24 hours, the first one started after adding the thin film and placing the sensor inside the conductive fluid. At first the sensors would work for smaller periods of time, but in the end they would be able to reach the 24-hour test. The first tests show that the sensor stopped working after 30-60 minutes. This was very awful, because it felt the addition of the thin film did not help at all.

The second time the sensors were used in the test they would sit in the conductive fluid for a couple of hours with no power running through the device. This was a step taken because on the first test the device seemed to fail after a while. Then it would start working again in air, after being cleaned. With these reactions, it was somewhat clear the sensor required some kind of conditioning, that is why it would sit for a couple of hours in the conductive fluid. The last test procedure extended the amount of time without power from a couple of hours to an entire day before starting to record actual data.

Placing the sensor inside the conductive fluid required the user to be aware that any type of conductivity through the copper lines would damage the sensor. This was avoided by using gloves when testing the sensor in the conductive fluid. In different occasions while testing this was forgotten and the sensor would fail due to skin contact with the copper lines.

Even though the thin film was an enhancement to the device, the sensors under the microscope did not show a color variation like they did with the protective layer version 1. Discoloration was not present on the surface of the device, like previously shown in Figures 3.21 and 3.22.

A sensor was submerged inside a Pyrex beaker with deionized water for testing purposes, the top of the beaker was covered with scotch tape to create a flat surface for the sensor. This would help prevent the sensor from falling inside the conductive fluid, and also create air gaps so that condensation would not occur due to the small amounts of heat produced from the heater. The beaker was placed inside an oven, to avoid any other air fluctuations present in the testing room.

The characterization laboratory at RIT was used for all the tests done to the sensors in Version 2, and the location of the computer was found to be in a very unique location. Right on top of the test setup a vent was located, and the room required constant ventilation due to the poor location of the room's thermostat. Thus the vent would be spitting cold air all the time, this sometimes caused fluctuations on the results when measuring the sensors in air. Though most of the time the sensors were inside a liquid, the air would have less of a chance affecting the results. But to avoid this issue, the entire setup was placed from being on top of the oven to inside the oven with the door closed. This would provide a more controlled environment, and have fewer uncertainties to worry about.

Figure 5.1 shows a picture of the test setup for a sensor in deionized water inside a beaker. This was primarily tested on top of the oven, the scotch tape on the top of the beaker was used to hold the piece that holds the sensor in place (see Figure 5.2).

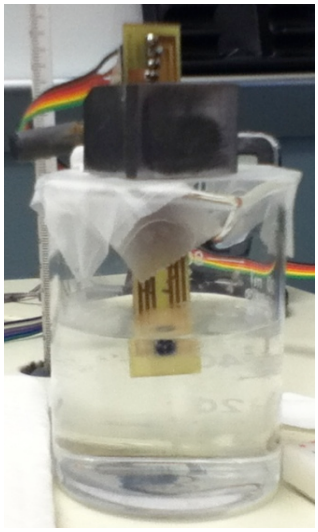

Figure 5.1 - Sensor I3 Inside Deionized Water for Long Term Testing

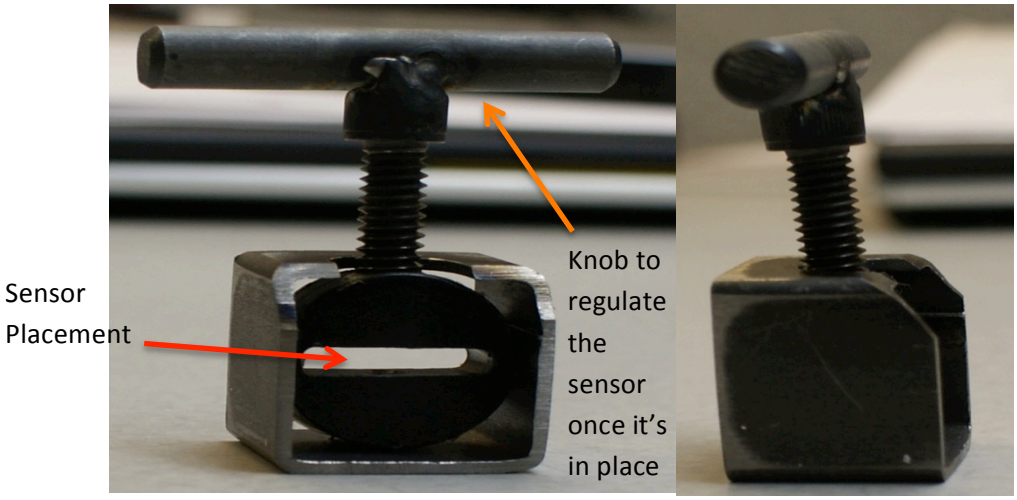

Figure 5.2 - Sensor Holder Piece that Fits Perfectly on Top of a Vial

The new piece holder (see Figure 5.2) was much easier to apply to the setup with the vials since it was custom made in house specifically for vial testing purposes. The main advantage of this device is that the sensor is placed in the middle of the vial without touching any of the sides, and it can be adjusted with a knob that regulates the sensors position. This keeps it straight as possible, as long as there is no extra epoxy on the sensor preventing it from sliding through the sensor placement location. Figure 5.4 shows a sensor wrongly placed inside a beaker with a conductive fluid without the actual piece holder, and also shows a representation of how the sensor should be located by the black perpendicular line. This would help prevent any variations in the testing procedure and keep everything under control.

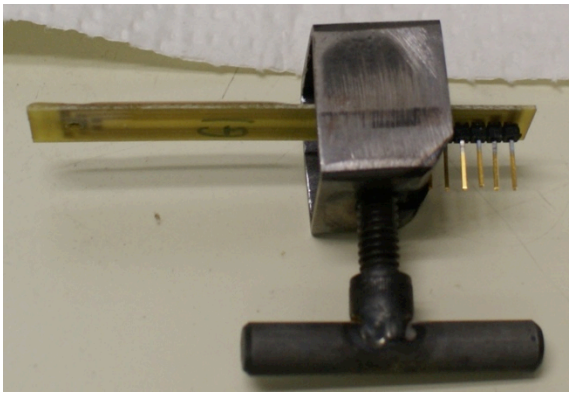

Figure 5.3 - Sensor G1 Placed Inside the Piece Holder

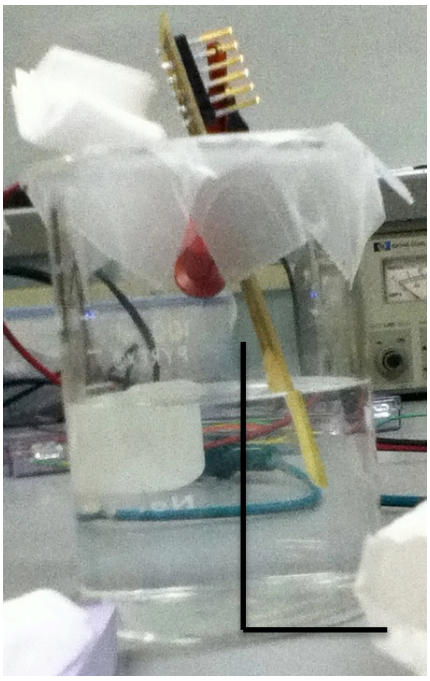

Figure 5.4 - Sensor in Deionized Water without Piece Holder

5.1.2 Sensor Test Results in conductive fluid

All sensors were tested in the same manner as stated in the previous section 5.1.1 by the three different test procedures. This would help determine the sensor would function properly for the 24-hour test. There is some conditioning required like previously stated, so that the sensor realizes it is in a conductive fluid. This improved the behavior of the device to operate for a longer time in a conductive fluid. The sensor would not require conditioning if it was tested in oil, since it is not a conductive fluid.

Out of the three sensors tested, I3 had the thickest layer of parylene C. It had a thin film measuring 1.93 μm, this was the first sensor that obtained an extra protective layer of parylene C. The idea at the time was the thicker the layer the better chance it would have against conductive liquid perspiration between the protective layer

and the actual substrate. This was seen previously in Version 1, when the sensor with epoxy or nail polish failed over time, due to the bubbles present in the protective layer. And also there was no actual protection to the device itself on top of the membrane, thus the actual substrate would be touching the conductive fluid. See Figure 5.5 for a preview after Version 2 is added and the sensor is placed in a conductive fluid.

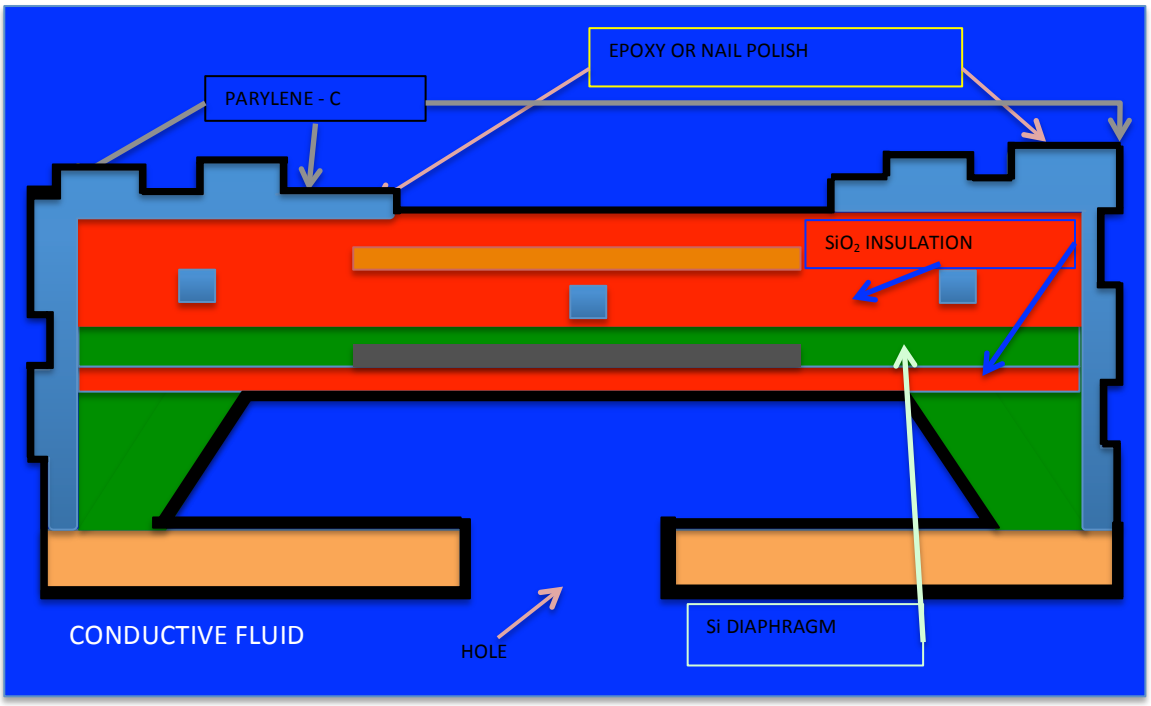

Figure 5.5 - Cross Section of Device with Version 2 in Conductive Fluid

These small observations done when testing version 1 were very important for the sensors performance in version 2. Thus the results presented below are the enhanced sensor, with a small variation in thickness and mass on the overall device. At the same time making the sensor more susceptible to chemical inertness, and water vapor transmission, or against moisture. This was a big problem in Version 1 thus Version 2 proofed that Parylene C is the best choice for this purpose.

Sensor K1 began working in the first trial for 10 minutes, afterwards the sensor would stop working. This meant that the sensors output would not be readable by Labview and no actual frequency response was obtained from the output. Therefore it would stop behaving like expected, but the sensor was still operational. Figure 5.6 explains the following relationship after a given amount of time the sensor would start to fade. This was not acceptable, and did not satisfy the requirements for this project, thus the main reason seemed to be that the thin film was not protecting it against conductive fluids.

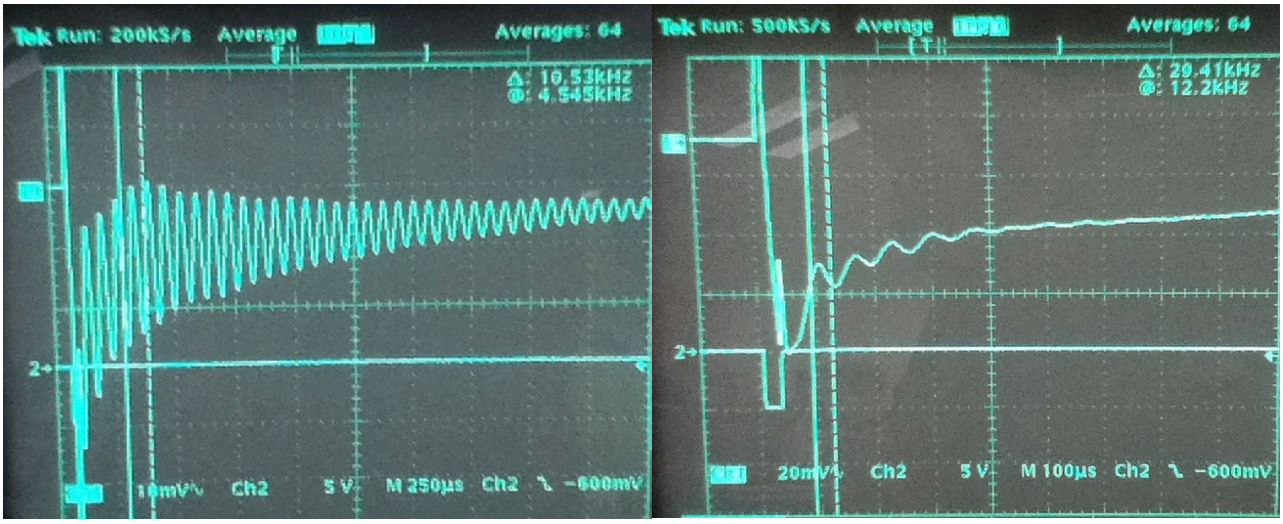

Figure 5.6 - Signal for the First 10 Minutes (left) After the Signal Starts to Fade (right)

Though the characteristics of parylene C are much better than epoxy or nail polish, the use of this material has been proven to work in conductive fluids like stated in [33] [32] [34] [35]. With this in hand, the sensor was cleaned to remove any conductive fluid residues as it was removed from the beaker. It was then re-tested in air, and the sensor worked again. This was a very good sign, because the sensor was still operational, it was not behaving in the liquid for more time which was the biggest factor from Version 1, as previously discussed in Section 3.3.5.

Due to these effects, something needed to change in the way this test was performed. A different procedure was applied with the same setup, this improved the results and the sensor was able to last longer. On this second attempt the sensor was able to record data for a longer period of time, it gained 57 minutes compared to the first test. Realizing this new test increased the functioning time for the sensor, a third attempt was done to prolong the time even further. Thus the sensor was left for nearly a day, submerged in the conductive fluid. With this new procedure it was possible to obtain good results past 24 hours from these devices with a protective layer of Parylene C.

This new procedure was applied to two different sensors and similar results were obtained, the sensors operated beyond the 24-hour test. This led to discovering the solution for the main problem that required conditioning the sensor. In this case it required them to remain submerged in the fluid for about a day without being activated. This would make the sensors operate for a longer period without affecting the results. Table 5.2 summarizes the results obtained from the devices tested in deionized water. All three sensors presented in the table

Table 5.2 - Information on Testing 3 Sensors in Deionized Water

	Time (mins)	Trial	Fo	Stdev	Amp	Stdev	Q Factor	Stdev
I3	67.5	1	7525	52.63	1.83E-04	1.66E-05	16.45	0.882
	4447	2	7413	118.39	7.23E-05	1.84E-05	31.92	3.222
K1	182	1	13213	1516.02	2.48E-04	1.01E-04	27.26	9.873
	1857.5	2	16233	434.70	7.34E-04	1.48E-04	56.36	4.471
J1	39.5	1	16394	331.25	4.79E-04	1.71E-04	27.46	4.434
	37.78	2	16424	271.65	2.12E-04	5.39E-05	24.49	3.777
	33.33	3	16586	326.51	1.63E-04	3.47E-05	31.62	5.784
	3041.56	4	16824	47.17	2.10E-04	2.43E-05	39.65	1.542

above show that after the 1st and 3rd try the devices lasted more than 24 hours in a conductive fluid. This states that for the first two try's the device was not "conditioned" properly, meaning the layer needed to adhere properly to the substrate, thus lasting less than a couple of hours. A factor is the expired Silane 172A and the way it evaporated and adhered to the substrate.

Overall the effect of placing the sensor in a conductive fluid tends to make the device decrease at first and then stabilize. This is seen in Figure 5.7, where the three different sensors are normalized and plot together in the same graph, though I3 is shown to last longer over time, they were all working appropriately until the user decided to stop running the test. The goal was for the sensors to operate past 24 hours, but for further testing I3 went close to 74 hours. The sensors worked in a conductive fluid for more than 24 hours, proving that parylene C is a good solution for underwater MEMS devices.

Even though each of the sensors worked beyond 24 hours, the best device was the output from J1 having a frequency of 16,824 ± 47.17 Hz for a period close to 51 hours. A very stable output compared to sensors I3 and K1 that varied through time. Sensor I3 and K1 had a similar output but were not as accurate as J1, they had standard deviations of 1.6% and 2.7% respectively. The data presented in Figure 5.7 also shows a gap in the recorded data for sensor K1, where it skipped a good portion and did not record anything for 14 hours. Until now that is wary because there is nothing to say what really happened in those hours. The only thing that could have happened is from the initial settings, the sensor might have been acting differently and not being able to record any data point. Also there are variations in which the device might have changed its frequency over time, due to the different forces applied inside the fluid.

On the other hand sensor I3 had a not so steady result of 7,413 ± 118.39 Hz, though it wasn't as close as J1 it is much better than K1. It obtained a quality factor of 31.92 ± 3.2, which seems to show that the quality factor increases due to the mass like previously stated, an enhancement to the design for all sensors. The same can be seen

on the results of the other two sensors after a trial or two. The most interesting results from I3 are that the measurements spikes in different portions were the readings vary in time 4, 18, 26, 8, 17 hours of recording. This is comparable to J1 because it is less steady, but more accurate than K1, which is all over the place.

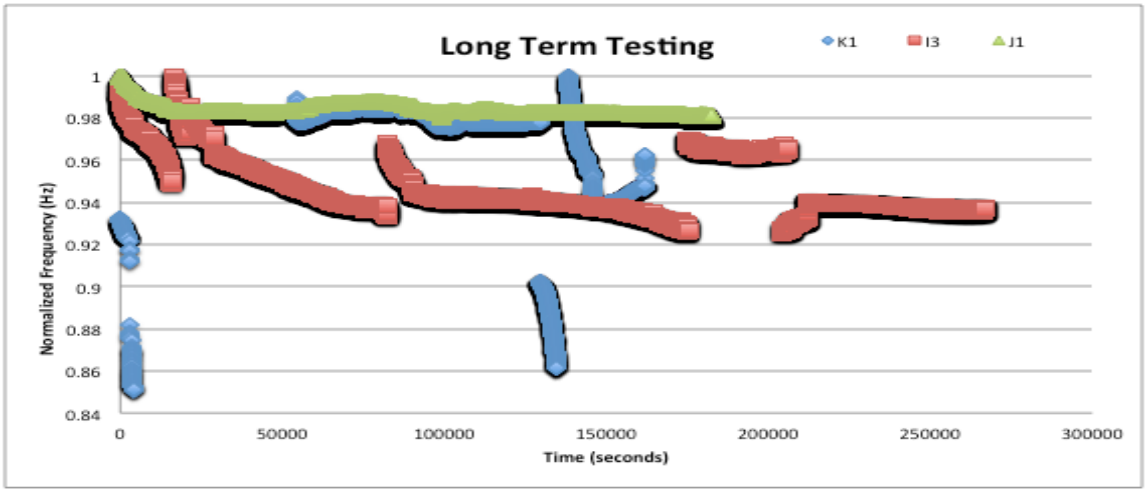

Figure 5.7 - Long Term Testing Results for Normalized Frequency for 3 Different Sensors

Figure 5.8 shows the amplitude data recorded from the sensors showing a similar response from the sensors, where J1 has the most stable response compared to K1 and I3. K1 and I3's response is spread all over, meaning that the sensor was changing its amplitude through out the time it was inside the fluid, having a variation of 20.2% and 25.4% respectively.

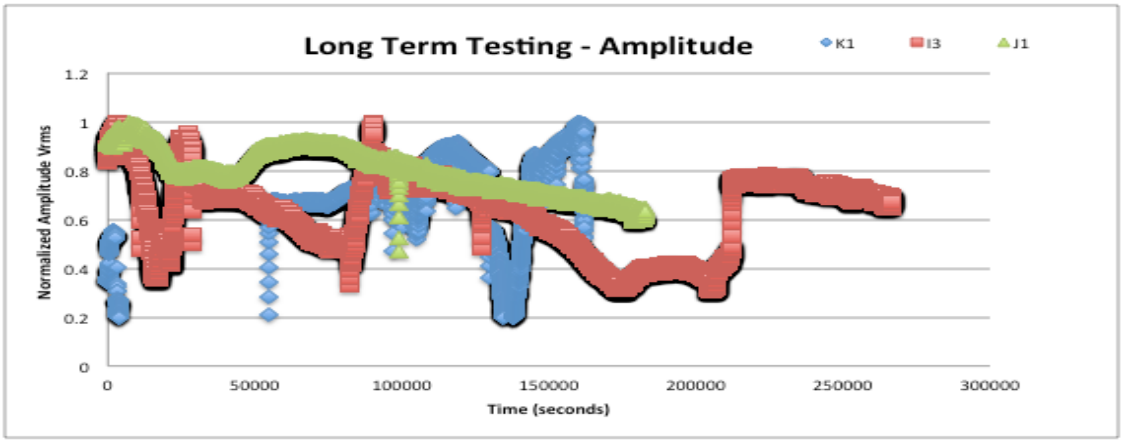

Figure 5.8 – Long Term Testing Results for Normalized Amplitude for 3 Different Sensors

As for the quality factor results from all the sensors it shows that J1 still remains at the top for being the most accurate one, its values only changed with a 3% variation. I3 on the other hand contains a lot of data points, even though it is stable it has a larger distribution of its values having a 10% variation. K1 with the huge gap in

between the data recorded has a smaller variation than I3 but definitely is not as stable as J1 with 8%. The quality factor values varied quite a lot between trials, they increased compared to their first one. This shows a similar correlation to their frequency results for K1 and J1 showing an increase while testing. On the other hand I3 showed the opposite.

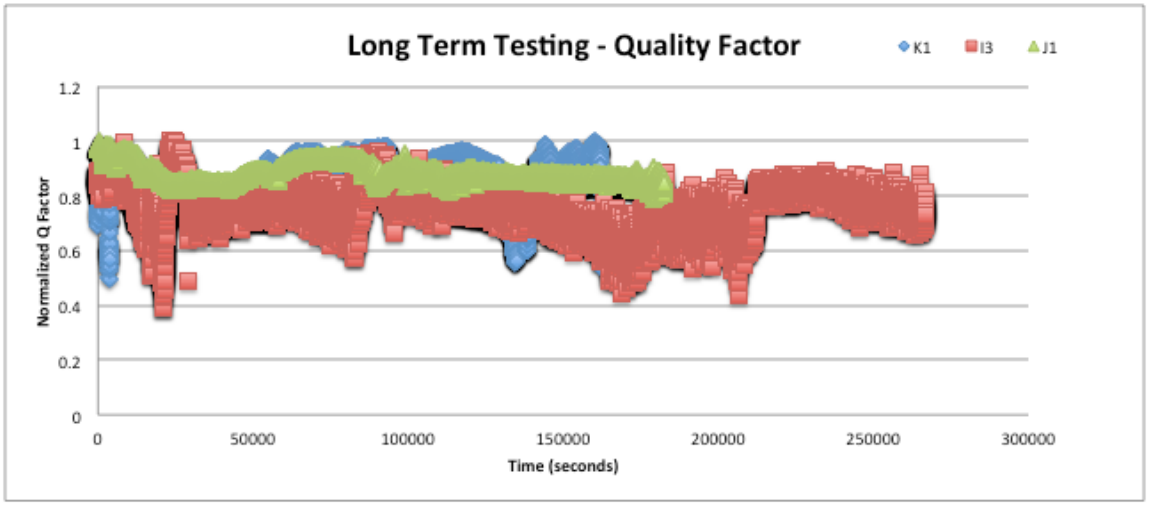

Figure 5.9 - Long Term Testing Results for Normalized Q Factor for 3 Different Sensors

Figure 5.10 represents the results from all the sensors that were tested in deionized water for long term testing. Overall they function past 1,440 minutes or 24 hours by being submerged in a conductive fluid without damaging the sensors performance and containing a protective layer of parylene C. Each of the devices tested required conditioning before testing them, thus it is possible to see the jump from less than 1 hour to working the full 24 hours and also the variation between the device without Parylene C and the ones with the protective layer.

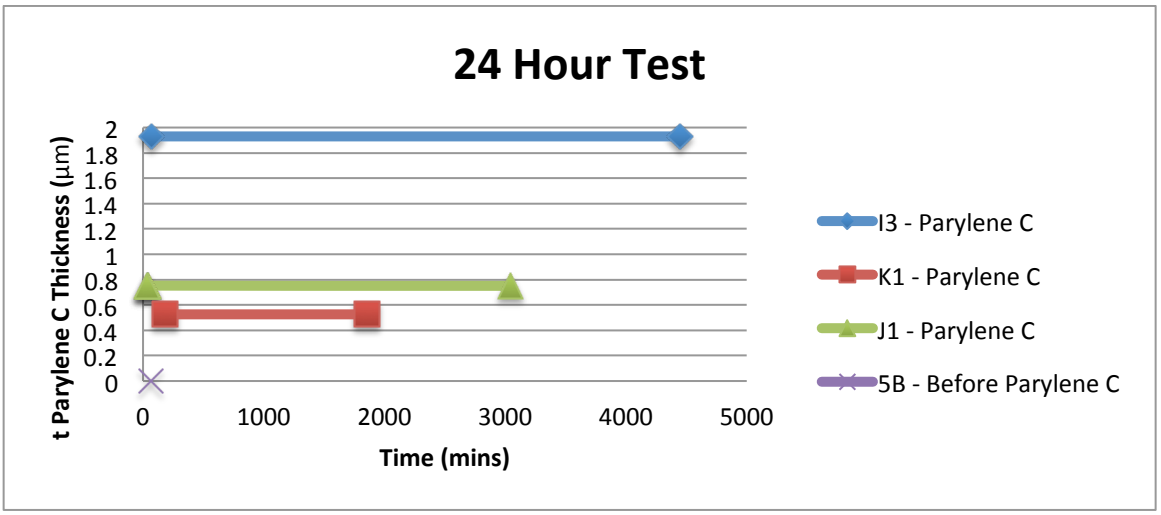

Figure 5.10 - Conductive Fluid Long Term Test

5.1.3 Problems while testing in conductive fluid

While testing the different sensors in deionized water, there were a couple problems regarding collecting data. One of the problems was the length of the data cable from the sensor to the circuitry board. Since the sensor was moved inside the oven, the length of the data cable needed to be longer. Thus a new cable was used in substitution of the old one, also the connections at the pins was a little problematic. The cable needed to be covered to prevent any short circuit between each of the soldered connections, see Figure 5.11.

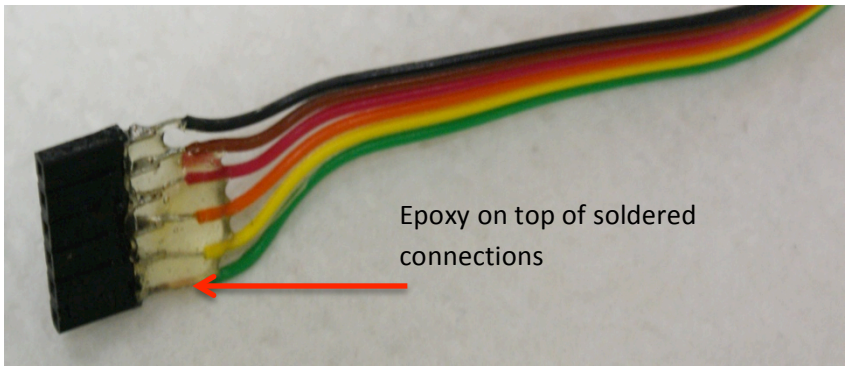

Figure 5.11 - Data Cable with Epoxy Around the Soldered Pins

After covering the soldered connections with epoxy, it saved a lot of devices from failing because now it had insulation against human skin. At the same time it made the end pinout cables sturdier when pressing it to the sensor. Once this cable got substituted into the setup taking results from different sensors inside the oven was easier, Figure 5.12 represents the new setup. A sensor is placed inside the vial filled with deionized water, together with the holder piece previously presented. It is also using the new longer cable, and protected with epoxy from the other cables and human skin conductivity. The piece holder uses an empty vial for support to prevent unbalancing the vial with the fluid.

Figure 5.12 - New Setup with Longer "insulated" Cable, Together with the Piece Holder and an Empty Vial

Other than that, another problem sometimes encountered was finding the right amount of voltage for the heater. Depending on the voltage applied for the sensor in air, and then placing it in a conductive fluid should be the same value, but that was not the case. Some devices did not have a reading for air even though the calculations would specify a 20μs pulse with a voltage range between 5V – 30V, nothing would occur. With this in mind, placing it in the conductive fluid without knowing the pulse or the voltage for the heater was a nightmare. Trying to find a pulse and the voltage that would make the sensor operate was a trial and error game. This is also explained in Section 3.1.3 were the pulse time is determined for sensors theoretically and through trial and error.

5.1.4 Summary of 24-hour test

Overall the sensor proved that it works in conductive fluids, which means that in theory it can work as a sensor to measure the viscosity of a fluid even if the liquid is conductive. The protective layer proves that it can withstand currents of up to 0.750 A through the heater, and 5 mA on the wheatstone bridge. At the same time a theoretical application of the sensors was assumed to determine how many times the sensor would actually be activated.

The sensor already proved it works for a full day without interruptions. With that test it's demonstrated that this viscosity sensor can be utilized for different applications. One of them is how many days the sensor can actually actuate before failing. This can be determined from the number of times the membrane vibrates in a given amount of time. Thus for the current application desired we are looking at the device to take a reading for x amounts of time for a day, depending on the number of averages read. The different values were deduced from a series of calculations presented in the following equations 5.1 – 5.5.

$$f_{input\ signal} * hrs * mins * secs = \#\ of\ membrane\ deflection \tag{5.1}$$

$$\#\ of\ membrane\ deflections * avg_{Q\ Factor} = Total\ \#\ of\ deflections \tag{5.2}$$

$$\frac{\#\ avgs_{osc.}}{f_{input\ signal}} = Every\ time\ a\ recording\ occur \tag{5.3}$$

$$\#\ avgs_{osc.} * \#\ \frac{recordings}{day} = Total\ \#\ \frac{avg_{osc.}\ recordings}{day} \tag{5.4}$$

$$\frac{\#\ of\ membrane\ deflections}{Total\ \#\ \frac{avg_{osc.}\ recordings}{day}} = \#\ days\ sensor\ should\ last \tag{5.5}$$

In theory these calculations can be utilized in many different ways, but for this application we are assuming the viscosity sensor is placed inside a vehicle to test the viscosity of a conductive fluid. Taking the data gathered

from device J1 it is possible to calculate the number of deflections this sensor can actuate and determine the duration of the sensors life.

Applying the previous equations to this application it is possible to say J1 in a period of 24 hours has deflected the membrane about 432,000 times in a up and down z-direction. Similarly it is possible to show that a value gets recorded every 12.8 seconds with an average of 64 recordings from the oscilloscope at a frequency of 5 Hz. Now that we have a value for the number of deflections occurring in a period of 24 hours at a frequency of 5 Hz, it is possible to calculate the total number of recordings per day with equation 5.4.

We are assuming that a recording throughout the day occurs every 4 times when the sensor is placed in its actual testing environment. Therefore it is possible to obtain a total of 256 average oscilloscope readings per day. Then apply equation 5.5 to determine the total # of days the sensor should last reading approximately 4 times a day. The outcome is a total of 1,688 days of operation given it reads 4 times throughout the day. In terms of years, the total amount of years the sensor should operate for is close to 4.6 years.

With these calculations we can determine the number total number of days the sensor should operate without failure. This will also require the device to be in a controlled environment and it is conditioned properly prior to its use.

5.2.0 Sensors with Parylene C in Conductive fluids at different viscosities

In this section different sensors were chosen to analyze conductive fluids at different viscosities. The fastest way to analyze these types of fluids was with a mixture between glycerol and water. Since the sensors were previously tested in deionized water, adding a viscous liquid to the mixture would help determine different viscosities and at the same time add the conductive property found in water. Therefore different percentages of glycerol were mixed with water for a determined volume to obtain various samples with varying viscosity values.

5.2.1 Glycerol

Glycerol or glycerin was chosen as the liquid to combine with water because it has a unique characteristic in which it can vary its viscosity property, its molecular formula is $C_3H_8O_3$. It is made from animal or vegetable sources, which are then applied to pharmaceutical and soap making industries. But for purposes of this project the main advantage of glycerin is altering its viscosity value by combining it with water. Other beneficial characteristics are that it is clear, viscous, odorless, sweet tasting, soluble in water and has a low toxicity level, thus easy to handle.

5.2.2 Glycerol Water Mixture

Adding water to glycerol helps reduce the viscosity of pure glycerol, which has a kinematic viscosity of 719.9 cSt or 905.7 cP at room temperature (25°C). Similarly this will help prove that the sensor works in conductive fluids at different viscosities. Most literature talks about glycerol concentrations to be measured by weight, thus most of the relevant tables will depend on the weight of the mixtures rather than volume. See Appendix section to find Table 5.8 which contains information on the viscosity of glycerin solutions, with dynamic viscosity values measured in cP or mPa*s.

5.2.3 Determining viscosity values of glycerol water mixtures at 25°C

One of the problems encountered while reading this table was the need to calculate values at room temperature (25°C) since they were not provided. Thus in order to obtain them an approach by Cheng [42] was applied. He is able to obtain an empirical formula that will determine the viscosity of the mixture for concentrations ranging from 0-100% at temperatures from 0-100°C. With this equation it is possible to calculate the viscosity of the glycerin solutions at different percentage weights at room temperature.

In order to choose the closest equation for this projects application, a table was created containing different equations discussed about in the paper to determine the viscosity of glycerol water mixtures. Table 5.3 has the summarized relevant information for the current project. Out of all the equations in the table, the closest one to our main approach is the one from Shankar and Kumar, but at the same time, it seems that the equation provided by Cheng which combines all three of them seems to be a more complete.

Table 5.3 - Summary of Different Equations to Determine Viscosity of Glycerol Water Mixtures

Authors	Viscosity Mixture Glycerol-Water	Variables	Problems
Chen & Pearlstein μ = Dynamic Viscosity	$\mu = A_1 e^{\left[A_2(T+273.15)^{-3}+A_3(T+273.15)+A_4(T+273.15)^{-1}\right]}$	μ = cP or 0.001 Ns/m^2 T = Temp. in °C $A_1 - A_4 = C_m$ C_m = Glycerol Concentration in mass	For Discrete Concentrations of $A_1 - A_4$ e.g. C_m = 40%, 50%, … 90%, 99% Other values require interpolation or extrapolations
Shankar & Kumar ν = Kinematic Viscosity	$\frac{ln(\frac{\nu}{\nu_w})}{ln(\frac{\nu_g}{\nu_w})} = C_m[1+(1-C_m)(B_1+B_2C_m+B_3C_m^2)]$	ν_g = Kin. Visc. of Glycerol ν_w = Kin. Visc. of water $B_1 - B_3$ = Temp. Coefficients (°C) C_m = Glycerol Concentration in mass	Only evaluated for 5 different temp. coefficients e.g. 10°C, 20°C, 30°C, 40°C, 50°C
Chenlo et. Al ν = Kinematic Viscosity	$\frac{\nu}{\nu_w} = 1 + 0.125C_{mol} * e^{\left(\frac{C_{mol}^{0.219}}{2.291[(T+273.1)/273.1]^3-1}\right)}$ $\nu_w = 0.09607 \times 10^{-6} e^{\left(\frac{2.9}{[(T+273.1)/273.1]^3}\right)}$	C_{mol} = mole fraction of glycerol T = Temperature (°C) ν_w = Kin. Visc. of water	This works for C_m values that have low values of glycerol concentrations **Deviations:** 9% for C_m = 40% 50% for C_m = 70%

The following equations are taken from Cheng [42] and applied to obtain measurements at room temperature (25°C). Where *a* and *b* are coefficients in Eqs 5.1 and 5.2 used for future calculations in Eq. 5.4. At the same time both coefficients only function correctly at temperatures ranging from 0°C – 100°C, just like it states in

Eq. 5.1. C represents the percentage value of weight concentration of glycerol. After calculating α it is possible to use Cheng's approach with Eq. 5.5.

$$0°C < T < 100°C \tag{5.1}$$

$$a = 0.705 - 0.0012T \tag{5.2}$$

$$b = (4.9 + 0.036T) * a^{2.5} \tag{5.3}$$

$$\alpha = 1 - C + \left[\frac{\left(a * b * c * (1 - C)\right)}{\left(a * C + b * (1 - C)\right)}\right] \tag{5.4}$$

$$\mu = \mu_{water}^{\alpha} * \mu_{Glycerol}^{(1-\alpha)} \tag{5.5}$$

$$\mu_{water} = 1.790e^{\left(\frac{(-1230-T)T}{(36100+360T)}\right)} \tag{5.6}$$

$$\mu_{Glycerol} = 12100e^{\left(\frac{(-1233+T)T}{9900+70T}\right)} \tag{5.7}$$

At first the values for 20°C from Table 5.2 were input to a table in excel, in order to compare them to the values from the calculations by Cheng. Two different approaches were evaluated using Eq. 5.5, the first one was using all of Cheng's assumptions which includes Eqs. 5.6 and 5.7 for a given temperature. On the second attempt, Eq. 5.5 was used without applying 5.6 and 5.7 but substituting them with fixed values for the dynamic (μ) values of water and glycerol. All of these values are dependent on temperature thus the results will vary accordingly.

From this point a new set of values for room temperature (25°C) were obtained for reference and to be applied to the previous equations. Using the calculated values from Cheng and the ones provided in [43], [44], [45] are summarized in the following table 5.4.

Table 5.4 - Information to Calculate Viscosity using Different References [42] [43]

	Glycerol % wt	Temperature (°C)			
		20		25	
Wiki	0	1.002	1412	0.91	910
Cheng	100	1.005	1413.8	0.893	905.7

Both set of values shown are compared and seem to be very similar, in the appendix section in Table 5.9 there are three different values shown next to each other. On the second column we have the Dorsey referenced values, then a polynomial fit was applied by using Excel (Figure 5.13) and shown on the third column. After that Cheng's approach was utilized which is located in the fourth column, and last but not least is the fifth column, which used Cheng's approach but does not include Eqs. 5.6 and 5.7. But actual fixed values for the viscosity of glycerol

and water. Overall the calculations match the results from [46] but for this project Cheng's equations will be used, thus the values from the fourth column are the best match.

At this point obtaining the viscosity values at room temperature (25°C) was the goal, thus a new set of results was compiled by applying the previous set of equations. In the appendix section in Table 5.10 it shows the calculated values at room temperature on the 3rd column and compares the Dorsey [46] values at 20°C and 30°C. With these results it is possible to state that Cheng's equations are very close in accuracy to the table presented in the appendix section Table 5.8.

5.2.4 Making the conductive fluid for different viscosity values

With the equations presented in the previous section it is possible to determine the dynamic and kinematic viscosities of glycerol and water mixtures depending on the percent weight of glycerol. Primarily this is done to understand if the sensor is capable of analyzing varying viscosity measurements in conductive fluids just like it did for oils. With this idea a procedure was elaborated to create different solutions for glycerol-water mixtures in order to vary its viscosity measurement and be able to use the tables created in the previous section.

In order to create the different solutions Eq. 5.8 was used to determine the Glycerol percent weight by dividing the weight of glycerol by the sum of the weight of glycerol and water.

$$Glycerol\ \%\ wt = \frac{wt\ C_3H_8O_3}{wt\ C_3H_8O_3 + H_2O} \tag{5.8}$$

This was a very tedious job because it required adding the different drops of water and glycerol together with a lot of precision and accuracy. For this to be constant and exact different volumetric flasks of 10 mL were used, but at the time volume was not the main factor to make these mixtures. The mixtures depended upon the weight of the glycerol and the total solution just like explained in Eq. 5.8. With this in mind, the density of glycerol was found in literature to be about 1.25802 $\frac{g}{mL}$ for 100% of glycerol at 25°C [47]. For verification purposes the value obtained from our trial are presented in Table 5.5 were the mass of the empty vial is subtracted from the total solution and the glycerol % weight is obtained. The density of 100% glycerol used was 1.2427 $\frac{g}{mL}$ with this value the different glycerin percent weights were calculated.

Table 5.5 - Determining Glycerin % Wt for Mixtures

Hypothetical Volume % Gly	Wt of Vial + Total Sln (g)	Wt of Total Sln (g)	Wt of Glycerin (g)	Calc. Glycerin % Wt	Kin. Visc. @ 25°C (cSt)
10	24.602	10.08	1.2427	12.33	1.177
20	25.252	10.73	2.4854	23.16	1.566
30	25.154	10.632	3.7281	35.06	2.294
40	25.614	11.092	4.9708	44.81	3.360
50	26.236	11.714	6.2135	53.04	4.953
60	25.733	11.211	7.4562	66.51	11.182
70	26.49	11.968	8.6989	72.68	18.074
80	26.263	11.741	9.9416	84.67	60.094
100	26.949	12.427	12.427	100	719.925

5.2.5 Glycerol Water Mixture tests

Figure 5.13 shows the different glycerol water mixtures created for test purposes in separate vials. With these vials ready to be used, the sensors with parylene C can be used to measure the viscosity of each of the fluids by obtaining their frequency, quality factor and amplitude.

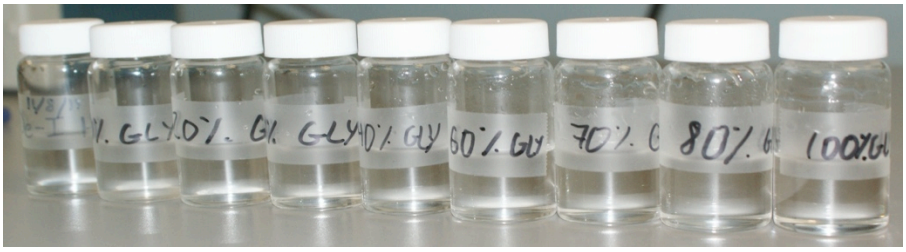

Figure 5.13 - Deionized Water and Glycerol Water Mixture Vials (10%-100% from Left to Right)

Three different sensors were chosen to test the vials conductive fluids. Table 5.6 shows the corresponding sensors characteristics.

Table 5.6 - Sensors Characteristics for Conductive Fluid with Varying Viscosity Test

ID	Wafer	h_{Si} (µm)	a (mm)	Heater Resistor		Old L2T	New L2T	Par-C t (µm)
				Type	Size (%)			
L1	4	15	1.75	N+ Poly	2	116.7	112.4	0.564
L2	4	15	1.75	P+	2	116.7	112.4	0.564
5B	4	15	1.75	N+ Poly	16	116.7	110.4	0.857

All the sensors used for this test have a new L2T ratio of close to 110 with their new diaphragm thickness. Previously they all had the same diaphragm thickness and length size, but varied in their size and type of heater resistor. Their protective layer thicknesses also varied, sensors L1 and L2 obtained 0.565 µm where as device 5B

added 0.857 µm. With these new characteristics the devices were tested in each vial for 20 minutes, the results are shown in the next section. The setup for these tests follows a similar procedure to the oil tests by using the piece holder inside the oven for a controlled environment. Figures 5.14 – 5.16 represent the sensors response of frequency, amplitude and quality factor from L1. Even though three sensors were tested, the best results obtained came from L1.

On the normalized frequency graph, Figure 5.14 it is possible to see that the theoretical calculations using Lamb and Kozlovsky's model follow a similar trend like oil tests. As viscosity increases, or the fluid becomes more viscous the frequency will tend to decrease, this is represented by the green dotted lines. This sensor was tested two times, the results from round 1 are presented by the light blue diamonds and round 2 by the red squares. The trend shows a decrease in frequency as viscosity increases just like in oil. There was a minor problem while testing the sensor for the first time using the different glycerol water mixtures. The device recorded a higher frequency reading for the 84.7% Glycerin vial test, but the second time the sensor was tested, the response improved.

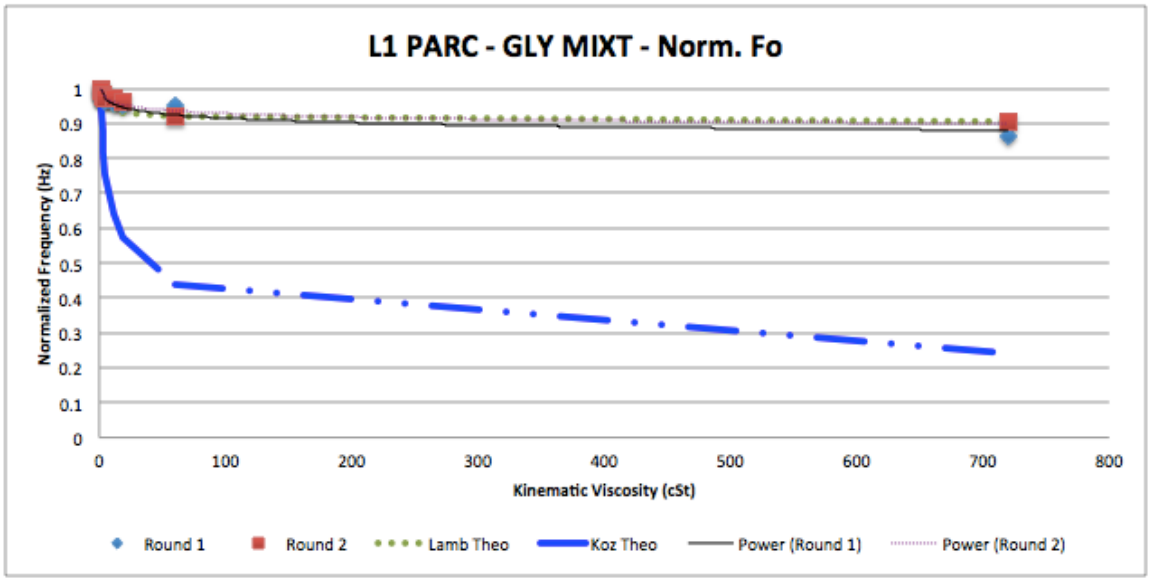

Figure 5.14 - L1 Normalized Frequency Response in Glycerol Water Mixtures

This has occurred previously in other sensors, were the frequency at a higher viscosity tends to increase rather than decrease. It is somewhat hard to explain why this happens, but keeping the same testing conditions and cleaning the sensor very thoroughly seems to help the results. On the other hand the overall test was a success because the device was able to capture data at varying viscosities in a conductive fluid. Figure 5.15 shows the response in terms of its normalized amplitude, though a similar response like the frequency is expected this was the

complete opposite. The different results were spread all over the graph and did not follow a trend. This can also be seen in Table 5.7 were the value of R^2 shown for both rounds is close to 0.40 rather than the theorized result by Lamb of a 0.89 or Kozlovsky 0.99. This factor is not reliable but shows the sensor is trying to follow the trend, due to the sensors minute measurements a small particle on the membrane can change the sensors performance.

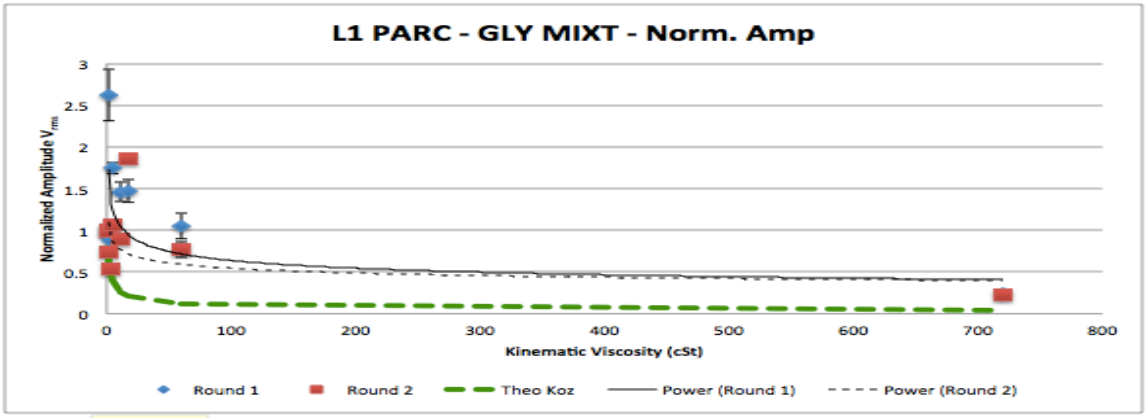

Figure 5.15 - Normalized Amplitude Response in Glycerol Water Mixtures

The results for quality factor from the sensor in conductive fluids with varying viscosities shows a slightly better response than the amplitude. Though the addition of the extra protective layer is very positive for the sensors output in producing more oscillations. Which is due to the extra mass, by exerting more force on the membrane. Figure 5.16 shows the results and similar to the frequency response shown in Figure 5.14 the data improved the second time. The red squares (round 2) demonstrate a much closer relationship to the theoretical calculations than

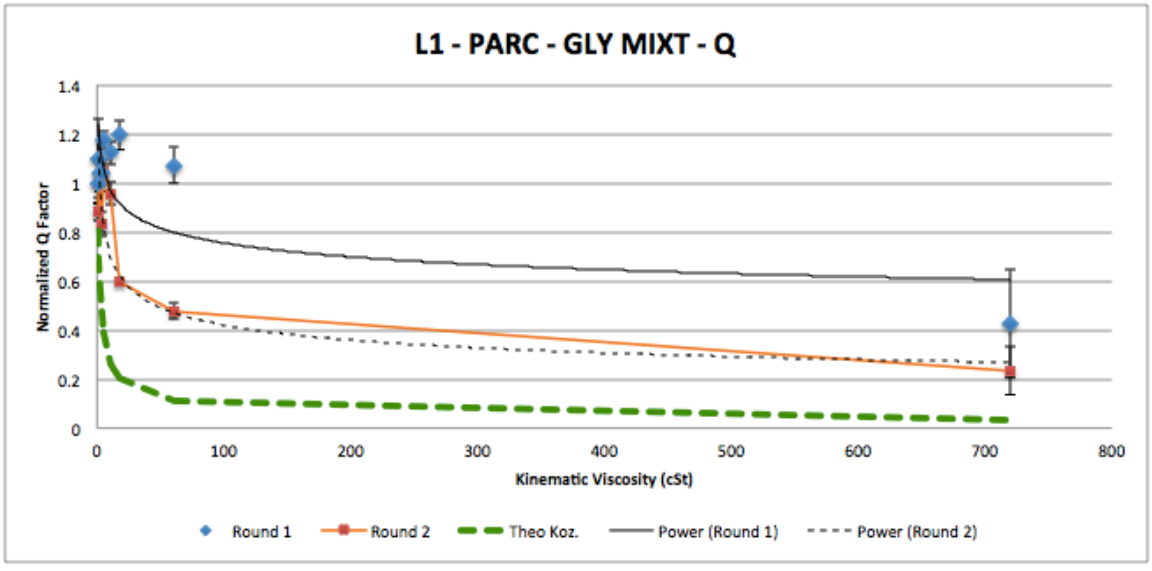

Figure 5.16 - Normalized Quality Factor Response in Glycerol Water Mixtures

the blue diamonds having an improved standard deviation from 8% to 5% of their values. But the quality factor values were affected sometimes when collecting the data, because Labview's code for Q depends upon the resonant frequency divided by the change in frequency, Eq. 2.33. This was previously explained in Section 2.2.0 Figure 2.12.

Table 5.7 - Power Law Fit to the Results from Device L1

	Freq Equations		Amp Equations		Q Equations	
	Y =	R^2	Y =	R^2	Y =	R^2
Lamb Theo	$0.9859x^{-0.015}$	0.89032	-	-	-	-
Koz. Theo	$1.075x^{-0.223}$	0.9976	$0.8545x^{-0.5}$	1	$0.8545x^{-0.5}$	1
Rnd 1	$1.0044x^{-0.019}$	0.88278	$1.8232x^{-0.218}$	0.48628	$1.2708x^{-0.108}$	0.51747
Rnd 2	$1.0013x^{-0.016}$	0.9397	$1.1363x^{-0.152}$	0.31427	$1.2071x^{-0.219}$	0.86812

Overall the frequency results seem to approach more with Lamb's theory rather than Kozlovsky, which includes the kinematic viscosity, *v*. But that does not prove that Kozlovsky's theory is wrong, because it uses the viscosity values, were as Lamb's theory does not. Ayela and Nicu [28] proved that liquids with a viscosity of up to 10 cP Lamb's method is the best to use. Where as if the viscosity of the liquid is higher than 10 cP then it is important to take into account the viscosity when applying to thin vibrating plates found in MEMS devices [25].

The main reason this would occur is due to the addition of an extra layer, this changes the characteristics of the materials, thus the L2T ratio is also changed due to the increase in mass and membrane thickness. Overall this test shows that the trend is followed, as viscosity increases the frequency decreases due to the change in density and viscosity of the fluid. The same is expected from the amplitude and the quality factor, but at times it seems that the two other factors are not as relevant as frequency in these tests, but they do help define the liquid under test with extra factors that may be useful for other tests. The measurement of quality factor should decrease due to the dampening of the vibrations as the viscosity of the fluids increase.

Generally this test proves that the sensor works in conductive fluids with varying viscosities. The experiment also shows that the results follow a similar trend compared to the theoretical data from Lamb and Kozlovsky's approach. At the same time it also shows that for viscosity values beyond 10 cSt or 10 cP the response varies more and more. Similar to the results in oil, the value of Q tend to decrease faster if it is past the 10 cSt mark. This is shown in the results as the values spread further apart from each other. The addition of parylene C as a protective layer is a success and does not damage the sensors performance, but actually enhances it due to the addition of mass on the membrane.

6.0 Repeatability & Accuracy

In this section the sensors repeatability and accuracy tests are run to determine whether the results recorded are not a replica and actually measure viscosity at different viscosity levels. It will also measure the variation of the data points under the same testing conditions just like if the sensors were mass produced and used to specifications. This test is focused more towards a repeatability and accuracy research environment, where the setup is controlled in a way most of the different factors are manageable.

6.1.0 Test Setup for Repeatability and Accuracy

The test setup for this section requires the sensor to be placed inside a vial without removing it in order to prevent any inconsistencies while recording data. This will also help the sensor to condition itself. The advantage of this test is that cleaning the sensor in between tests is not required. In previous tests this cleaning method has shown to have some effect on the readings. The voltage applied to the device was only activated for a minute to record data, and then turned off for 60-minute intervals.

But for this test varying the frequency would change the time period according to the frequency applied. Thus decreasing the frequency would prolong the time the heater was on, where as if the frequency increased the opposite would occur. The input signals characteristics changed from a frequency of 1 Hz and 20 Hz, this would help determine what frequency is the fastest one to heat up the sensor. With this approach it is possible to find the correct frequency value that will speed up the heating of the sensor and be able to make the sensor operate to its full capabilities.

Some of the problems encountered before changing the frequency were that the sensor did not produce the results the team aimed for. The main reason for this was the frequency at which it operated was not the optimal. Therefore the heater did not warm up fast enough for the oscillation to occur, thus the actual time period for 5 Hz is 0.2 seconds. With 0.2 seconds it seemed it was too slow, consequently higher and lower frequencies were chosen.

As for the accuracy portion of the test setup, the team focused on obtaining results with the same sensor and trying to see how close to the actual results it would be possible to achieve. The sensor has been previously tested on different glycerol water mixtures of 10% - 100%. Testing the device in a 90% solution might help prove that it is able to follow the trend. This would help prove that the sensor can be accurate regardless of knowing the mixture composition.

6.2.0 Results for Repeatability

Sensor J5 was used for all of these tests and they are plotted in the following Figure 5.1. The results show that the repeatability tests were done at a frequency of 1 Hz and 20 Hz for a 53.04% glycerol water mixture. At the same time the results at 20 Hz show a larger variation compared to the ones at 1 Hz. It crosses the 44.81% and 35.06% glycerol mixtures mark, which is a problem. This means that the actual sensor is taking measurements of more than one kind of glycerol water mixture, even though it has been in the 53.04% the entire time. The sensor lacks repeatability, but then again this is also due to the actual mixtures, they were not mixed properly. They might contain a different viscosity value at different percentages, but it seems that under 10 cSt the sensor does not seem to differentiate 44.81% and 53.04%.

Similarly the results of each of the glycerol water mixtures for sensor J5 have a contradicting result on their standard deviation. At 44.81% and 53.04% their standard deviations overlap on top of each other. This affects the results, but like any other prototype sensor, it has its disadvantages leading into future improvements. With these results it seems that at 1 Hz the sensor is more stable than at 20 Hz, even though both measure the viscosity of 1 or 2 different viscosity values.

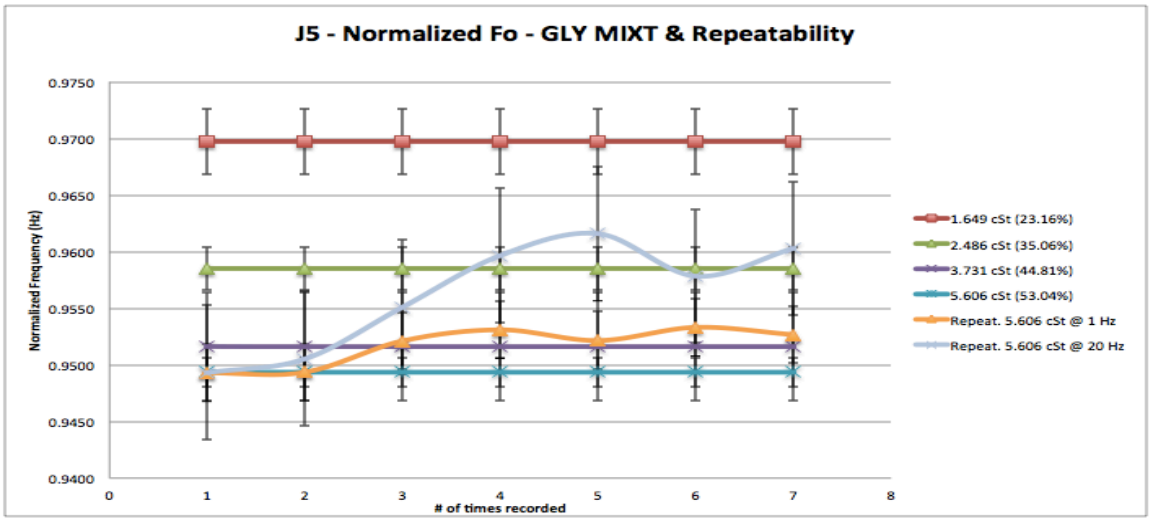

Figure 6.1 – Normalized Frequency Results for Repeatability of Sensor J5 at 1 Hz and 20 Hz

The results for quality factor and amplitude are not shown at the time because it was deduced that out of the three results obtained form the sensor frequency had the best characteristic representation of the different fluids, second came Q and then the amplitude. With the previous test we can conclude that input frequency of 1 Hz is pretty close to the actual calibrated data. Thus a different repeatability test with an 84.67% Glycerol water mixture is performed to see what happens at a higher viscosity value, 85.6 cSt.

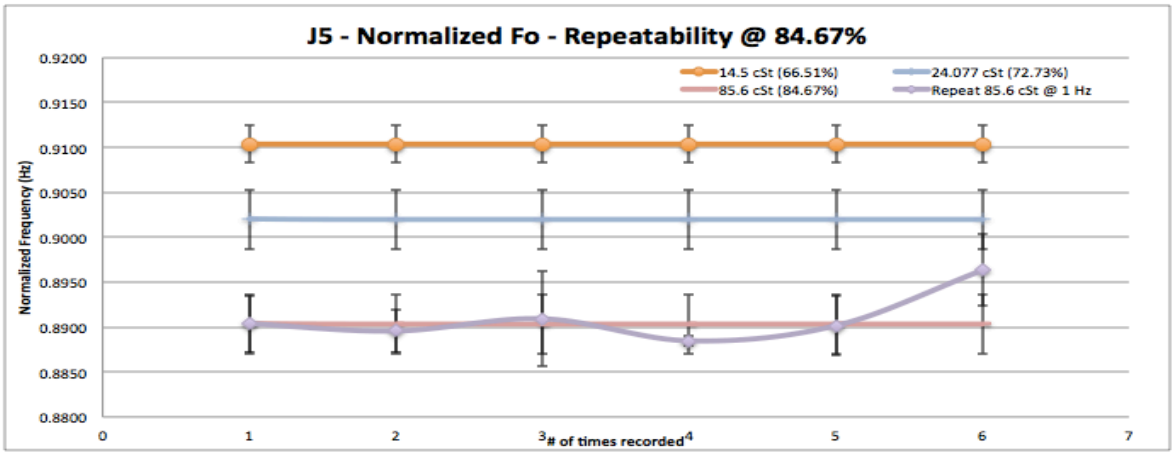

Figure 6.2 - Repeatability at 84.67% Glycerol Water Mixture at a Frequency of 1 Hz

Figure 5.2 shows the results of the repeatability test at 1 Hz for an 84.67% Glycerol water mixture. The test shows that the result is close enough to the actual calibrated measurement, with a slight variation at the last minute. Overall the results show a pretty close relationship in which it does not vary as much as the low viscosity measurement. For higher viscosities the sensor behaves like expected.

6.3.0 Results for Accuracy

For this test sensor J5 was also used to measure accuracy of a random percentage of glycerol water mixture. A higher and a lower viscosity were utilized, as random samples, to see the different results, just like the repeatability test. Figure 5.3 and 5.4 show the actual results of the low and high samples tested. Just like previously stated, Q and amplitude are not good factors that represent viscosity regardless of the varying samples.

Similar to the repeatability results at a lower viscosity the sensor does not fully difference between the low viscosity values. Where as if we go beyond 10 cSt the variation is much higher since the liquid is more viscous, thus the sensor does see a difference, and it is accurate enough that it is possible to follow the actual trend.

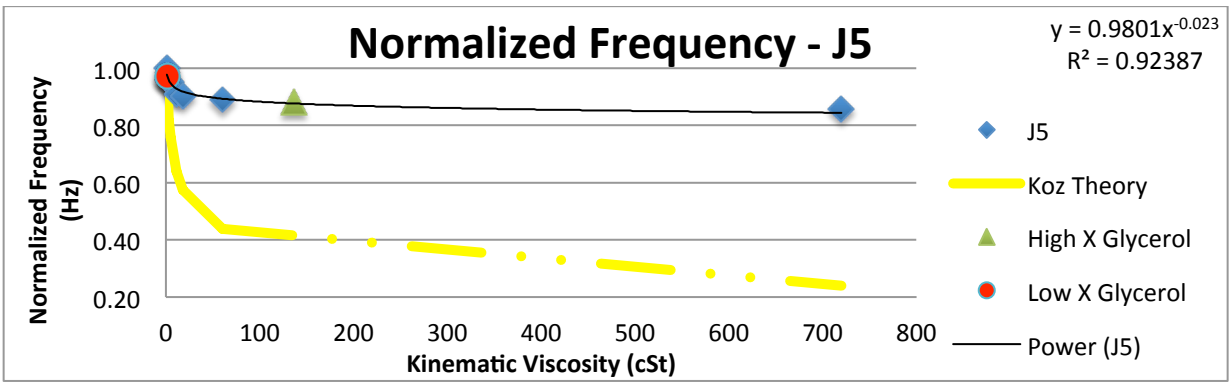

Figure 6.3 - Accuracy Test at High and Low Viscosity Measurements Using Sensor J5

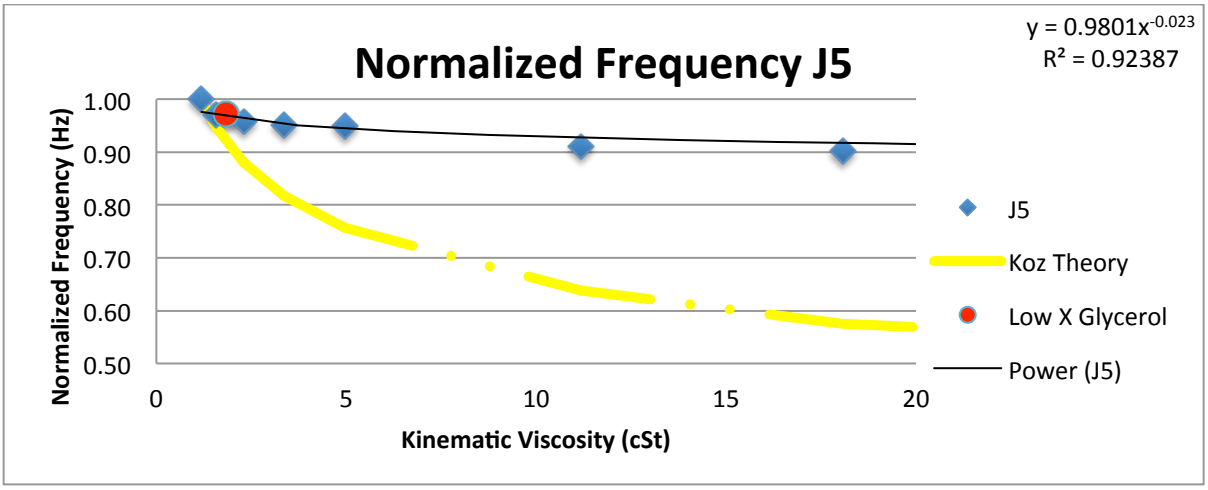

Figure 6.4 - Accuracy Test Zoomed in for the Low Viscosity Measurement Using Sensor J5

6.4.0 Conclusion for Repeatability & Accuracy

Overall the sensor repeats the readings at higher viscosities rather than low because of the higher viscous liquids, and increasing density. For values less than 10 cSt the sensors performance is operational, but needs to improve the sensitivity factor. For these tests the input frequency of the pulse was determined to have a faster and better response at 1 Hz rather than 20 Hz. For the accuracy test, a similar result is seen in the data, in which at low viscosities the sensor has trouble in determining the frequency, amplitude and quality factor. But when it is tested in a higher viscosity value, the sensor is able to determine the right frequency, and the Q and amplitude vary constantly.

The overall picture is that the sensor is able to detect a variation in frequency more than the quality factor or the amplitude response. This is also important because adding the protective layer of Parylene C definitely changes the sensors characteristics. This influences in the response that it actually portrays. Similarly to the results shown in Section 4.0, the trends are able to follow the theoretical calculations to a certain extent.

7.0 Conclusions

Adding Parylene C as a protective layer for a post fabrication process is a possible solution. Having various sensors already produced and ready for testing, together with a post process fabrication that did not alter the sensors performance was achieved. The protective layer had a thickness varying between 0.4 μm – 1.93 μm, regardless of the thickness they all protected the sensors from conductive fluids. Most of the problems seen with the protective layer Version 1 were avoided once Version 2 was applied. The main reason the sensors failed, were due to a thin passivation layer, and no actual protection on top and below the membrane. Just like seen in Figures 3.8 and 3.20.

With the addition of Version 2 it is possible to obtain results after conditioning the sensor in a conductive fluid. Similarly long-term tests show that the sensor is capable to work in conductive fluids past 24 hours. And the current sensor can be applied to a machine that has a conductive fluid that requires to monitor its viscosity.

The sensors characteristic change with the addition of parylene C, the tests for before and after parylene C in oils for different viscosities show a frequency, amplitude and Q variation. The results follow the theoretical calculations and it is possible to determine the outcome. Similarly glycerol water mixtures with varying viscosity values were tested for frequency, amplitude and Q. The results show a trend that is determined by the theoretical calculations, and clearly show a similar response. Out of the three results, frequency is the main factor that helps characterize the response more than amplitude and Q.

Overall the sensors have proven to work in conductive fluids with varying viscosity with the protective layer of parylene C without damaging the sensor's performance.

7.1.0 Future work

Some improvements for the sensor after doing so many tests to it with the current protective layer are to look for a substitute of epoxy to improve the packaging method. At the same time a further investigation at long term tests is required to deduce whether conditioning is only required once or the sensor actually requires it to be conditioned all the time before placing it in conductive fluids.

Another test that would have been very good to see results from is varying the temperature (0 – 100°C) in a conductive fluid. A similar test was done in air with varying temperature, and the results show a hysteresis effect, but it varies according to each sensors characteristic. Each sensor contains a different measurement of thickness, length of the membrane, and heater material.

One of the main problems during testing was observed when placing the sensor inside a vial. Many different times as the sensor was placed inside a vial or in a liquid, the back hole where the fluid would enter gained a bubble or two. The main reason for this was the material of the PCB is not hydrophilic, which helps adhere water to its surroundings. This would also help increase the sensitivity, because most of the issues while recording data were seeing with the bubble not letting the fluid flow freely. Maybe the size of the cavity should be bigger for the liquid to flow freely. And finally once all of these issues have been addressed, the sensor should be able to test it in biological applications.

8.0 Appendix

Table 1A – Results from Screening Experiment

Details							
ID	**Device #**	**a-Size (mm)**	***Resistor***		**R_heater (Ω)**	**V_Bridge (mV)**	**CT2L**
			Type (P+ / Poly)	**Size (35%, 16%, 2%)**			
1C	1	1.75	P	2%	60	78.7	116.7
	2	1	P	35%	217	12.8	66.7
	3	1	Poly	2%	46.7	35.7	66.7
2A	**4**	1	Poly/P+	2%	52	11.5	66.7
	5	1	Poly	16%	70	95.7	66.7
	6	1	Poly	1%	100	-16.7	66.7
	7	1	P	2%	309	30.5	66.7
	8	1	P/P+	2%	267	1.105	66.7
	9	1	Poly	2%	90	-50.7	66.7
	10	1	P	35%	239	161	66.7
	11	1.75	P	16%	270	42.24	116.7
	12	1	P	2%	380	25.7	66.7
	13	1	P	16%	248	50.187	66.7
	14	1	P	2%	283	78.5	66.7
4A	15	1.75	P	16%	255	-20.3	116.7
	16	1	Poly	1%	140	61.05	66.7
	17	1	Poly	35%	98.5	-70.352	66.7
	18	1	Poly	16%	118	61.213	66.7
	19	1	P	1%	257	92.518	66.7
3A	20	2.5	Poly/P+	35%	71.8	37.502	166.7
6C	**21**	1.75	P	2%	232	55.6	116.7
	22	1	P	35%	216	42.8	66.7
	23	1	P	16%	226	71.854	66.7
	24	1	P/P+	2%	273	5.5	66.7
	25	1	Poly / P+	2%	125	-12.2	66.7
	26	1.75	Poly	35%	71.9	-49.2	116.7
2C	27	1.75	Poly	2%	77.963	76.25	116.7
	28	1	Poly	16%	77.8	36.7	66.7
3C	29	2.5	P	16%	221	-20.1	166.7
4C	30	2.5	P	2%	221	-102.4	166.7
	31	1	P	1%	255	-54.465	66.7
	32	1	P	16%	225	-199.78	66.7
5C	33	1.75	P	35%	242	-65.9	116.7
	34	1.75	P	16%	???	16.305	116.7
	35	1	P / P+	2%	272	14.035	66.7
	36	1	Poly / P+	2%	63.8	10.741	66.7

How to use the Parylene Coater in the CMP laboratory at RIT?

1. Adding Parylene – C Dimer to Parylene Coater Tool
    a. Remove foil and heating tape surrounding evaporation lid
    b. Unscrew and remove clamp
    c. Open Evaporation Chamber and remove previous boat if any
    d. Clean the lid with Micro-90 and wipe
    e. Create a boat for tool* (made out of Aluminum Foil)
    f. Create a smaller boat**
    g. Weigh smaller boat*** (tare boat)
    h. Add Dimer*** (X grams depending on desired thickness)
    i. Record weight of dimer for later calculations
    j. Add Dimer to boat for tool, place boat for tool inside evaporation chamber
    k. Close evaporation chamber lid, wrap heating tape and aluminum foil to prevent heat from escaping to atmosphere

2. Clean Chamber
    a. Clean lid with a wipe and Micro-90 (re-agent)
    b. Clean inside of chamber with wipe and Micro-90, make sure O-ring is clean from debris and pick up any extra material (aka. Parylene C film) from inside the chamber

3. Placing wafer or device inside chamber
    a. Place wafer or device in the middle of the disc, equidistant from all sides, facing up.
    b. Make sure that it will not fall from rotating platform or it will hit the exhaust vent.
    c. Cover the chamber with the lid

4. Move knob, PUMP SWITCH to pump air out of the chamber
5. Press the blue button and keep pressed until the ALM (alarm) lights are completely on all the way, else the tool is going to shut off. (This is a safety check)
6. Let the machine run
    a. Turn the heat knobs on
    b. Turn the cryo-cooler on
    c. Once all gauge levels are OK press START button
7. Start Run

*Look at Figure 4.15

**Look at Figure 4.16

***Look at Figure 4.11 and 4.16

***This step requires you to go in the SMFL laboratory and use the scale in the first wet etch bench

Table 2A - Viscosity of Aqueous Glycerin Solutions in (cP) or (mPa*s) [48] [46]

Viscosity of Aqueous Glycerine Solutions in Centipoises/mPa*s											
Glycerin % Wt	Temperature (°C)										
	0	10	20	30	40	50	60	70	80	90	100
0	1.792	1.308	1.005	0.8007	0.656	0.5494	0.4688	0.406	0.3565	0.3165	0.2838
10	2.44	1.74	1.31	1.03	0.826	0.68	0.575	0.5	-	-	-
20	3.44	2.41	1.76	1.35	1.07	0.879	0.731	0.635	-	-	-
30	5.14	3.49	2.5	1.87	1.46	1.16	0.956	0.816	0.69	-	-
40	8.25	5.37	3.72	2.72	2.07	1.62	1.3	1.09	0.918	0.763	0.668
50	14.6	9.01	6	4.21	3.1	2.37	1.86	1.53	1.25	1.05	0.91
60	29.9	17.4	10.8	7.19	5.08	3.76	2.85	2.29	1.84	1.52	1.28
65	45.7	25.3	15.2	9.85	6.8	4.89	3.66	2.91	2.28	1.86	1.55
67	55.5	29.9	17.7	11.3	7.73	5.5	4.09	3.23	2.5	2.03	1.68
70	76	38.8	22.5	14.1	9.4	6.61	4.86	3.78	2.9	2.34	1.93
75	132	65.2	35.5	21.2	13.6	9.25	6.61	5.01	3.8	3	2.43
80	255	116	60.1	33.9	20.8	13.6	9.42	6.94	5.13	4.03	3.18
85	540	223	109	58	33.5	21.2	14.2	10	7.28	5.52	4.24
90	1310	498	219	109	60	35.5	22.5	15.5	11	7.93	6
91	1590	592	259	127	68.1	39.8	25.1	17.1	11.9	8.62	6.4
92	1950	729	310	147	78.3	44.8	28	19	13.1	9.46	6.82
93	2400	860	367	172	89	51.5	31.6	21.2	14.4	10.3	7.54
94	2930	1040	437	202	105	58.4	35.4	23.6	15.8	11.2	8.19
95	3690	1270	523	237	121	67	39.9	26.4	17.5	12.4	9.08
96	4600	1580	624	281	142	77.8	45.4	29.7	19.6	13.6	10.1
97	5770	1950	765	340	166	88.9	51.9	33.6	21.9	15.1	10.9
98	7370	2460	939	409	196	104	59.8	38.5	24.8	17	12.2
99	9420	3090	1150	500	235	122	69.1	43.6	27.8	19	13.3
100	12070	3900	1410	612	284	142	81.3	50.6	31.9	21.3	14.8

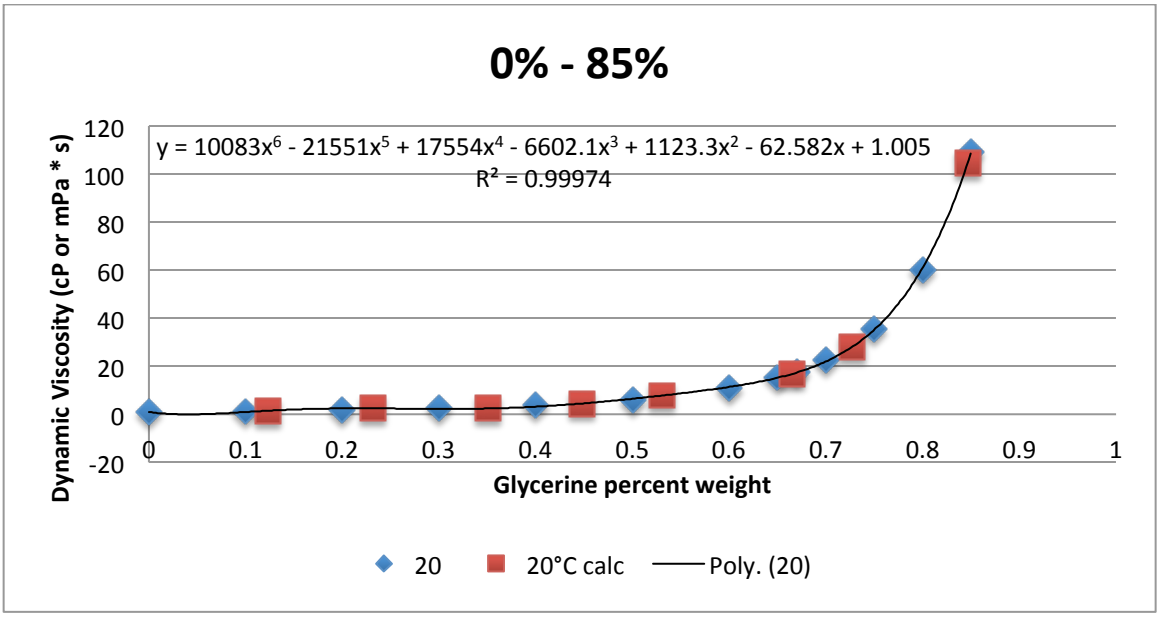

Figure 1A - Calculated and Dorsey Values at Different Glycerin Percent Weights

Table 3A - Calculated Values of Viscosity for Different Glycerin Percent Weights at 20°C

% GLY wt	Dynamic Visc. (cP or mPa*s)			
x	y table Dorsey	y calc Excel	μ_mixture Cheng-1	μ_mixture Cheng-2
0	**1.005**	1.005	1.005	1.002
10	**1.31**	0.93	1.29	1.28
12.33	--------'	1.47	1.37	1.37
20	**1.76**	2.44	1.72	1.71
23.16	--------'	2.45	1.90	1.89
30	**2.5**	2.24	2.40	2.39
35.06	--------'	2.41	2.91	2.90
40	**3.72**	3.17	3.58	3.57
44.81	--------'	4.51	4.45	4.44
50	**6**	6.48	5.78	5.77
53.04	--------'	7.81	6.83	6.81
60	**10.8**	11.42	10.45	10.42
65	**15.2**	15.22	14.82	14.79
66.51	--------'	16.83	16.62	16.58
67	**17.7**	17.42	17.26	17.22
70	**22.5**	21.99	22.02	21.97
72.73	--------'	28.11	27.95	27.89
75	**35.5**	35.26	34.57	34.49
80	**60.1**	61.06	58.07	57.96
84.67	--------'	104.62	101.71	101.52
85	**109**	108.68	106.16	105.96
100	**1410**	--------'	1413.831	1412

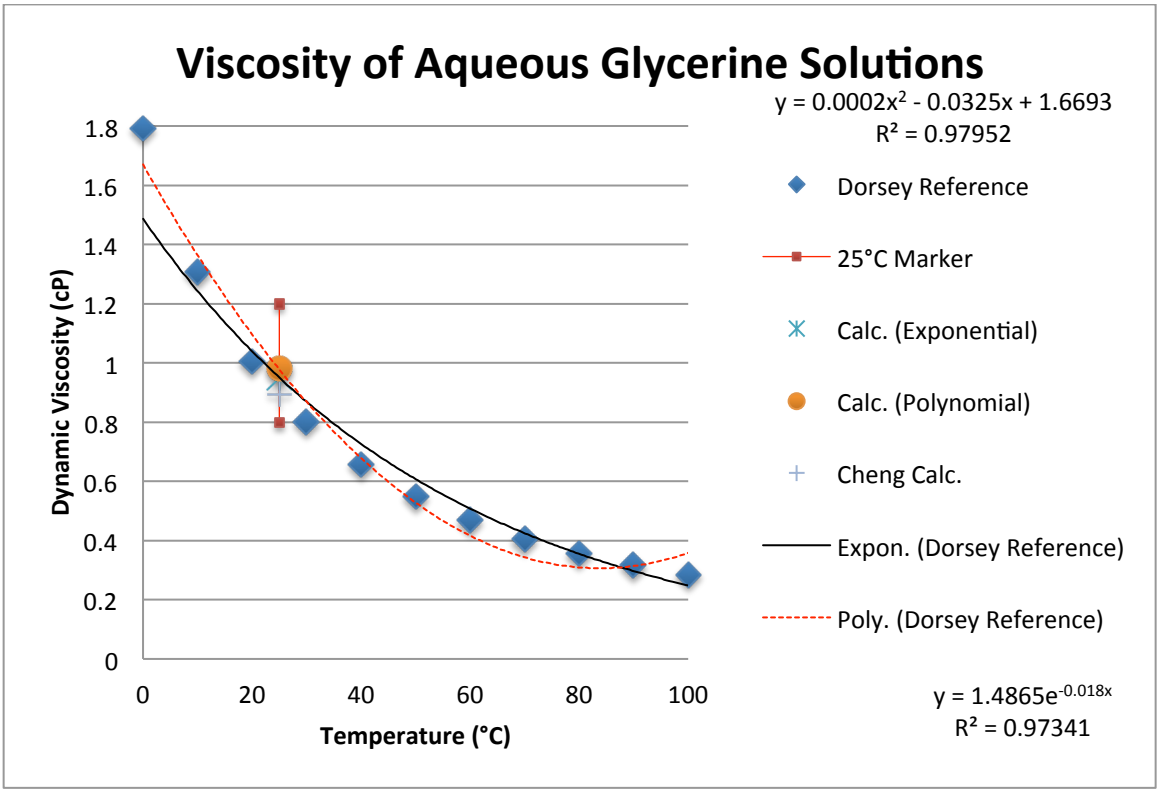

Figure 2A - Determining Dynamic Viscosity at 25°C [46]

Table 4A - Calculated Values Compared with Dorsey Reference as Temperature is Increased the Viscosity Decreases

% GLY wt	Dynamic Visc. (cP or mPa*s)		
	At 20°C	At 25°C	At 30°C
x	y table Dorsey	μ_mixture Cheng-1	y table Dorsey
0	1.005	0.893	0.8007
10	1.31	1.136	1.03
12.33	--------'	1.207	--------'
20	1.76	1.498	1.35
23.16	--------'	1.649	--------'
30	2.5	2.067	1.87
35.06	--------'	2.486	--------'
40	3.72	3.026	2.72
44.81	--------'	3.731	--------'
50	6	4.785	4.21
53.04	--------'	5.606	--------'
60	10.8	8.398	7.19
65	15.2	11.711	9.85
66.51	--------'	13.054	--------'
67	17.7	13.534	11.3
70	22.5	17.055	14.1
72.73	--------'	21.396	--------'
75	35.5	26.179	21.2
80	60.1	42.871	33.9
84.67	--------'	73.077	--------'
85	109	76.119	58
100	1410	905.680	612

9.0 Works Cited

[1] Ivan Puchades and Lynn F. Fuller, "A Thermally Actuated Microelectromechanical (MEMS) Device for Measuring Viscosity," *Journal of Microelectromechanical Systems*, vol. 20, no. 3, pp. 601-608, 2011.

[2] Laurent Dr. Auret. (2008, May) Neosens discusses about its unique innovative sensors based on MEMS technology to monitor continuously fouling phenomenon in any liquid environment. [Online]. http://www.i-micronews.com/interview.asp?id=33

[3] L Ristic and M Shah, "Trends in MEMS Technology," in *WESCON*, Phoenix, 1996.

[4] Amy C. Richards Grayson et al., "A BioMEMS Review: MEMS Technology for Physiologically Integrated Devices," in *Proceedings of the IEEE*, 2004.

[5] Eric Mounier, "MEMS Market and New Applications," in *Integration Issues of Miniaturized Systems*, Brussels, 2008.

[6] Kaigham J. Dr. Gabriel, "MicroElectroMechanical Systems (MEMS)," in *IEEE Aerospace Conference Proceedings*, Arlington, 1997.

[7] p-wholesale.com. Automotive Pressure Sensor. [Online]. http://www.p-wholesale.com/cn-pro/5/297to1/automotive-pressure-sensor-12223861-284223.html

[8] Bosch AG. (2008, April) Bosch Media Service. [Online]. http://www.bosch-presse.de/presseforum/details.htm?txtID=3593&locale=en

[9] Mona E. Zaghloul and David J. Nagel. (1999) The Teaching of MicroElectroMechanical Systems (MEMS).

[10] Y.J. Zhao et al., "A MEMS Viscometric Glucose Monitoring Device," in *The 13th International Conference on Solid-State Sensors, Actuators and Microsystems*, Seoul, 2005.

[11] Robert W. Stark, Stefan Burghardt, and Marc Hennemeyer, "Cantilever Micro-rheometer for the Characterization of Sugar Solutions," Munich, 2008.

[12] P Rust and J Dual, "NOVEL METHOD FOR GATED INDUCTIVE READOUT FOR HIGHLY SENSITIVE AND LOW COST VISCOSITY AND DENSITY SENSORS," in *Solid State Sensors, Actuators and Microsystems Conference* , Beijing, June 2011, pp. 1088-1091.

[13] Libo Zhao, Guiming Zhang, Zhuangde Jiang, and Zhigang Liu, "A MEMS Resonator-type Viscosity Sensor Based on Triangular Cantilever," in *Mechanic Automation and Control Engineering (MACE), 2010 International Conference*, Wuhan, 2010.

[14] Oliver Brand, Jennifer M English, Sue Ann Bidstrup, and Mark G Allen, "Micromachined Viscosity

] Sensor for Real-Time Polymerization Monitoring," in *International Conferencee on Solid-State Sensors and Actuators. Transducers*, Chicago, 1997.

[15] Yook-Kong Yong, John Vig, and Arthur Ballato, "Straight Crested Wave Analysis of Quartz MEMS Ring Electroded Mesa Resonators," in *Ultrasonics Symposium, 2002*, Munich, 2002.

[16] Yook-Kong Yong, Mihir S Patel, and Masako Tanaka, "Estimation of Quartz Resonator Q and other Figures of Merit by an Energy Sink Method," in *Frequency Control Symposium and Exposition*, Vancouver, 2005.

[17] C Riesch et al., "A Micromachined Suspended Plate Viscosity Sensor Featuring IN_PLANE Vibrations and Integrated Piezoresistive Readout," in *Solid-State Sensors, Actuators and Microsystems Conference, Transducers*, Denver, 2009.

[18] D. Sparks et al., "Dynamic and kinematic viscosity measurements with a resonating microtube," in *Sensors and Actuators A: Physical*, Christchurch, 2009.

[19] Wikipedia.org. (2011, December) Joule Heating. [Online]. http://en.wikipedia.org/wiki/Joule_heating

[20] Wikipedia.org. (2011, December) Wheatstone Bridge. [Online]. http://en.wikipedia.org/wiki/Wheatstone_bridge

[21] Stig Ekelöf, "The Genesis of the Wheatstone Bridge," *Engineering Science and Education Journal*, vol. 10, no. 1, pp. 37-40, February 2001.

[22] Burr-Brown Corporation. (1998, July) Octopart Base. [Online]. http://octopart.com/ina101hp-texas%2Binstruments-414167

[23] Bruno A Boley and Jerome H Weiner, *Theory of Thermal Stresses*. Malabar: Krieger Publishing Company, 1988.

[24] Philip M Morse and K. Uno Ingard, *Theoretical Acoustics*. Princeton: McGraw-Hill Inc, 1968.

[25] Y Kozlovsky, "Vibration of Plates in Contact with Viscous Fluid: Extension of Lamb's Model," *Journal of Sound and Vibration*, vol. 326, no. 1-2, pp. 332-339, 2009.

[26] Horace Lamb, "On the Vibrations of an Elastic Plate in Contact with Water," in *Proceedings of the Royal Society*, London, 1920.

[27] R.D. Blevins, "Formulas for Natural Frequency and Mode Shape," in *Van Nostrand Reinhold*, New York, 1979.

[28] Cédric Ayela and Liviu Nicu, "Micromachined Piezoelectric Membranes with High Nominal Quality Factors in Newtonian Liquid Media: A Lamb's Model Validation at the Microscale," *Sensors Actuators B Chemical*, pp. 860-868, May 2007.

[29] O Brand, H Baltes, and U Baldenweg, "Ultrasound Transducer Using Membrane Resonators Realized with Bipolar IC Technology," in *IEEE Workshop on MEMS*, Oiso, 1994.

[30] Biye Wang, "Considerations for MEMS Packaging," in *High Density Microsystem Design and Packaging and Component Failure Analysis*, Shanghai, 2004.

[31] A Lapicki et al., "Functionalization of Micro-Hall Effect Sensors for Bio Medical Applications Utilizing Superparamagnetic Beads," in *Digests of the IEEE International Magnetics Conference*, Nagoya, 2005.

[32] Sie-Yu Li, Chih-Chao Hsu, Shi-Zheng Lin, and Ru-Min Chao, "A Novel Design of Piezo-Resistive Type Underwater Acoustic Sensor Using SOI Wafer," in *OCEANS*, 2006.

[33] D Hanley and J Martin, "A Test of Parylene as a Protective Circuitry for Microcircuitry ," , Cambridge.

[34] Yong Xu et al., "Underwater Shear-Stress Sensor / Micromachined Thermal shear-stress Sensor for Underwater Applications," in *Journal of Microelectromechanical Systems*, 2005.

[35] Jie Zhu et al., "A Novel Technique to Cover Microfluidic Systems with Parylene-C," in *Nano/Micro Engineered and Molecular Systems (NEMS)*, 2010.

[36] Hung-I Kuo, Rui Zhang, and Ro W.H., "Development of micropackage technology for biomedical implantable microdevices using parylene-C as water vapor barrier coatings," in *IEEE, Sensors*, Kona, 2010.

[37] X Huang et al., "A MEMS Differential Affinity Sensor for Continuous Glucose Detection," in *Transducers '11*, Beijing, 2011.

[38] MNX. Material: Polyimide Film. [Online]. https://www.memsnet.org/material/polyimidefilm/?keywords=Polyimide

[39] PECVD Silicon Nitride. [Online]. http://www.mit.edu/~6.777/matprops/pecvd_sin.htm

[40] Wikipedia.Org. (2012, January) Fused quartz - Wikipedia, the free encyclopedia. [Online]. http://en.wikipedia.org/wiki/Fused_silica

[41] Specialty Coating Systems. (2010, June) SCS Parylene Coatings. [Online].

] http://scscoatings.com/what_is_parylene/parylene_properties.aspx?gclid=COS_qvrwq7ECFYeo4AodBF0AWA

[42] N.S. Cheng, "Formula for Viscosity of Glycerol Water Mixture," in *Industrial Engineering Chemical Research*, Nanyang, 2008, pp. 3285-3288.

[43] Wikipedia Org. (2012, April) Glycerol - Wikipedia, the free encyclopedia. [Online]. http://en.wikipedia.org/wiki/Glycerol#cite_note-Viscosity_of_Glycerol_and_its_Aqueous_Solutions-1

[44] The Engineering Toolbox. (--, --) Water - Dynamic and Kinematic Viscosity. [Online]. http://www.engineeringtoolbox.com/water-dynamic-kinematic-viscosity-d_596.html

[45] First Ten Angstroms. (--, --) Dispensing Glycerol and othe High Viscosity Liquids. [Online]. http://www.firsttenangstroms.com/faq/GlycerolViscosity.html

[46] N. E. Dorsey, "The Properties of ordinary water substance," *Q. J. R. Meteorological Society*, vol. 81, no. 347, pp. 132-133, January 1955.

[47] Glycerine Producers Association, *Physical Properties of Glycerine and its solutions*. New York, USA: Glycerine Producers Association, 1963.

[48] The Dow Chemical Company. (2009, September) OPTIM Glycerine Viscosity. [Online]. https://dow-answer.custhelp.com/app/answers/detail/a_id/3600/~/optim-glycerine-viscosity

[49] Liu Yaxin, Chen Liguo, and Sun Lining, "A MEMS Flow Sensor and Its Application in Adaptive Liquid Dispensing," in *International Conference on Measuring Technology and Mechatronics Automation*, Hunan, 2009.

[50] Jae Hong Park, Kiyoung Choi, Dong-Yeon Lee, Jaesool Shim, and Tae Song Kim, "Resonant Properties of Piezoelectric Cantilever Transducers Fabricated on the SiC Membrane," in *Nano/Micro Engineered and Molecular Systems*, Kaohsiung, 2011.